Hybrid supracolloidal structures through interface driven assembly

By

Catheline A. L. Colard

A thesis submitted in fulfilment of the requirements for the degree of Doctor of Philosophy in Chemistry

University of Warwick, Department of Chemistry

September 2010

Table of contents

Figures

Tables

Acknowledgments

This work would have not been achieved without the precious discussions, advice and collaboration with numerous people at the University of Warwick and elsewhere.

I am fortunate to have had the opportunity to work within the Bon Polymer Colloid group, part of the material cluster of the Department of Chemistry since October 2006. First of all I am very grateful to my promoter Assoc. Prof. Stefan Bon for giving me the chance to join his team, for his precious enthusiasm and numerous ideas and also the opportunity to present my research and network through internationally leading conferences/journals.

I also would like to address special thanks to my industrial supervisor Dr. habil. Wolf-Dieter Hergeth at Wacker Chemie AG (Burghausen, Germany). This work would not have happened without the developed scientific research proposal and their industrial financial support. Thank you for your advice and guidance during this project.

Special thanks go to all the past and present members of the Bon Polymer Colloid group. Thank you Nadia and Nicole (our post-docs) for your precious help and encouragements, Pat especially for your guidance when I started and Roberto for your contribution in our collaborative work. Thank you all for interesting discussions, fun times in the labs and coffee breaks - Pat, Rich, Nadia, Roberto, Tom, Andy, Nick, Nicole, Adam, Rong, Attyah, Gabit, Yunhua, and other students, visitors, undergrads and masters.

I would like to thank Dr. James Covington (School of Engineering), Sara Fortuna and Dr. Alessandro Troisi (Department of Chemistry), as well as Dr. habil. Wolf-Dieter Hergeth, Barbara Hager and Dr. Reinhard Härzschel (Wacker Chemie AG, Germany) for interesting discussions and their involvement in our successful collaborative works.

I acknowledge Steve York, Dr. Richard Dobedoe, Jane Green and Ian Portman for their training and help with electron microscopes (Department of Physics and School of Biology), Birmingham Science city Innovative for some of the equipment used in this research (Uses for Advanced Materials in the Modern World (West Midlands Centre for Advanced Materials Project 2) with support from Advantage West Midlands (AWM) and partly funded by the European Regional Development Fund (ERDF)), and Dr. K. Kindlay (John Innes Centre), and staff from Quorumtech, Gatan, and Zeiss Cambridge UK for assistance with cryo-electron microscopy.

I also would like to thank everybody who has encouraged me all the way or at some stages of the accomplishment of this work. You know how much your presence and your support in those times have been important to me; I am really grateful for those fortunate moments. Not mentioning again friendships within the Bon group, I also would like to name mi Pepes Sole, Sarah and Haz, also Agnieszka & Michal, Zsuzsa, Flo, Julien, Ofelia, Schumi, Vicky, Stacy, Gaidad, Ale, Dave, Martin, Paul, Jen, Sarah, Lucie, Claire, Mike, Raj, Ant, Alex, Shmyalla, Ofe, Michael, and Zoe.

Special thanks go to my Belgian friends, who were there for me over the internet and/or whenever I managed to visit Belgium, Xa, Pit, Cathy, Alex & Ju, Ben, Val, Marie, Leen and Oana.

Most importantly I would like to thank my family. I am especially grateful for the continuous support from my Mummy and I also would like to thank Papounet José, Boubou, Marraine & Tonton, mon frérot Oli & Maëlle, Bon Papa, Tit & Parrain, Papa & Adi, Isa & Didier.

Declaration

I hereby declare that this thesis consists of my own work, and that it has not previously been submitted for any previous degree at any institution. Production of powders *via* spray-drying and their application tests in tile adhesive formulations, presented in Chapter V, were carried out at Wacker Chemie AG (Burghausen, Germany) in the Polymer Research division, research laboratories of Dr. Wolf-Dieter Hergeth and Dr. Reinhard Härzschel. Tests of the reinforced hybrid polymer foams as gas sensors in Chapter VI were carried out in collaboration with Dr. James Covington in the School of Engineering of the University of Warwick, and cryo-SEM analyses were performed with assistance of Dr. K. Kindlay (John Innes Centre), and staff from Quorumtech, Gatan, and Zeiss Cambridge UK.

Where other sources of information have been used, they have been acknowledged and referenced.

Signature: *Catheline Colard* Date: *17th September 2010*

Abstract

We investigated different strategies for the preparation of armoured polymer particles. Inorganic nanoparticles, such as clay platelets and Ludox colloidal silica grades, were used as solids-stabilisers in processes such as miniemulsion, suspension and/or emulsion polymerisations. These nanoparticles were either assembled at liquid-liquid interfaces for the stabilisation of monomer droplets or adsorbed onto solid surfaces in the case of poly(vinyl acetate) latex particles. Colloidal assembly was promoted by modifying the pH and/or the ionic strength of the dispersion medium, thereby tuning the surface properties of the nanoparticles. When prepared in miniemulsion polymerisation, latexes with controlled particle size distributions were obtained. Their diameter was dictated by the amount of solids-stabiliser (Laponite clay) or by the dimensions of the building blocks (Ludox colloidal silica).

We developed a versatile emulsion polymerisation process leading to silica-armoured poly(vinyl acetate) particles and showed that quantitative disc centrifugation analyses throughout the polymerisation process unravelled mechanistic aspects of particle formation and growth. Stability of the armoured particles was studied in dispersion and after spray-drying the hybrid dispersions. The thickness of the silica shell on the polymer particles had an important role in limiting polymer inter-diffusion upon film formation. The obtained powders were tested as additives in cement-based formulations for tile adhesives. However, desired performance characteristics were not obtained in comparison to standard formulations.

Soft polymer composite foams were prepared through freeze-drying a mixture of colloids. ‘Large-soft’ particles of poly(vinyl laurate) reinforced by an armouring layer of ‘small-hard’ nanoparticles of colloidal silica led to the formation of highly porous open-cell foams. Upon addition of a third conducting colloidal component, this newly designed material proved promising results as a gas sensor.

Abbreviations

(FEG-)SEM	(Field Emission Gun-) Scanning Electron Microscopy
AIBN	2,2′-azobis(2-methylpropionitrile
C-black	Carbon black
CPS	Disc Centrifuge Particle Sizing
D_I	Dispersity index (often called Polydispersity index)
DLS	Dynamic Light Scattering
DSC	Differential Scanning Calorimetry
d_z	Hydrodynamic Diameter
Exp.	Experiment
FCC	Face-centred cubic
HCP	Hexagonal close-packed
KPS	Potassium persulfate
NaSS	Sodium styrene sulfonate
NMR	Nuclear Magnetic Resonance
PS	Poly(styrene)
PVAc	Poly(vinyl acetate)
PVL	Poly(vinyl laurate)
PVOH	Poly(vinyl alcohol)
PVPiv	Poly(vinyl pivalate)
SDS	Sodium dodecyl sulfonate
TEM	Transmission Electron Microscopy
V-65	2,2'-azobis(2,4-dimethyl valeronitrile)
VAc	Vinyl acetate

VEOVA-10	Vinyl neodecanoate (mixture of isomers)
VL	Vinyl laurate
VPiv	Vinyl pivalate
T_g	Glass transition temperature
X_m	Monomer conversion

Chapter I.

General introduction

This chapter introduces the field of interface and colloid science. Key colloidal properties and assembly mechanisms for the formation of raspberry-like particles are described. This introduction is followed by the main objectives of this thesis which are put into their industrial context and finally, the research of each following chapter is briefly outlined.

I.1. Interface and colloid science[1]

Interface and colloid science is a branch of physical chemistry studying heterogeneous systems composed of at least one dispersed phase (not soluble) in a dispersion medium. Each of the constituting phases can be either at a state of gas, liquid or solid. A *colloid* can be defined as a substance composed of a system of particles, which also can be referred to as *colloids*, with linear dimensions in the range of about 10^{-9} to 5×10^{-7} m dispersed in a continuous medium. Nature provides us with numerous colloidal dispersions, such as natural rubber latex extracted from rubber trees, or milk which is an emulsified butter fat dispersion. Graham identified colloidal particles for the first time in the 1860s and discussed the constitution and properties of matter.[2-3] He described the presence of colloids between the liquid and crystalline states which in the case of silicic acid gels depended on their hydration, solubility, and concentration. Nowadays, colloid science plays a significant role in technological developments including a wide range of industrial sectors such as pharmaceuticals, biotechnology, nanotechnology, food industry, and building industry.

Colloids can be classified in two categories: *lyophilic colloids* for solvent loving particles and *lyophobic colloids* for solvent hating particles. Lyophilic colloid sols are thermodynamically stable. However most colloidal dispersions are lyophobic meaning that the energy associated with creating and maintaining the large area of contact between dispersed particles and dispersion medium is significant. Thermodynamically unstable, these lyophobic particles can only be dispersed if their surface properties cause repulsion between particles to prevent

them from aggregating over long periods. In this case, the barrier to undergo coagulation is kinetic and the system is called *metastable*. In this work, lyophobic systems are considered and our study concerns dispersions of liquids in liquids and solids in liquids.

I.2. Stabilisation of lyophobic colloids

As a result of their individual thermal motion, also called random *Brownian motion*, dispersed particles can potentially collide. These inter-particle shocks combined with attraction forces, such as van der Waals interactions, lead to aggregation of the colloids. If two spheres are at close proximity and in a vacuum, the following expression approximates the attractive potential energy, V_a:

$$V_a = -\frac{A a}{12 H} \qquad \textbf{Equation I-1}$$

Where a is the radius of the spheres, and H is their minimum distance of separation. A is the *Hamaker constant*, characteristic of the material of the particles at the microscopic molecular or atomic interactions, which is reduced by the self-attraction of the medium in the case of a liquid dispersion.

Different mechanisms of stabilisation or destabilisation tend to prevent or provoke coagulation of dispersed solid particles. The term flocculation generally refers to a reversible aggregation process. Four main categories of colloidal stability are presented in this section.

I.2.1. Electrically charged colloids

To overcome attraction forces, particles can be stabilised by possessing surface charges. Covalently bound or adsorbed, these charges induce the formation of an *electrical double layer*. Due to the requirement of electroneutrality, an identical but oppositely charged layer of ions, so-called surface ions, and a diffuse layer of mobile ions will be generated with ions present in the continuous phase. Some ions are strongly adsorbed onto the (particle) surface and form an inner sub-layer which is called the *Stern layer*. The electric potential, V_r, inside the electric double layer is expressed by the following equation:

$$V_r = V_s \exp(-KH) \qquad \textbf{Equation I-2}$$

Where V_s is the surface electric potential, H is the distance from the surface and K is the characteristic thickness of the diffuse layer, called the *Debye length*, which depends on the ionic strength of the medium. The hydrodynamic diameter includes the thickness of this layer, meaning this is not an absolute measure of the actual dimension of the colloid. This influences measurements when determining particle size distributions by dynamic light scattering, see Appendix A, section A.3. The potential stability of electrically charged colloidal systems can be evaluated by the magnitude of the zeta potential as measured by electrophoretic light scattering, see Appendix A, section A.2.

Elaborated models to calculate the repulsive free energy between electrically charged lyophobic particles have been developed. The "DLVO theory" was developed in parallel in two groups, by Derjaguin and Landau[4] and, Verwey and Overbeek[5] in the 1940s. It combines van der Waals attractions

between particles and the existence of the electrical double layer. When two particles are brought together, due to their random thermal motion, known as their *Brownian motion*, the cloud of their counter-ion layers will overlap. A higher ionic concentration between the particles than elsewhere leads to an increase of the free energy of the system, either in terms of electrochemical potential or osmotic pressure, which brings solvent from outside, both creating a driving force for repulsion between the particles. The combination of the electrostatic repulsion potential, to the van der Waals attraction and Born repulsion potentials is represented in Figure I-1 as a function of distance from the surface of a spherical particle. The primary minimum is generally so deep that the energy to separate two particles from there is close to be infinite. However, the presence of a secondary minimum in the resulting potential energy curve explains thermodynamically the reversible flocculation[6] already observed in the 1910's for clay[7] and silver sol.[8]

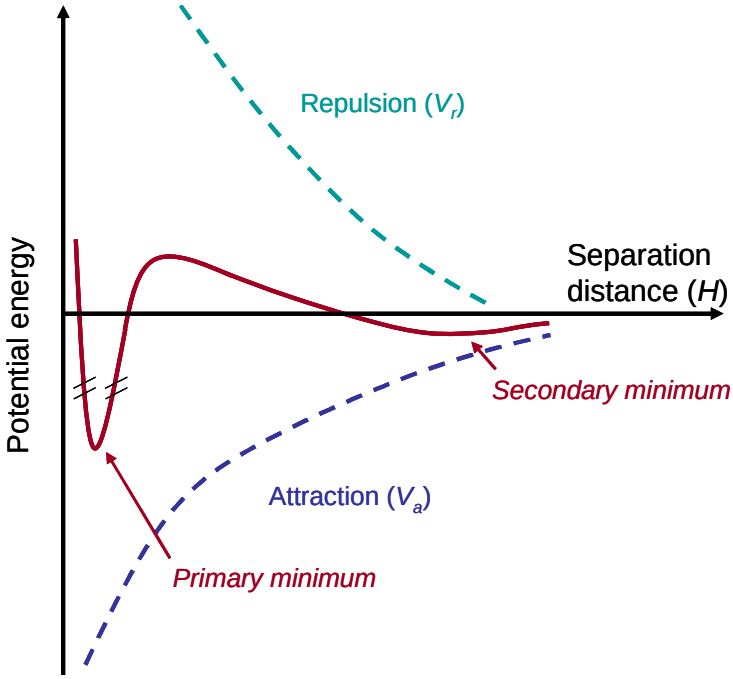

Figure I-1. Schematic representation of the total potential energy (red line) obtained by adding the van der Waals attraction potential, V_a, and the electrostatic and Born repulsion potentials, V_r, as a function of distance between two spherical particles. The height of the repulsive barrier indicates system stability.

I.2.2. Sterically stabilised colloids

Steric stabilisation, already described by Napper in the late 1960's,[9-13] is obtained by adsorption of non ionic macromolecules; typically, hydrophilic or amphiphilic polymers are used and are referred to as *protective colloids*.[14] The particles interact only when their protective polymeric layers start overlapping. The interpenetration of the polymer chains is called the compression region. The main effects contributing to effective repulsion, or in other words to limited compression, are the elastic and osmotic terms from the deformation and the solvation effects of the polymeric chains, respectively. Commonly used in industrial processes for many decades,[15-17] this polymeric layer serves as anti-

caking or suspending agent and often enhances the properties of a material when film formed.

I.2.3. Depletion effect

The depletion effect involves the presence of free macromolecules (or nanoparticles) controlling stabilisation or flocculation of uncharged dispersed colloids. The polymer chains remain in the continuous liquid phase being inert or repulsive to the polymeric surface or if all the adsorption-sites are occupied. The attractive force between dispersed particles and free macromolecules having no direct interactions between them was reported by Asakura and Osawa in 1958.[18] They found that this force acts around the particles in the range of the diameter of the macromolecules and its magnitude is of the order of the osmotic pressure of the solution of macromolecules. This stipulates that the average segment density in free polymer is less near any surface than in the bulk phase. Therefore, when approaching two polymer particles this engenders expulsion of free macromolecules and creates regions of lower and higher concentrations of free polymer. Flocculation is induced if the attraction and expulsion of the pure solvent remaining between the particles occurs. This effect was studied for common polymers such as poly(acrylic acid)[19] and poly(methyl methacrylate) (PMMA).[20] The *bridging effect* observed for the latest induced aggregation of the PMMA latex synthesised in emulsion polymerisation. The reason for this was due to the presence of free polymer chain formed from predominant nucleation in the aqueous phase as a result of high monomer water solubility. A model of the interactions between uncharged macromolecules and micron spheres, suggested and compared with experiments by Feigin and Napper in the

early 80s,[21-22] argued that kinetic stabilisation can also result if the generated repulsion is strong enough. Lekkerkerker *et al.* calculated this entropic depletion force, attractive or repulsive, between large spheres and avoiding smaller particles[23-24] or rod-like macromolecules.[25]

I.2.4. Image charge effect

The feature of *image charge effect* is well known in classical electrostatics but is essentially described in theoretical work.[26-31] Complex simulations calculate the interaction forces by considering charge density and the charge distribution (dielectric constant) for polarisable matter. A simple description of the image charge effect can be given as follows: when a charged particle is brought close to a solid surface, the dielectric response of the medium leads to a polarisation potential that counteracts the external charge. This material is divided into point charges which are called the image charges.[32] The resulting electrical force between the particle and the solid surface follows the Coulomb's law; that is to say that the magnitude between two point charges is proportional to the magnitude of both electrical charges and inversely proportional to the square of the distance separating the two points. The effective interaction of an interface and an electrolyte, image charge effects plus the deformation of the colloidal ion atmosphere by the interface, can be attractive or repulsive. Based on the electrical double layer model, Klein and von Grünberg investigated the consequences of a high accumulation of ion distributions next to charged objects in electrolyte solutions, thereby modelling realistic examples such as the adsorption of DNA on a cationic membrane.[28] They found that due to double-layer forces a charged colloid suspended in an electrolyte is repelled from a like-

charged planar wall, and somehow, it was experimentally demonstrated that a precise measurement of these double-layer forces acting on a colloid near a glass surface can be used to determine surface charge densities using total internal reflection microscopy.[33] Recently, Leunissen *et al.* conducted an interesting study on the electrostatic stabilisation effects of polymer colloids on oil-water interfaces.[34] Non-wetting particles but strongly bound to the oil-water interfaces were found to form surprisingly stable emulsions that can crystallise. Based on electrostatic effects, the mechanism of haloing stabilisation is described in section I.4.3.

I.3. Fabrication of supracolloidal structures

Based on the definition of supramolecular chemistry, which is the science beyond the molecules, their interaction and assembly, *supracolloidal chemistry* refers to the assembly of colloidal components for the formation of complex structures. *Nanocomposites* can be defined as materials having two or more phases and at least one of the constituent can be identified as colloid in the final product.

Advanced colloidal assembly strives towards for mimicking natural systems although the nano/microstruture of today's most advanced composites has yet to achieve the order and sophisticated hierarchy of hybrid materials built up by living organisms in nature.[35] Drug delivery systems[36] or supports for tissue regeneration[37] are only examples of important challenges for both colloid scientists and the healthcare industry in this case. Colloidal assembly has been studied and developed to control size and shape[38] of nanomaterials in order to fabricate, for instance, organised crystals with interesting optical and magnetic

properties,[39-41] electrical circuits,[42] or materials of modulated tensile strength and ductile behaviours.[43]

Armes *et al.* recently published a review entitled: *"Colloidal nanocomposite particles: quo vadis?"* in which they focused on the increased interest in the development of polymer-silica latex particles over the last two decades.[44] The term *hybrid* colloid is often used to define organic-inorganic colloidal systems; a broader definition also pertains to materials composed of at least two kinds of incompatible organic polymers.[45-46] One interesting morphological class of hybrid polymer latexes is those showing an armoured supracolloidal structure in which inorganic nanoparticles are assembled onto and adhere to the surface of the polymer latex spheres. These armoured hybrid morphologies when applied to waterborne coatings feature for example scratch resistance,[47-49] flame retardancy of the resulting films,[50] or profound synergistic effects as an additive in waterborne pressure sensitive adhesives.[51] Teixeira and Bon recently reviewed the different strategies for the preparation of hybrid nanocomposite polymer latex particles.[52] These colloidal interactions have been proven to be highly complicated. The next section relays key theories, models and types of colloidal stability of interest for this work.

I.4. Interaction mechanisms for the preparation of solids-stabilised latex particles

Ramsden was the first person, in 1903, to mention the presence of solids in the surface-layers of solutions and suspensions and studied the separation of those solids.[53] Not a long time later, in 1907, Pickering reported the stabilisation

of emulsions with insoluble emulsifiers.[54] The term Pickering stabilisation, or Pickering emulsion, relates to his pioneering work and describes consequently the directed assembly of colloidal particles onto emulsion droplets. Herein, three types of system are distinguished: (i) the adherence of nanoparticles at liquid-liquid interfaces for the stabilisation of liquid droplets, (ii) the adsorption of nanoparticles on solid substrates such as larger polymer particles and (iii) finally a brief description of the haloing phenomenon is given.

I.4.1. Particle wettability at liquid-liquid interfaces

An explanation for the phenomenon of Pickering stabilisation was given by the theory of emulsification reported by Finkle *et al*. in 1923.[55] This theory suggests that the particles are partially wettable by the two phases involved. In 1954, Wiley described that freshly prepared Pickering emulsions could undergo limited coalescence before a stable set of solids-stabilised oil droplets in water was obtained. Factors affecting the "limiting size" of the droplets in oil-in-water emulsions were discussed.[56]

A 2-D model of the interactions of a monolayer of polystyrene spheres trapped at a water/air interface was reported by Pieranski in 1980.[57] The energy profile of a particle of radius *R* demonstrates why they can adhere to the interface. This model assumes a smooth and continuous liquid-liquid interface, absence of gravity, a smooth surface of the spherical particle and negligible line tension at the three phase contact line. A schematic representation is shown in Figure I-2.

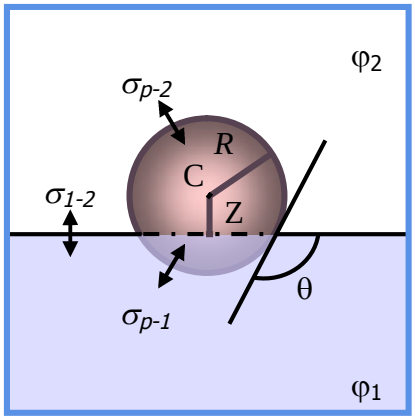

Figure I-2. Schematic representation of a solid spherical particle of radius *R* sitting at the interface of φ_1 and φ_2 a distance Z from the centre C. $\sigma_{p-1}, \sigma_{p-2}, \sigma_{1-2}$ are the surface/interfacial tensions between the particle and φ_1, the particle and φ_2 and the two phases respectively and θ is the three-phase contact angle.

The energies between the particle and the phase 1 (φ_1), the particle and the phase 2 (φ_2) and between the two phases are reported in Equations (I-3) to (I-5) respectively:

$$E_{p-1} = \sigma_{p-1} . 2\pi R^2 (1 - \breve{z}) \qquad \textbf{Equation I-3}$$

$$E_{p-2} = \sigma_{p-2} \cdot 2\pi R^2 (1 + \breve{z}) \qquad \textbf{Equation I-4}$$

$$E_{1-2} = -\sigma_{1-2} \cdot \pi R^2 (1 - \breve{z}^2) \qquad \textbf{Equation I-5}$$

Where $\breve{z} = Z/R$ is the dimensionless vertical coordinate measured from the centre C, with respect to the level of the phase 1. $\sigma_{p-1}, \sigma_{p-2}, \sigma_{1-2}$ are the surface/interfacial tensions between the particle and φ_1, the particle and φ_2 and the two phases respectively.

The total energy, *E*, is the summation of the energies given in Equations (I-3) to (I-5) and $E_{unit} = \pi R^2 \sigma_{1-2}$ is defined to scale the surface energies, so that the energy $\tilde{E}$ is written:

$$\tilde{E} = E / E_{unit} \qquad \textbf{Equation I-6}$$

Using Equation (I-7) and Equations (I-4) to (I-6), respectively, the following quadratic function is found:

$$\tilde{E} = \breve{z}^2 + 2(a-b)\breve{z} + 2a + 2b - 1 \qquad \textbf{Equation I-7}$$

Where, $a = \sigma_{p-2} / \sigma_{1-2}$ and $b = \sigma_{p-1} / \sigma_{1-2}$

The parabola of this function depends on the values of interfacial tension but in the case of successful adherence of the particle at the interface, the minimum energy $\tilde{E}_{\min}$ will appear for values of $\breve{z}$ comprised between -1 and +1 as represented in Figure I-3.

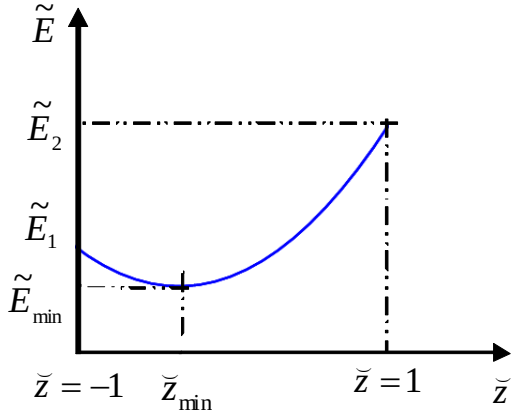

Figure I-3. Potential energy curvature of a solid particle leaving the interface to go in φ_1 ($\tilde{E}_1$) or in φ_2 ($\tilde{E}_2$) where, $\breve{z}_{\min}$ is the vertical coordinate of the centre *C*, position of the particle at the liquid-liquid interface, at minimal energy ($\tilde{E}_{\min}$).

Consequently, $\Delta\tilde{E}_1 = \tilde{E}_1 - \tilde{E}_{\min}$ and $\Delta\tilde{E}_2 = \tilde{E}_2 - \tilde{E}_{\min}$ represent the quantities of energy required to the particle to move in phase 1 and in phase 2 respectively.

Clint and Taylor found that the energy required to remove the particle from the interface into phase 1 or 2 becomes independent from the surface tensions between both liquids and the particle (σ_{P-1}, σ_{P-2}) by using the following Young's equation for equilibrium at the three-phase contact line:[58]

$$\sigma_{p-2} - \sigma_{p-1} = \sigma_{1-2} \cos\theta \qquad \textbf{Equation I-8}$$

Where θ is the three-phase contact angle describing the position at which the particle sits at the interface.

The general expression of the energy is then expressed as:

$$E = \pi R^2 \sigma_{1-2} \left(1 \pm \cos\theta\right)^2 \qquad \textbf{Equation I-9}$$

The sign in the brackets is negative for θ < 90 º, when the particle is removed into the water and positive for θ > 90 º, when it is removed into the oil phase. The radius *R* of a particle and the interfacial tension between the two liquids σ_{1-2} are generally known. Due to its simplicity this equation is often used to calculate the energy with which a particle could be held at an interface.[59-61]

Hence, solids particles are used as emulsifier and their effectiveness in stabilising emulsion droplets, sometimes called Pickering emulsions, is tuned by the surface properties of the particles and the nature of the liquid phases. Levine *et al.* demonstrated that the electrical double layer, solvation and solid elastic

repulsive interactions are negligible in comparison to the energy depth of a single particle.[62] They also concluded that in equilibrium partitioning virtually all the particles should be deposited on the emulsion droplets when enough interface area is created. Recent advances using this strategy for the formation of supracolloidal structures and the importance of line tension are described in Chapter III.

I.4.2. Colloidal assembly by controlled heterocoagulation

Assembly of solids particles through *heterocoagulation* refers to their adsorption onto a surface which can result from several types of interactions. Controlled adhesion of nanoparticles around larger particles is commonly achieved through hydrogen bonding interactions or ionic bonds leading to stable colloidal nanocomposites. The theory of heterocoagulation was developed by Hogg *et al.* who were the first to present, in 1966, a quantitative theory derived from the diffuse double layer theory. They described the kinetics of coagulation of different hypothetical colloidal species under various conditions such as the concentration of potential-determining ions, the total concentration of ionic species in the supporting electrolyte, the particle size and the relative proportions (in terms of numbers of particles) of the two solid components.[63] In 1976, Schott experimentally investigated the flocculation of a suspension constituted of positively and negatively charged colloids and attributed this phenomenon to a heterocoagulation process, *i.e.* charge neutralisation of bismuth subnitrate by bentonite (clay).[64] A common approach consists of adding a co-monomer for the synthesis of the polymer beads for the formation of acid-base interactions with nanoparticles. In 1982, Tamai *et al.* investigated the

deposition of cationic polystyrene latex prepared by using *N,N*-dimethylaminoethyl methacrylate as co-monomer on polyacrylonitrile, polyamide, and polyester fibres as a function of pH.[65] Many systems have been reported over the last few years using similar strategies and are developed in Chapter IV.

I.4.3. Haloing stabilisation

Lewis *et al.* reported in 2001 a new stabilisation mechanism for which the presence of a critical volume of highly charged nanoparticles (hydrous zirconia) would enhance the stabilisation of microspheres negligibly charged (silica).[66] The nanoparticles were arranged in halos around the microspheres. This was supported by zeta potential analysis showing an effective charge build-up of the microspheres. However they observed by scanning angle reflectometry that nanoparticles did not adsorb on the surface of the microspheres. This mechanism was then investigated by means of direct simulation which showed that haloing stabilisation occurs over a window of nanoparticle concentrations and also sensitively depends on nanoparticle charge and colloid-nanoparticle size asymmetry.[67-69]

Direct force measurements between a silica sphere attached to the cantilever of an atomic force microscope and a silica flat surface demonstrated with increasing concentration in zirconia nanoparticles a transition from an attractive to a repulsive force *via* a meta-stable peak observed in the presence of different concentration in zirconia nanoparticles.[70] Another example involving aluminium oxide microspheres stabilised by highly charged cerium oxide was described and investigated at different value of pH and weight fractions of nanoparticles

by Karimian and Babaluo.[71] Rheological properties, colloidal stability, and 3-D structure of assembled colloids through this mechanism have been highlighted by Rhodes and Lewis.[72] They showed that halo-stabilised suspensions exhibit Newtonian flow behaviour whereas an increase in the apparent viscosity and degree of shear thinning was observed for the flocculated suspension, at lower or higher concentration in stabilising nanoparticles.

I.5. Objectives and outline of the thesis

In this thesis, the formation of supracolloidal structures is explored using interface-driven assemblies as a strategy to form armoured composites. Inorganic and polymer colloids in the range of nanometers to micrometers are used as building blocks. Several routes for the synthesis of polymer particles armoured with inorganic nanoparticles are developed and we also investigate the arrangement and packing of those nanoparticles on the polymeric spheres and their tendency in prohibiting film formation of the polymer particles.

The industrial goal of this project, agreed with Wacker Chemie AG, is to investigate and design the use of nanoparticles as solid stabilisers for the synthesis of poly(vinyl esters) latexes. The final product should ideally be in the format of redispersible powders. The application lying behind the development of those armoured latexes/redispersible powders is to be utilised as additives in cementitious applications. Polymer modified dry mix mortars, or one pack systems, are of great importance for the construction industry. Conventionally poly(vinyl alcohol) is used as protective colloid for the synthesis of poly(vinyl acetate) based latexes, and is added to the latexes during spray-drying to prevent the particles from film forming and obtain redispersible powders.

Silica particles show direct compatibility in the formulation as cement is notably composed of clay, sand and calcium silicates. Therefore, our purpose is to investigate different types of silica nanoparticles for the stabilisation of polymer particles prepared *via* several polymerisation processes such as miniemulsion, suspension and emulsion polymerisation. Particle behaviour and stabilisation mechanisms are studied for better understanding and to be able to target a solids-stabilised system with no addition of any co-monomer, surfactant or macromolecules which usually increase the cost of production.

In spite the hydrophilicity of vinyl acetate and its tendency to hydrolyse, the composition of the armoured latex should have the highest possible ratio poly(vinyl acetate)/poly(vinyl neodecanoate-based). Criteria such as pH and composition need to be addressed to optimise the solids-stabilised polymerisation process to specifics for industrial applications. Solids content of the latexes should be increased as much as possible, reaching typically above 50 wt%. Mechanistic and kinetic aspects of the process have to be studied and optimised to tune the particle size distribution. Currently, latexes in the size range of 800 nm – 5 micron in diameter are used commercially. Colloidal stability of the prepared latexes has to be achieved at high value of pH and high ionic strength to mimic the chemistry in cement applications, *i.e.* pH 12 with high concentration in calcium cations. Film formation of the scaffolded solids-stabilised dispersions should be prevented during spray-drying and the powders could be tested in cementitious applications to conduct a comparative study to current commercial additives produced by Wacker Chemie AG.

We present here a brief overview of each chapter:

Chapter II extends the use of Laponite clay discs as solid stabiliser in Pickering miniemulsion polymerisation. Previous work on armoured latex particles of polystyrene and various hydrophobic (meth)acrylates were made upon solidification by polymerisation of the monomer droplets stabilised with Laponite clay platelets and particle size distribution was controlled by the amount of stabilisers. In our case, special consideration was given to the synthesis of clay – poly(vinyl esters) latexes, specifically using vinyl acetate and vinyl laurate. Limitations and drawbacks in preparing poly(vinyl esters) latexes in a miniemulsion process and using clay platelets as solid-stabilisers are addressed.

Chapter III focuses on the assembly of silica nanoparticles at liquid-liquid interfaces for the synthesis of oil-in-water or water-in-oil emulsions. We developed this strategy to prepare armoured polymer latexes of micron- and submicron-sizes using free radical suspension and miniemulsion polymerisation processes and investigated the preparation of high solids content hybrid polymer latexes. Dimensions of the building blocks were found to have an influence on the average particle size of the prepared latexes and we also studied their packing patterns on the latex particles.

Chapter IV is dedicated to the development of a versatile emulsion polymerisation process in which solid nanoparticles are used as stabiliser for the simple fabrication of armoured nanocomposite of poly(vinyl acetate) latexes. Key mechanistic events of solids-stabilised emulsion polymerisations are described and we demonstrate the use of disc centrifugation as a quantitative

tool to determine the fate of nanoparticles in their use as solids-stabilisers.

Chapter V covers the investigation of the role of the silica nanoparticles armouring the polymer latexes. By increasing the pH better colloidal stability was obtained until coalescence occurred at high ionic strength. In the spray-drying process the thickness of the silica shell had an important role in limiting polymer inter-diffusion upon film formation. A series of powder coatings made through spray-drying of the armoured polymer latexes were tested as additives in cement-based formulations for tile adhesives. Desired performance charactersistics, however, were not obtained in comparison to standard formulations.

Chapter VI describes the fabrication of nanocomposite reinforced soft polymer foams, which were built by freeze-drying a mixture of colloids dispersed in water, thereby using ice-crystals as template for the porous structure. “Soft” polymer latex particles film-formed and the cell walls were covered by “hard” nanoparticles which maintained the foam structure by enhancing its robustness. Addition of carbon black as a third colloidal component led to conducting nanocomposite foams which could be used as promising gas sensors.

The main conclusions and the industrial outlook of this thesis are highlighted in **Chapter VII**.

I.6. References

1. Hunter, R. J., *Foundations of colloid science*. 2nd Ed. ed.; Oxford University Press Inc.: 2001.

2. Graham, T., *J. Chem. Soc., Trans.* **1864,** *17*, 368-371.

3. Graham, T., *J. Chem. Soc., Trans.* **1864,** *17*, 318-327.

4. Deryagin, B.; Landau, L., *Acta Physicochim. URS* **1941,** *14*, 633-62.

5. Verwey, E. J. W.; Overbeek, J. T. G., *Theory of the Stability of Lyophobic Colloids*. Elsvier Pub. Co.: 1948; p 216.

6. Overbeek, J. T. G., *J. Colloid Interf. Sci.* **1977,** *58* (2), 408-422.

7. Bleininger, A. V., *Tran. Am. Ceram. Soc.* **1911,** *12*, 504-16;3.

8. Oden, S., *Z. Physik. Chem.* **1912,** *78*, 682-707.

9. Napper, D. H., *J. Colloid Interf. Sci.* **1969,** *29* (1), 168-70.

10. Napper, D. H., *J. Colloid Interf. Sci.* **1970,** *33* (3), 385-93.

11. Napper, D. H., *J. Colloid Interf. Sci.* **1970,** *32* (1), 106-14.

12. Napper, D. H., *J. Colloid Interf. Sci.* **1977,** *58* (2), 390-407.

13. Napper, D. H.; Netschey, A., *J. Colloid Interf. Sci.* **1971,** *37* (3), 528-35.

14. Fitch, R. M., *Polymer Colloids: A Comprehensive Introduction*. Academic Press Limited: 1997; p 364.

15. Walker, I. F. U.S. Patent 2519088, 1950.

16. Wesslau, H.; Wilhelm, H.; Wolf, H.; Faulhaber, G. DE. Patent 62-70057 1244409, 1967.

17. Whiteley, T. E.; Perry, E. J. FR Patent 1444543, 1966.

18. Asakura, S.; Oosawa, F., *J. Polym. Sci.* **1958,** *33* (126), 183-192.

19. Liang, W.; Tadros, T. F.; Luckham, P. F., *Langmuir* **1994,** *10* (2), 441-6.

20. Chu, H.-H.; Hsu, X.-C., *J. Appl. Polym. Sci.* **1994,** *51* (9), 1653-1658.

21. Feigin, R. I.; Napper, D. H., *J. Colloid Interf. Sci.* **1980,** *74* (2), 567-571.

22. Feigin, R. I.; Napper, D. H., *J. Colloid Interf. Sci.* **1980,** *75* (2), 525-541.

23. Lekkerkerker, H. N. W.; Widom, B., *Physica A* **2000,** *285* (3-4), 483-492.

24. Mao, Y.; Cates, M. E.; Lekkerkerker, H. N. W., *Physica A* **1995,** *222* (1-4), 10-24.

25. Mao, Y.; Cates, M. E.; Lekkerkerker, H. N. W., *Phys. Rev. Lett.* **1995,** *75*, 4548.

26. Winter, H., *J. Phys. Condens. Matter* **1996,** *8* (49), 10149-10183.

27. Hatlo, M. M.; Lue, L., *Soft Matter* **2008,** *4* (8), 1582-1596.

28. Klein, R.; Von Grunberg, H. H., *Pure Appl. Chem.* **2001,** *73* (11), 1705-

1719.

29. Banchio, A. J.; Gapinski, J.; Patkowski, A.; Häußler, W.; Fluerasu, A.; Sacanna, S.; Holmqvist, P.; Meier, G.; Lettinga, M. P.; Nägele, G., *Phys. Rev. Lett.* **2006,** *96*, 138303.

30. Denton, A. R., *Phys. Rev. E* **2007,** *76* (5-1), 051401/1-051401/11.

31. Denton, A. R., *J. Phys. Condens. Matter* **2008,** *20* (49), 494230/1-494230/8.

32. Jackson, J. D., *Classical Electrodynamics*. Third ed.; John Wiley & Sons, Inc.: 1999.

33. von Grunberg, H. H.; Helden, L.; Leiderer, P.; Bechinger, C., *J. Chem. Phys.* **2001,** *114* (22), 10094-10104.

34. Leunissen, M. E.; van Blaaderen, A.; Hollingsworth, A. D.; Sullivan, M. T.; Chaikin, P. M., *P. Natl. Acad. Sci. U.S.A.* **2007,** *104* (8), 2585-2590.

35. Wei, W.; Yang, Z., *Adv. Mater.* **2008,** *20* (15), 2965-2969.

36. Duran, J. D. G.; Arias, J. L.; Gallardo, V.; Delgado, A. V., *J. Pharm. Sci.* **2008,** *97* (8), 2948-2983.

37. Freemont, T. J.; Saunders, B. R., *Soft Matter* **2008,** *4* (5), 919-924.

38. Stebe, K. J.; Lewandowski, E.; Ghosh, M., *Science* **2009,** *325* (5937), 159-160.

39. Pileni, M. P., *Cryst. Res. Technol.* **1998,** *33* (7-8), 1155-1186.

40. Yodh, A. G.; Zimmerli, G. *Entropically driven self-assembly of colloidal crystals on templates in space*; University of Pennsylvania, Philadelphia, PA, U.S.: 2002; 1-16.

41. van Dillen, T.; van Blaaderen, A.; Polman, A., *Mater. Today* **2004,** *7* (7-8), 40-46.

42. Velev, P. O. D., Assembly of Electrically Functional Microstructures from Colloidal Particles. In *Colloids and Colloid Assemblies*, Prof. Frank, C., Ed. Wiley-VCH: 2004; 437-464.

43. Bonderer, L. J.; Studart, A. R.; Gauckler, L. J., *Science* **2008,** *319* (5866), 1069-1073.

44. Balmer, J. A.; Schmid, A.; Armes, S. P., *J. Mater. Chem.* **2008,** *18* (47), 5722-5730.

45. Guyot, A.; Landfester, K.; Joseph Schork, F.; Wang, C., *Prog. Polym. Sci.* **2007,** *32* (12), 1439-1461.

46. Alexandre, M.; Dubois, P., *Mater. Sci. Eng.* **2000,** *28* (1-2), 1-63.

47. Xue, Z.; Wiese, H. US Patent 7094830, 2003.

48. Bauer, F.; Flyunt, R.; Czihal, K.; Buchmeiser, M. R.; Langguth, H.; Mehnert, R., *Macromol. Mater. Eng.* **2006,** *291* (5), 493-498.

49. Tiarks, F.; Leuninger, J.; Wagner, O.; Jahns, E.; Wiese, H., *Surf. Coat. Int.* **2007,** *90* (5), 221-229.

50. Porter, D.; Metcalfe, E.; Thomas, M. J. K., *Fire Mater.* **2000,** *24* (1), 45-52.

51. Wang, T.; Colver, P. J.; Bon, S. A. F.; Keddie, J. L., *Soft Matter* **2009,** *5* (20), 3842-3849.

52. Teixeira, R. F. A.; Bon, S. A. F., *Adv. Polym. Sci.* **2010,** *ASAP*.

53. Ramsden, W., *Proc. R. Soc. London, Sect. A* **1903,** *72*, 156-164.

54. Pickering, S. U., *J. Chem. Soc. Trans.* **1907,** *91*, 2001-2021.

55. Finkle, P.; Draper, H. D.; Hildebrand, J. H., *J. Am. Chem. Soc.* **1923,** *45*, 2780-8.

56. Wiley, R. M., *J. Coll. Sci. Imp. U. Tok.* **1954,** *9*, 427-37.

57. Pieranski, P., *Phys. Rev. Lett.* **1980,** *45* (7), 569-72.

58. Clint, J. H.; Taylor, S. E., *Colloid Surface* **1992,** *65* (1), 61-67.

59. Binks, B. P.; Clint, J. H., *Langmuir* **2002,** *18* (4), 1270-1273.

60. Binks, B. P., *Curr. Opin. Colloid In.* **2002,** *7* (1,2), 21-41.

61. Xu, H.; Melle, S.; Golemanov, K.; Fuller, G., *Langmuir* **2005,** *21* (22), 10016-20.

62. Levine, S.; Bowen, B. D.; Partridge, S. J., *Colloid Surface* **1989,** *38* (2), 325-343.

63. Hogg, R.; Healy, T. W.; Fuerstenau, D. W., *Trans. Faraday Soc.* **1966,** *62* (6), 1638-51.

64. Schott, H., *J. Pharm. Sci.* **1976,** *65* (6), 855-861.

65. Tamai, H.; Hamada, A.; Suzawa, T., *J. Colloid Interf. Sci.* **1982,** *88* (2), 378-84.

66. Tohver, V.; Smay, J. E.; Braem, A.; Braun, P. V.; Lewis, J. A., *P. Natl. Acad. Sci. U.S.A.* **2001,** *98* (16), 8950-8954.

67. Liu, J.; Luijten, E., *Phys. Rev. Lett.* **2004,** *93*, 247802.

68. Karanikas, S.; Louis, A. A., *Phys. Rev. Lett.* **2004,** *93*, 248303.

69. Liu, J.; Luijten, E., *Phys. Rev. E* **2005,** *72*, 061401.

70. Hong, X.; Willing, G. A., *Langmuir* **2009,** *25* (9), 4929-4933.

71. Karimian, H.; Babaluo, A. A., *J. Eur. Ceram. Soc.* **2006,** *27* (1), 19-25.

72. Rhodes, S. K.; Lewis, J. A., *J. Am. Ceram. Soc.* **2006,** *89* (6), 1840-1846.

Chapter II.

Laponite clay – poly(vinyl esters) latexes prepared *via* miniemulsion polymerisation

This chapter extends the use of Laponite clay discs as solid-stabiliser in Pickering miniemulsion polymerisation. Previous work on armoured latex particles of polystyrene and various hydrophobic (meth)acrylates were made upon solidification by polymerisation of the monomer droplets stabilised with Laponite clay platelets and particle size distribution was controlled by the amount of stabilisers. In our case, special consideration was given to the synthesis of clay – poly(vinyl esters) latexes, specifically using vinyl acetate and vinyl laurate. Limitations and drawbacks in preparing poly(vinyl esters) latexes in a miniemulsion process and using clay platelets as solid-stabiliser are addressed.

II.1. Introduction

Solids-stabilised emulsions and assembly of supracolloidal arrays recently gained considerable commercial interest in important applications such as the food industry, cosmetics, and coatings. Over the last 10 years, Armes *et al*. have investigated several systems by inserting alcoholic silica sols in dispersion polymerisation processes.[1-5] Notably, they studied the case of polystyrene latexes and used different types of initiators (oil soluble, cationic) and reported the preparation of lightly cross-linked poly(4-vinyl pyridine)/silica nanocomposite particles as an interesting new class of pH-responsive particulate emulsifiers for oils of varying polarity at around neutral pH.[6] Lewis and co-workers described that a stable colloidal system of negligible charged silica spheres could be obtained upon addition of a critical volume fraction of highly charged nanoparticles of hydrous zirconia.[7] These nanoparticles did not adsorb onto the silica spheres, and the stabilisation mechanism was referred to as "haloing". The mechanisms of different types of colloidal interaction and pioneering works on their driven assemblies at liquid-liquid or solid-liquid interfaces are described in Chapter I, see section I.4.

In 1996, Velev *et al.* described the synthesis of hollow supracolloidal structures *via* assembly of polystyrene latex at the liquid-liquid interface of emulsion droplets.[8-9] The synthesis of selectively permeable capsules composed of colloidal particles was reported by Dinsmore *et al.,* who tentatively named these supracolloidal structures "colloidosomes".[10] Recently they also published a temperature – responsive system in which the colloidosomes composed of poly(*N*-isopropylacrylamide-*co*-acrylic acid) microgel particles were formed by self-assembly.[11] Paunov *et al.* have shown the preparation of colloidosomes with

a gelled aqueous core stabilised by a shell of agarose.[12-13] Magnetic Pickering emulsifiers were studied by Fuller *et al.*.[14] They demonstrated the ability to induce triggered macroscopic phase separation of solid-stabilised emulsions using paramagnetic particles at an oil/water interface upon application of external magnetic fields. Russel *et al.* reported on supracolloidal capsules of quantum dots using both radical and ring-opening metathesis polymerisation techniques to cross-link vinyl benzyl and norbornene functional quantum dots, respectively.[15-16] Most of those studies use particles with diameters in the range of submicron to few microns. The use of smaller solids-stabilisers, such as cadmium selenide nanoparticles, can direct nanoparticle assembly at liquid-liquid interfaces, the small particle size giving rise to an interfacial adsorption energy comparable to a few times the thermal energy.[17]

Our interest lies in the formation of supracolloidal structures by polymerising submicron monomer droplets which have solid particles adhered to their interface *via* a miniemulsion polymerisation process. Early pioneering works were undertaken by Hohenstein *et al.* in 1946 describing the polymerisation of olefins and diolefins notably in suspension polymerisation in which some experiments used solid particles as stabiliser.[18-19] Our group demonstrated the utility of the building blocks assembly at liquid-liquid interfaces for the formation of reactor vessels and their buckling behaviour of giant droplets upon evaporation of its content.[20] We further developed this strategy to prepare for the first time polymer latexes with a Pickering miniemulsion polymerisation process.[21] Armoured latex particles of polystyrene and various hydrophobic (meth)acrylates were made upon solidification by polymerisation of the monomer droplets stabilised with Laponite clay platelets.

Laponite RD is a synthetic trioctahedric hectorite clay, composed of two tetrahedral silica sheets and a central octahedral magnesia sheet with a density of 2.570 g cm^{-3} and a general chemical formula which can be written as follows: $[Si_8(Mg_{5.45}Li_{0.4})O_{20}(OH)_4]Na_{0.7}$. The overall negative charge accompanied with the positive charges located between the silica sheets, and therefore at the rim of the disc, confer to those particles unique and very complex colloidal properties. Stable dispersions at high pH showed different types of gel structures by X-ray scattering measurements[22] and the mechanisms of swelling and dispersion of several clays into individual particles has been described.[23-24] The addition of salt reduces the critical flocculation concentration at which gels are formed which is opposite to the behaviour of spherical particles acting as isotropic liquids upon compression of the double layer. At low ionic strength, an unconnected face-face alignment of clay discs is suggested responding to dominating electrostatic repulsions, whereas at higher ionic strength, the so-called "house-of-card"[25] structure was observed. Although, recent simulations suggested the configuration of "overlapping-coins" to be the most favourable.[26] Amongst various investigations, atomic force microscopy experiments lately addressed the dispersity of the particle size and revealed its disc-liked shape to be about 25 to 35 nm in diameter with thickness of *ca.* 1 nm.[27] Those dimensions are of suitable order for the stabilisation of droplets of submicron sizes as confirmed by previous group work on Pickering miniemulsion polymerisations using nanosized Laponite clay discs as stabiliser.[21]

Ashby and Binks reported a systematic study on the stability of oil-in-water emulsion droplets using Laponite RD as Pickering stabiliser for different concentrations in salt.[28] They only observed the formation of stable emulsions of

toluene, water and Laponite RD clay particles under the conditions where the clay are flocculated, for concentrations in sodium chloride not lower than 0.1 M, and at intermediate concentrations in particles, that is to say 1.0 to 3.5 wt%. At higher clay content, shearing difficulties were encountered caused by the high viscosity of the dispersion. No phase inversion was observed for variety of oil and polar oils and even at high oil volume fraction due to the hydrophilic nature of Laponite RD clay.[21] The average droplet size was found to be strongly affected by the oil volume fraction but did not depend on the clay concentration. Binks also observed a limited Ostwald-ripening effect and suggested a mechanism for which the droplet interface is quickly fully-covered by the clay, hence inhibiting further oil diffusion. Stability of the system is provided not only from the suggested Pickering stabilisation of the liquid-liquid interface but also from the network or moderately viscous gel formed by the Laponite discs in the aqueous medium. Those clay particles were already integrated in polymerisation processes in late 50's, as published by Wiley in two patents. One patent describes the use of clay as thickener for suspension polymerisation and the other one is on quiescent suspension polymerisation including the use of colloidal particles as stabiliser.[29-30] Combination of two types of clay in an emulsion polymerisation process also stabilised by anionic surfactant showed enhancement of the colloidal stability of the final latexes for which Choi *et al.* suggested an ensemble of potential factors.[31-32] Stability would be achieved not only from the electrostatic repulsive charges between the clay particles and the anionic surfactant or from their adsorption onto the latex spheres acting like steric barriers, but also by creating barriers when forming layers within the continuous aqueous phase and increasing the viscosity thereby reducing the

latex particles mobility and lowering the impact and the probability of collisions between them.

Solids-stabilisers were employed successfully in (mini)emulsion polymerisation processes, but always in presence of other surfactants and/or co-monomers.[32-33] The use of nanosized clay particles in absence of molecular surfactants allowed successful stabilisation of styrene miniemulsion droplets.[21] A mechanistic approach described the Pickering miniemulsion polymerisation kinetics of styrene, as well as the extension to a series of hydrophobic monomers.[34] The average particle size distributions of the latexes could be tailored with the concentrations in monomer and synthetic clay used. A semi-empirical model based on the hypothetical equilibrium of Laponite clay discs distributed between the aqueous phase (excess) and onto the latex surfaces (Pickering stabiliser) allowed prediction of the latex particle sizes. Recent work on the preparation of ‘‘soft–hard’’ poly(lauryl acrylate) – Laponite hybrid particles made *via* Pickering miniemulsion polymerisation led to marked mechanical property enhancements when these nanocomposite supracolloidal particles were blended at various low concentrations with a standard poly(butyl acrylate-co-acrylic acid) latex for application as a waterborne pressure-sensitive adhesive.[35]

In this chapter, the development of Laponite clay-stabilised poly(vinyl esters) latexes of submicron sizes *via* miniemulsion polymerisation was investigated. Limitations of this process are addressed to meet up with industrial requirements, *i.e.* latexes with high overall solids contents and “pH-friendly”, giving special consideration to the sensitivity of the monomer/polymer to undergo hydrolysis.

II.2. Experimental

II.2.1. Materials

Vinyl acetate and vinyl laurate monomers were purchased from Aldrich at purities ≥ 99.0% and 98.0%, respectively and, unless specified, were used as received. The hydrophobe *n*-Hexadecane was purchased from Aldrich and sodium chloride was purchased from BDH, both at reagent grade purity. The clay used was Laponite RD and was kindly donated by Rockwood Additives Ltd. V-65 initiator (2,2'-azobis(2,4-dimethyl valeronitrile)) was kindly donated by Wako Specialty Chemicals and AIBN initiator (2,2′-azobis(2-methylpropionitrile)) was purchased from VWR International, both used as supplied. Oil soluble dye (2,4-dihydroxy-4'-nitroazobenzol) was purchased from Aldrich. NaCl (Laboratory reagent grade, Fisher Scientific) and deionised water purged by nitrogen. Dialysis tubing cellulose membranes (33 mm flat diameter), purchased from Aldrich, were washed for few minutes under running water. Ammonia was purchased from Fisher at S.G. 0.88 (35%) concentration in water. Silicon wafers (used as sample holders for characterisations by scanning electron microscopy (SEM)) were kindly donated by Wacker Chemie AG.

II.2.2. Equipment

The monomer miniemulsion was formed in an aqueous clay dispersion using a high shear force created by an Ultra-Sonic probe, Branson 450 W digital sonifier at 70% amplitude, after being mixed using an IKA WERKA, Ultra Turrax, T25 basic set at 24000 rpm. Monomer conversions were checked by ^{1}H NMR analyses on a Bruker AC400 in deuterated chloroform. Particle size distributions were performed by dynamic light scattering on a Malvern

Instruments Zetasizer 3000HSa. The pH of the dispersions was recorded using a Knick pH meter 765 Calimetic and Labworldsoft, laboratory software IKA, for online measurements. Viscosities were measured on a Brookfield Model DV-II+ viscometer equipped with a LV1, LV2 or LV3 spindle. Scanning electron microscopy was performed on a ZEISS supra 55VP FEGSEM.

II.2.3. Laponite stabilised poly(vinyl laurate) latexes in miniemulsion polymerisation

Laponite RD (1.0 g, 10 wt% based on monomer) was added to deoxygenated H_2O (100.0 g) and sonicated for 4.5 min at 70% amplitude with a 30 s pause every minute. While the sonication had started, NaCl (0.57 g, 0.1 M) was added to the aqueous phase. The oil phase containing vinyl laurate (10.0 g, 9.3% solids), *n*-hexadecane (0.4 g, 4 wt%) and V-65 (2,2'-azobis(2,4-dimethyl valeronitrile)) (0.05 g, 0.5 wt%) was poured into the Laponite RD dispersion. The two phases were mixed using an Ultra Turrax for 2 min. The resulting suspension was sonicated for 6.5 min at 70% amplitude with a 30 s pause every minute in an ice bath to prevent early polymerisation. The formed miniemulsion was bubbled through with N_2 for 20 min minimum in a round-bottomed flask. The latex was collected after overnight polymerisation under N_2, heating at 51 ºC (10 hour half-life temperature) and gentle stirring. Monomer conversions, X_m, were determined by ^{1}H NMR spectroscopy. The analysis of a ^{1}H NMR spectrum is given as an example in Appendix B, section B.1. All latexes were dialysed against deionised water with modified pH (9-10) by addition of ammonia. Formulation of all the samples and their average particle diameter, d_z, and dispersity index, D_I, determined by dynamic light scattering of the dialysed samples can be found in Table II-1. Exact masses of reagents are reported in

Table B.2 (Appendix B, section B.2). Note that when using AIBN initiator, polymerisation reactions were conducted at 65 ºC, the 10 hour half-life temperature of AIBN.

Table II-1. Overall clay and oil contents, final monomer conversions X_m, hydrodynamic diameters d_z and dispersity indices D_I of the different clay-stabilised poly(vinyl laurate) latexes prepared in miniemulsion polymerisation.

Experiment	***Overall clay content/ wt%***	***Overall oil content/ wt%***	***X_m/ %***	***d_z/ nm***	***D_I/ -***
CC-1-123	0.89	9.30	91	266.7	0.15
CC-1-124	0.88	9.25	89	268.1	0.16
CC-1-047	0.44	9.14	93	393.4	0.24
CC-1-048	0.67	9.31	93	296.3	0.18
CC-1-043	0.89	9.32	92	297.0	0.21
CC-1-049	1.11	9.29	92	242.1	0.14
CC-1-050	1.33	9.29	93	239.0	0.15
CC-1-107	0.63	9.23	88	313.5	0.18
CC-1-108	0.89	9.27	87	281.7	0.19
CC-1-109	1.23	9.18	85	270.1	0.21
CC-1-110	1.49	9.16	83	235.3	0.15
CC-1-193A	0.45	9.37	94	453.5	0.32
CC-1-194A	0.67	9.37	94	329.6	0.27
CC-1-196A	1.00	9.35	94	243.7	0.13
CC-1-197A	1.33	9.29	96	238.3	0.12
CC-1-198	0	9.29	89	271.4	0.16

II.3. Results and discussion

The preparation of solids-stabilised poly(vinyl esters) latexes with synthetic Laponite clay was investigated using a miniemulsion polymerisation process. Three successive experimental steps were undertaken. Firstly, the dispersion of the Laponite clay particles in the aqueous phase was prepared by ultrasonication (step (1)). Then, the formation of oil-in-water miniemulsion droplets was obtained by pre-emulsifying and sonicating the hydrophobic phase, a mixture of monomer, oil soluble initiator and hydrophobe, into the clay dispersion using an homogeniser (Ultra-Turrax) and a sonifier (Ultra-Sonic probe), as represented in Figure II-1 (step (2)). Finally, polymer latex particles were formed by solidifying the miniemulsion monomer droplets upon thermal polymerisation (step (3)). Flocculation of the Laponite clay discs,[25-26] necessary to induce their stabilising effect on the monomer miniemulsion droplets,[28, 34] was provoked by adding salt in step (1).

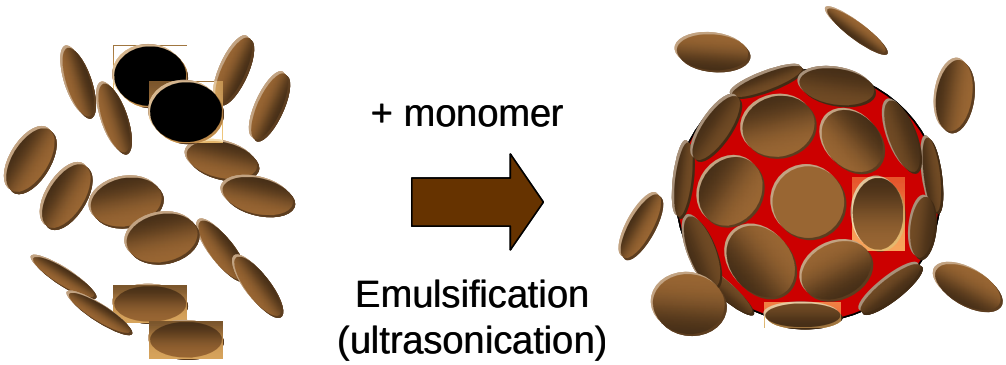

Figure II-1. Cartoon of the formation of armoured oil-in-water miniemulsion droplets of monomer using clay platelets as stabiliser (step (2)).

II.3.1. Experimental restrictions in alkaline conditions: Case of vinyl acetate monomer

Schork *et al.* already discussed the synthesis of poly(vinyl acetate) latexes *via* miniemulsion polymerisation in terms of robust nucleation, limited role of monomer diffusion, and higher shear stability compared to macroemulsion polymerisation.[36] However, in our experiments we used this process in presence of dispersed Laponite clay particles which imposed a high value of pH due to their structural nature.[25-26] Particular attention is therefore given to the preparation of vinyl acetate miniemulsions due to its sensitivity to hydrolyse.[37-38] The degradation of vinyl acetate monomer in alkaline medium produces acetic acid (pK_a = 4.75) and acetaldehyde (see Figure B-4, Appendix B) and was followed by performing pH measurements. The pH of *ca.* 10 wt% vinyl acetate, containing 4 wt% hexadecane (based on monomer) in 1.0 wt% clay dispersion was recorded to drop from about 9.5 to 7.5 during the ultrasonication process (step 2). (See Appendix B, section B.4 for details on pH measurements.)

For this reason no stable miniemulsion of vinyl acetate monomer could be obtained using Laponite clay nanoparticles as stabiliser. After conducting this work, Jung *et al.*[39] reported in 2007 the successful synthesis of poly(vinyl acetate) – montmorillonite (clay) nanocomposite microspheres by low-temperature suspension polymerisation at a 1 wt% concentration in clay treated with cationic surfactant. However, they underlined the limitation of the process by also a marked increased in the hydrolysis rate of vinyl acetate or in the saponification rate of the polymer using 1, 2 and 5 wt% clay dispersions.

The miniemulsion polymerisation process using Laponite clay nanoparticles as stabiliser was then investigated using vinyl laurate monomer (VL). Bearing

an eleven carbon alkyl side chain increasing its hydrophobicity, this monomer has a lower water solubility (< 0.001 g L^{-1} at 20 ºC) than vinyl acetate (23 g L^{-1} 20 ºC),[a] and is therefore less prone to hydrolyse when emulsified in alkaline aqueous phase.

II.3.2. Poly(vinyl laurate)/clay latexes

A series of poly(vinyl laurate)/clay latexes was prepared in miniemulsion polymerisation following the three steps previously described. Stable low glass transition latexes (~ 10 wt% solids content) were obtained using 0.4 to 1.5 overall wt% of Laponite clay platelets. The amounts of water, sodium chloride salt, monomer, *n*-hexadencane and initiator were kept constant (that is to say 100.0 g, 0.57 g, 10.0 g, 0.4 g and 0.05 g, respectively or halved batches), see Table II-1 in the experimental part for overall weight contents and Table B.2 and B.3 (Appendix B) for all quantities. The role of *n*-hexadecane (hydrophobe) was to limit the diffusion of monomer between droplets, also called Ostwald-ripening. When a hydrophobe is used in conjunction with the monomer, broadening of the particle size distribution is thereby minimised. In our case, *n*-hexadence is approx. 10^3 less soluble in water than vinyl laurate monomer.[b]

II.3.2.1. Thermal and shear stability

Stability/coalescence of the miniemulsion droplets of vinyl laurate monomer formed in presence of Laponite clay particles in step (2) was investigated macroscopically. An oil soluble dye (2,4-dihydroxy-4'-nitroazobenzol) was used

[a] Values provided by the supplier Wacker Chemie AG

[b] Water solubilities from supplier: <0.001 g L^{-1} for vinyl laurate at 20 ºC and 0.0009 mg L^{-1} for hexadecane at 25 ºC.

to facilitate the observation of the partial phase separation of the oil (monomer) emulsified in water. Samples with overall contents of *ca.* 10 wt% vinyl laurate, 4 wt% hexadecane (based on VL monomer) and 1 wt% clay in aqueous dispersion were typically used.

No ripening of the miniemulsion droplets was observed macroscopically for temperatures up to 90 ºC over 24 hours. This demonstrates successful limitation of monomer diffusion, known as Ostwald ripening effect, and a sufficient barrier towards flocculation and coalescence of the miniemulsion droplets. V-65 and AIBN initiators were both used at their corresponding 10 hour half-life temperature of 51 ºC and 65 ºC, respectively, and we considered this had no effect on the particle size distribution of the prepared latexes.

Although Schork *et al.* demonstrated by dynamic light scattering measurements that miniemulsions are more shear stable than similar macroemulsions,[36] we found that droplet coalescence still occurred overtime in our experiments. Increased shear instability of vinyl laurate miniemulsions was observed for higher shear fields (magnetic stirring). As droplets bump into each other with higher kinetic energy, it was logical to monitor faster coalescence. Shear field (stirring speed) was adjusted to minimise coalescence only ensuring homogeneity of the reaction mixture.

II.3.2.2. Investigation of potential aqueous phase events

Less monodisperse latexes with dispersity indices between 0.12 and 0.32 were obtained. This could be attributed to several phenomena. Coalescence of the monomer miniemulsion droplets can lead to higher dispersity of the resulting latex. However, it is known that narrow dispersities can be achieved by taking advantage of the limited coalescence phenomenon occurring in solids-stabilised

systems of emulsion droplets.[40-42] As discussed in the previous paragraph, shear coalescence of the droplets was observed but minimised by adjusting the stirring speed of the miniemulsion. Another phenomenon to be avoided is the formation of new particles throughout the polymerisation process by secondary nucleation. The importance of potential aqueous phase events during the radical polymerisation has been studied in our system by adding a water soluble radical scavenger, sodium nitrite ($NaNO_2$). Laponite clay stabilised – monomer miniemulsion droplets were prepared in a batch of 9.3 wt% overall monomer and 9.6 wt% of clay platelets, based on monomer. This miniemulsion was split into two parts (entries CC-1-123 and CC-1-124 in Table II-1 and B.2 in Appendix B). Based on the water phase, 73 mM of $NaNO_2$ was added to one of the sample (CC-1-124) prior heating/polymerising the monomer droplets. Sampling was performed throughout the polymerisation process to follow monomer conversion measured by ^1H NMR spectroscopy and final particle size distribution analysed by dynamic light scattering. No distinctive difference between the two samples was found; see Figure II-2 and Table II-1.

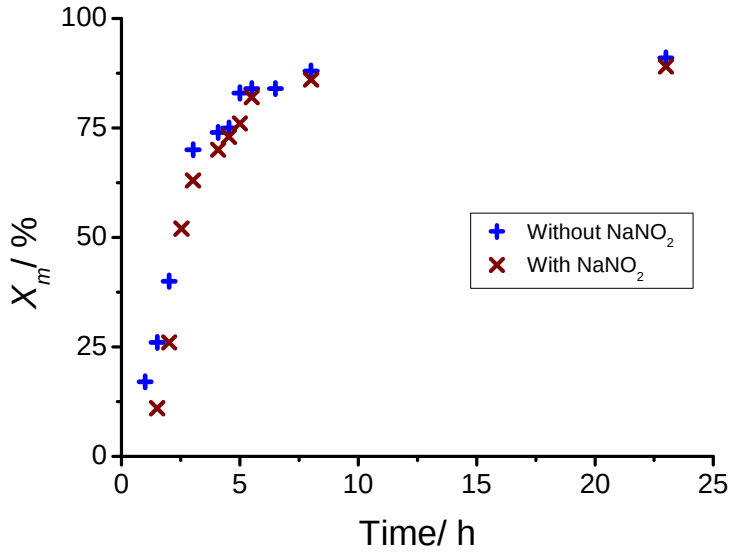

Figure II-2. Monomer conversion followed by ^{1}H NMR spectroscopy in the presence of a water soluble scavenger ([×], CC-1-124) and without ([+], CC-1-123).

This corroborates with the fact that the water solubility of vinyl laurate monomer is really low, thereby minimising the potentiality of having aqueous phase events. This is also in line with previous work in our group where the preference of using an oil soluble initiator rather than water soluble was already underlined and suggested that the clay particles at the interface could complicate radical entry and exit events when using a water soluble initiator.[21]

II.3.2.3. Effect of the concentration in Laponite clay on the latex particle size

By varying the amount of Laponite clay particles, we investigated its stabilising effect on the size of the monomer miniemulsion droplets, hence the size of the polymer latex particles obtained. As previously reported by our group for the synthesis of Laponite-stabilised polystyrene latexes, smaller latex particles were obtained when using Laponite clay dispersions of higher solids content. This resulted from the partitioning of the clay discs between the aqueous phase and the monomer miniemulsion droplet interface. We also

observed that the droplet/latex particle size was inversely proportional to the viscosity of the flocculated (*via* salt) clay dispersions which increased linearly with their solids content, see Appendix B (section B.4.1). However, if related, this was opposite to the trend observed in other systems. Higher viscosities of the continuous phase are known to stabilise larger droplets. For instance Snabre and Magnifotcham reported in 1998 on the formation and rise of bubble stream in a viscous liquid.[43] They observed that in intermediate and high flow rate regime, surface tension forces are negligible and either viscous or inertia forces determined the bubble size. We could postulate that in our system the viscosity was negligible during the sonication process but became effective once the sonication probe was stopped, thereby bringing a stabilisation effect to the system.

The average diameters of all clay-stabilised poly(vinyl laurate) latexes were measured by dynamic light scattering (see Table II-1) and are plotted (excepted last entry) as a function of the amounts of clay platelets in the water phase in Figure II-3.

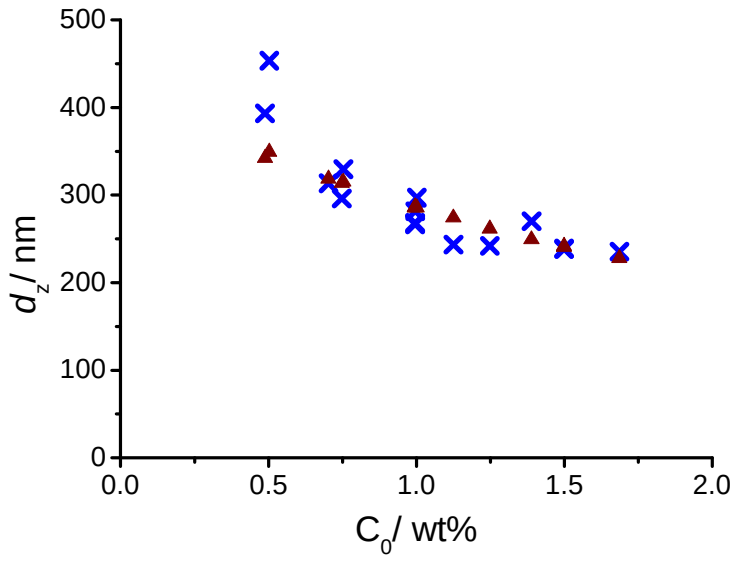

Figure II-3. Graph of the hydrodynamic average diameter d_z of the clay-stabilised poly(vinyl laurate) latexes versus the overall amount of clay platelets [×] (and calculated values from the fitted model [▲], see Figure II-4).

Antonietti *et al.*[44] and Wu[45-46] discussed simple models to predict the size of spherical microemulsions whereby monomer cores were surrounded by surfactant molecules. Analogous to these, Bon and Colver developed a basic semi-empirical model to predict the average particle size of Pickering stabilised latexes. It correlates the average particle size with the amounts of clay, defining the excess of clay particles in the aqueous phase, C_{excess}, expressed as a function of the initial concentration of clay in the water phase, $C_{excess} = f(C_0)$.[34]

They demonstrated *via* series of miniemulsion polymerisations that average particle size was controlled and could be predicted. The built-up model implied several assumptions as follows: uniform clay and miniemulsion monomer droplet sizes, 2-D square packing and full coverage of the clay discs on the monomer droplets, and building blocks of negligible sizes compared to the size of the colloidosomes, therefore the Laponite clay discs interact on a flat surface. The average diameter was measured by DLS and the excess in particles (m_{excess})

was calculated with the following equations (for details report on Appendix B, section B.4.2):

$$m_{excess} = m_0 - \frac{3}{2}\pi \left(\frac{\rho_{part}}{\rho_{oil}}\right)\left(\frac{h_{part}}{d_{oil}}\right) m_{oil} \qquad \textbf{Equation II-1}$$

$$C_{excess} = \frac{m_{excess}}{m_{water}} \qquad \textbf{Equation II-2}$$

$$C_0 = \frac{m_0}{m_{water}} \qquad \textbf{Equation II-3}$$

Where m_0 is the amount of Laponite clay, ρ_{part} and ρ_{oil} are the densities of the Laponite clay particles and the "oil-polymer" phase, respectively. d_{oil} is the average diameter of the solids-stabilised droplets determined by DLS measurements, h_{part} corresponds to the thickness of the Laponite clay discs and finally m_{oil} and m_{water} are the amounts of monomer and water in the latex, respectively.

By plotting C_0 versus C_{excess} previously defined (Equations II-2 and II-3), a linear trend is obtained (Figure II-4) for the series of experiments (see Table II-1, and Tables B-2 and B-3 in Appendix B, last entry excluded). Linear trends of the clay-stabilised polystyrene latexes reported by Bon and Colver[34] are also displayed for comparison (using 4 and 8 wt% hexadecane, dashed and dotted lines, respectively).

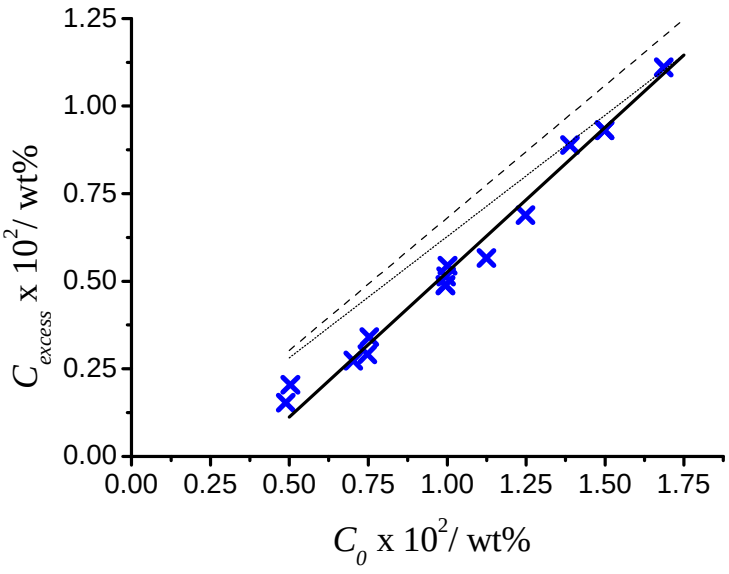

Figure II-4. The calculated excess concentration of Laponite clay discs supposedly remaining in the aqueous phase, C_{excess}, versus the initial overall concentration in clay particles in water, C_0, for the clay-stabilised poly(vinyl laurate) latexes. (———) is the corresponding linear fit of equation C_{excess} = (1-0.1741) C_0 – 0.0030. For comparison, (- - - -) and (·····) were the linear fits found by Bon and Colver in the case of clay-stabilised polystyrene latexes of equations C_{excess} = (1-0.2438) C_0 – 0.0008 and C_{excess} = (1-0.3076) C_0 – 0.0006, using 4 and 8 wt% of hexadecane based on monomer, respectively.[34]

Although C_{excess} can be expressed as a first-order polynomial function $f(C_0)$, there is a noticeable increase in the slope in the case of poly(vinyl laurate) latexes compared to polystyrene latexes[34] (using 4 wt% hexadecane based on monomer in both cases). Being closer to unity, this revealed a different partitioning of the clay platelets between the aqueous phase and onto the surface of the latex particles. In comparison to the polystyrene composite system, a smaller influence of clay platelets on the size of the polymer latex particles was obtained for poly(vinyl laurate) latexes (in the range of *ca*. 200 to 450 nm in diameter). At concentrations of clay in the water phase, C_0, lower than 1.25 g g^{-1}, the shift of the linear fit of the clay-stabilised poly(vinyl laurate) latexes to smaller values of C_{excess} indicated the formation of smaller polymer particles

than in the case of solids-stabilised polystyrene latexes. We suggested that partial loss of the control on the particle size distribution occurred and this gave rise to the possible in situ formation of surfactant upon hydrolysis of monomer, see reaction scheme presented in Figure II-5. Although this was not detected by NMR spectroscopy of the dried films of the polymer latexes (see appendix B, section B-1), the occurrence of this unwanted reaction was indirectly verified by the preparation of poly(vinyl laurate) latexes using a miniemulsion polymerisation process in alkaline medium without addition of any stabiliser (clay, co-monomer or surfactant). The emulsification of vinyl laurate in water following the same procedure but without addition of sodium hydroxide did not lead to the formation of a stable miniemulsion. This proved the formation of stabilising species, *i.e.* sodium laurate surfactant, when emulsification of vinyl laurate monomer was conducted in basic aqueous medium.

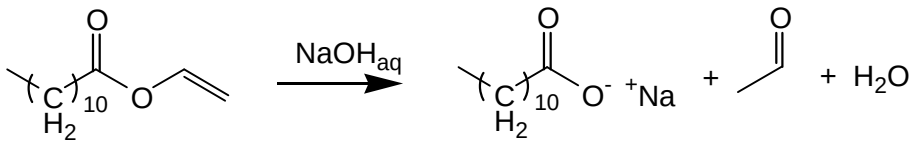

Figure II-5. Hydrolysis reaction scheme of vinyl laurate monomer in alkaline medium leading to the formation of sodium laurate and acetaldehyde.

Although the water solubility of vinyl laurate is very low, the high energy input *via* sonication and the high surface area created during the emulsification process are favourable factors for partial hydrolysis of the monomer in alkaline medium.

By stabilising the monomer – aqueous phase interface, the surfactant molecules prevent the Laponite clay particles from adhering to the interface to form colloidosomes, as represented in Figure II-6. The partitioning equilibrium

of the Laponite clay platelets is therefore shifted to the dispersed state rather than onto the water – monomer droplets interface. Surfactant molecules are less strongly bonded to the interface than solid particles, so that the previously mentioned phenomenon of limited coalescence in solids-stabilised emulsion systems might not apply anymore in this case. This could lead to more important ripening effects and could explain the resulting less monodisperse latexes with D_I ranging from 1.12 to 1.32 (see Table II-1).

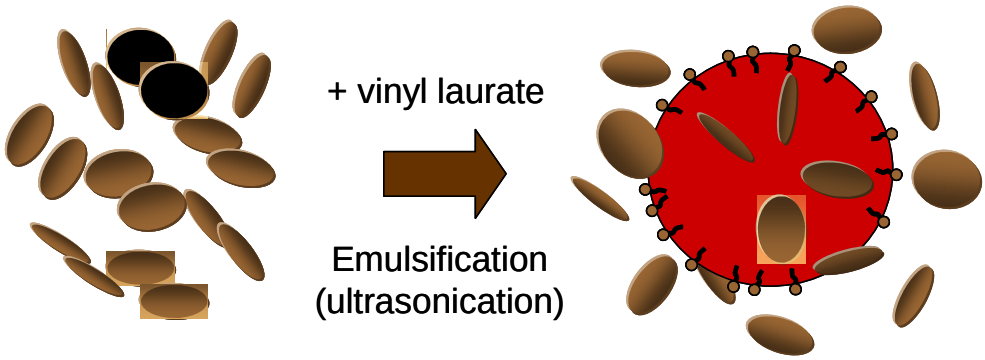

Figure II-6. Cartoon of the formation of miniemulsion droplets of vinyl laurate in the presence of clay platelets as stabiliser (step (2)).

II.4. Conclusions

In conclusion, stable poly(vinyl laurate) latexes were obtained *via* a miniemulsion polymerisation process in presence of flocculated Laponite clay particles. Control of the size of the polymer particles was poor which indicated limited or nonexistent adsorption of the Laponite clay onto the miniemulsion droplets of monomer. This was attributed to the in situ formation of surfactant sodium laurate displacing the portioning of the clay discs to the water phase. Poly(vinyl acetate) latexes could not be prepared using Laponite clay as stabiliser due to the important hydrolysis of the monomer during the emulsification process.

Laponite clay platelets are therefore not an ideal solid stabiliser to be used for the formation of armoured latex particles of the investigated poly(vinyl esters), and also displayed limited solids content which is unsuitable for industrial purposes as in this case high solids content latexes are targeted.

II.5. References

1. Barthet, C.; Hickey, A. J.; Cairns, D. B.; Armes, S. P., *Adv. Mater.* **1999,** *11* (5), 408-410.

2. Percy, M. J.; Barthet, C.; Lobb, J. C.; Khan, M. A.; Lascelles, S. F.; Vamvakaki, M.; Armes, S. P., *Langmuir* **2000,** *16* (17), 6913-6920.

3. Percy, M. J.; Armes, S. P., *Langmuir* **2002,** *18* (12), 4562-4565.

4. Han, M. G.; Armes, S. P., *Langmuir* **2003,** *19* (11), 4523-4526.

5. Schmid, A.; Fujii, S.; Armes, S. P., *Langmuir* **2005,** *21* (18), 8103-8105.

6. Fujii, S.; Read, E. S.; Binks, B. P.; Armes, S. P., *Adv. Mater.* **2005,** *17* (8), 1014-1018.

7. Tohver, V.; Smay, J. E.; Braem, A.; Braun, P. V.; Lewis, J. A., *P. Natl. Acad. Sci. USA* **2001,** *98* (16), 8950-8954.

8. Velev, O. D.; Furusawa, K.; Nagayama, K., *Langmuir* **1996,** *12* (10), 2374-84.

9. Velev, O. D.; Furusawa, K.; Nagayama, K., *Langmuir* **1996,** *12* (10), 2385-91.

10. Dinsmore, A. D.; Hsu, M. F.; Nikolaides, M. G.; Marquez, M.; Bausch, A. R.; Weitz, D. A., *Science* **2002,** *298* (5595), 1006-1009.

11. Dinsmore, A. D., *Langmuir* **2006**.

12. Noble, P. F.; Cayre, O. J.; Alargova, R. G.; Velev, O. D.; Paunov, V. N., *J. Am. Chem. Soc.* **2004,** *126* (26), 8092-8093.

13. Cayre, O. J.; Noble, P. F.; Paunov, V. N., *J Mater Chem* **2004,** *14* (22), 3351-3355.

14. Melle, S.; Lask, M.; Fuller, G. G., *Langmuir* **2005,** *21* (6), 2158-2162.

15. Lin, Y.; Skaff, H.; Boeker, A.; Dinsmore, A. D.; Emrick, T.; Russell, T. P., *J. Am. Chem. Soc.* **2003,** *125* (42), 12690-12691.

16. Skaff, H.; Lin, Y.; Tangirala, R.; Breitenkamp, K.; Boker, A.; Russell, T. P.; Emrick, T., *Adv. Mater.* **2005,** *17* (17), 2082-2086.

17. Lin, Y.; Skaff, H.; Emrick, T.; Dinsmore, A. D.; Russell, T. P., *Science* **2003,** *299* (5604), 226-229.

18. Hohenstein, W. P.; Mark, H., *J. Polym. Sci.* **1946,** *1*, 127-45.

19. Hohenstein, W. P.; Mark, H., *J. Polym. Sci.* **1946,** *1*, 549-80.

20. Colver, P. J.; Chen, T.; Bon, S. A. F., *Macromol. Symp.* **2006,** *245-246*, 34-41.

21. Cauvin, S.; Colver, P. J.; Bon, S. A. F., *Macromolecules* **2005,** *38* (19), 7887-7889.

22. Saunders, J. M.; Goodwin, J. W.; Richardson, R. M.; Vincent, B., *J. Phys. Chem. B* **1999,** *103* (43), 9211-9218.

23. Norrish, K., *Discuss. Faraday Soc.* **1954,** *18*, 120-134.

24. Mongondry, P.; Tassin, J. F.; Nicolai, T., *J. Colloid Interf. Sci.* **2005,** *283* (2), 397-405.

25. Van Olphen, H., *An Introduction to Clay Colloid Chemistry*. 2nd ed.; John Wiley & Sons: 1977.

26. Jo̎nsson, B.; Labbez, C.; Cabane, B., *Langmuir* **2008,** *24* (20), 11406-11413.

27. Balnois, E.; Durand-Vidal, S.; Levitz, P., *Langmuir* **2003,** *19* (17), 6633-6637.

28. Ashby, N. P.; Binks, B. P., *Phys. Chem. Chem. Phys.* **2000,** *2* (24), 5640-5646.

29. Wiley, R. M. U.S. Patent 2,886,559, 1959.

30. Wiley, R. M. U.S. Patent 2,932,629, 1960.

31. Choi, Y. S.; Wang, K. H.; Xu, M.; Chung, I. J., *Chem. Mater.* **2002,** *14* (7), 2936-2939.

32. Choi, Y. S.; Xu, M.; Chung, I. J., *Polymer* **2005,** *46* (2), 531-538.

33. Tiarks, F.; Landfester, K.; Antonietti, M., *Langmuir* **2001,** *17* (19), 5775-5780.

34. Bon, S. A. F.; Colver, P. J., *Langmuir* **2007,** *23* (16), 8316-8322.

35. Wang, T.; Colver, P. J.; Bon, S. A. F.; Keddie, J. L., *Soft Matter* **2009,** *5* (20), 3842-3849.

36. Schork, F. J.; Poehlein, G. W.; Wang, S.; Reimers, J.; Rodrigues, J.; Samer, C., *Colloid Surface A* **1999,** *153* (1-3), 39-45.

37. Rostovskii, E. N.; Ushakov, S. N.; Barinova, A. N., *Izv. Akad. Nauk SSSR, Ser. Khim.* **1958**, 59-63.

38. Fujii, K.; Ukida, J.; Matsumoto, M., *J. Polym. Sci.* **1963,** *1*, 687-91.

39. Jung, H. M.; Lee, E. M.; Ji, B. C.; Deng, Y.; Yun, J. D.; Yeum, J. H., *Colloid Polymer Sci.* **2007,** *285* (6), 705-710.

40. Arditty, S.; Whitby, C. P.; Binks, B. P.; Schmitt, V.; Leal-Calderon, F., *Eur. Phys. J. E* **2003,** *11* (3), 273-281.

41. Binks, B. P.; Clint, J. H., *Langmuir* **2002,** *18* (4), 1270-1273.

42. Destribats, M.; Schmitt, V. r.; Backov, R. n., *Langmuir* **2009,** *26* (3), 1734-1742.

43. Snabre, P.; Magnifotcham, F., *Eur. Phys. J. B* **1998,** *4* (3), 369-377.

44. Antonietti, M.; Bremser, W.; Mueschenborn, D.; Rosenauer, C.; Schupp, B.; Schmidt, M., *Macromolecules* **1991,** *24* (25), 6636-43.

45. Wu, C., *Macromolecules* **1994,** *27* (1), 298-9.

46. Wu, C.; Yan, C.-Y., *Macromolecules* **1994,** *27* (16), 4516-20.

Chapter III.

Solids-stabilised emulsion droplets for the preparation of silica-armoured polymer latexes[a]

In this chapter, we used silica nanoparticles instead of surfactant molecules to stabilise liquid-liquid interfaces for the synthesis of oil-in-water or water-in-oil emulsions. We developed this strategy to prepare armoured polymer latexes of micron- and submicron-sizes using free radical suspension and miniemulsion polymerisation processes and investigated the preparation of high solids content hybrid polymer latexes. Dimensions of the building blocks were found to have an influence on the average particle size of the prepared latexes and we also studied their packing patterns on the latex particles.

[a] Part of this work was published

1. Fortuna, S.; Colard, C. A. L.; Troisi, A.; Bon, S. A. F., *Langmuir* **2009,** *25* (21), 12399-12403.

III.1. Introduction

Silica particles, such as colloidal silica or fumed silica, can adhere to oil – water interfaces and stabilise emulsion droplets against coalescence.[2-8] Surface chemistry of these colloids is controlled to obtain partial wetting of the two liquid phases. Since silica particles have hydroxyl groups on their surface, their surface charge density and electrical double layer thickness are greatly sensitive to the pH and the ionic strength of the phase in which they are dispersed. The lyophilicity of the inorganic SiO_2 particles and thus their wettability characteristics with the dispersion medium and the dispersed phase can be tuned. The properties of the media can be changed upon addition of salt for instance or alternatively the colloidal surface can be modified with a variety of reagents. For example, exposure of silica particles to organo-silanes with functional groups, such as octyltrimethoxysilane, gives the particles a more hydrophobic character.[9-10]

Fine-tuning of the lyophilicity of the particles will not only determine its efficiency to stabilise emulsion droplets but will also dictate the type of emulsion formed, oil-in-water (o/w) or water-in-oil (w/o). The *Bancroft rule* states that "the phase in which a molecular emulsifier is more soluble constitutes the continuous phase."[11] However, the preparation process can also determine the type of emulsion; some *anti-Bancroft* systems and catastrophic phase inversions have also been reported in the literature.[4-5, 8, 12-14] Avoiding additional chemical modification of the surface, bare silica particles have been employed as solid stabiliser. However, inefficient stabilisation of o/w emulsions has often been improved upon addition of co-stabiliser, such as surfactant or polymer.[15-20] Hassander *et al.* reported on the stabilisation mechanism of highly stable

paraffin oil emulsions using colloidal silica nanoparticles (Ludox) combined with a co-stabiliser, such as poly(vinylpyrrolidone) or cetyltrimethylammonium bromide (CTAB) surfactant.[15] They described the necessity of a two step mechanism involving (i) agglomeration of the silica particles induced by the co-stabiliser and (ii) adsorption of agglomerates of silica particles at the oil/water interface. Midmore developed this strategy for the preparation of high oil volume fraction (0.75) of Ludox stabilised o/w emulsions.[16] Using hydroxypropyl cellulose as co-stabiliser, reversible flocculation of the silica was obtained by varying the pH. Adsorption of co-stabiliser on the silica nanoparticles was controlled by the amount of silanol groups (thereby pH) present on the silica surface as electrostatic repulsion between particles was reduced and hydrogen bonding interactions increased.[21] Recently, Chevalier *et al.* reported the use of bare fumed silica nanoparticles for the preparation of stable o/w Pickering emulsions.[22] When employing vinyl monomers as oil, solids-stabilised latexes can be prepared upon free radical polymerisation of the o/w emulsion droplets. Early pioneering works were undertaken in the 40's and late 50's by Hohenstein *et al.* and Wiley who notably reported on the suspension polymerisation process using solid particles as stabiliser.[23-26] In 2001, Landfester *et al.* reported the synthesis of polymer/silica nanocomposites in a variety of structures and compositions by using a miniemulsion polymerisation process.[27] They reported a hedgehog morphology where the silica nanoparticles act as Pickering stabilisers, however, their surfactant free miniemulsion polymerisation process required the use of a basic co-monomer as a "coupler". In addition, they also investigated the influence of the addition of a cationic or anionic surfactant. The overall size of the particles was in the 100 nm region and controlled by the

amount of silica. Chen, J.-F. *et al.*[28] and Chen, M. and co-workers[29] reported on the preparation of polystyrene/nano-SiO_2 composite microspheres with a raspberry morphology *via* Pickering miniemulsion polymerisation.

The armoured structure of the polymer particles confers new properties to the materials such as tendency to deform and film-form the hybrid polymer particles for instance. The packing organisation of the nanoparticles is of practical importance in applications such as the film formation of armoured polymer latexes in waterborne coatings. The determination of the packing geometry of identical spheres or circles onto a spherical surface is often referred to as the Thomson problem,[30] generalised later by Tammes. In 3D close-packing of identical spheres in HCP or FCC lattices, 12 nearest neighbours of each sphere can be identified. This number, also known as the 3D Kissing number, is an exact solution of the Tammes problem. When we look at an isolated cluster of 13 spheres in such a lattice, it becomes apparent that each of the 12 spheres assembled onto the central one has 5 neighbours (excluding the central sphere). The deviation from having 6 nearest neighbours in a 2D hexagonal packing arrangement on a flat surface is a direct effect of the curvature of the surface. In every spherical system, 12 of these so-called defects must be present. When the central sphere becomes larger, more neighbours can be accommodated on its surface. Examples include a football or its chemical equivalent, a C_{60} buckyball,[31-32] which is composed of 12 pentagons and 20 hexagons. Bausch *et al.* investigated very large systems with the assembly of thousands of microspheres of identical size onto emulsion droplets.[33-34] They showed that the generic rule of 12 defects prevailed in the form of five- and seven-neighbour line defects, or grain boundary scars. Intriguing questions are the following:

What happens if we look at systems of intermediate size, or in other words, what would the packing organisation be when hundreds of particles are assembled onto a sphere? What would happen to the self-assembled equilibrium packing structure if our building blocks were not all the same size?

To try to answer these questions, we investigated the use of different grades of silica particles as solids-stabilisers for the preparation of oil-in-water and water-in-oil emulsions by tuning their surface properties. We studied the assembly of silica nanoparticles of various sizes on the liquid-liquid interfaces of small submicrometre-sized droplets of styrene prepared *via* miniemulsion polymerisation. Packing patterns of the single-armoured layer of spherical nanoparticles of silica (*i.e.* Ludox TM-40) on the surface of poly(styrene) latex particles was analysed and discussed in terms of the particle size dispersity of the silica nanoparticles. Emulsions with high fractions of the dispersed phase were achieved and limitations towards droplets coalescence were corroborated with our model relating generated interface (droplet size) and amounts in silica particles. Targeted high solids content polymer latexes were successfully prepared *via* miniemulsion and suspension polymerisation. It is noteworthy to mention that no surfactant, nor the use of auxiliary hydrophilic co-monomer such as (meth)acrylic acid, or ionic initiator is required. To the best of our knowledge this is the first time that armoured silica-polymer nanocomposite particles were made on such a large and convenient scale.

III.2. Experimental

III.2.1. Materials

All monomers were purchased from Aldrich or subsidiary companies at 96% or greater purities. All the monomers were used as received. *n*-Hexadecane and an aqueous solution of hydrochloric acid (0.1010 M or AnalaR grade, *i.e.* 32%) were purchased from Aldrich and sodium chloride was purchased from BDH, all at reagent grade purity. Grades of Ludox ® colloidal silica sols (solids content), TM-40 (40 wt%), HS-40 (40 wt%) and SM-30 (30 wt%), were purchased from Aldrich and fumed silica HDK/SLM ® powders (HDK D05, HDK N20, SLM 149/1, SLM 149/2, HDK HKS-D, HDK H20, HDK H2000) were kindly donated by Wacker Chemie AG. Ludox nanoparticles are of approximate spherical shape and about 5 to 25 nm in diameter depending on the grade. Fumed silica powders are aggregates of about 100 nm in diameter made of primary particles of diameter between 5 to 30 nm. V-65 initiator (2,2'-azobis(2,4-dimethyl valeronitrile)) was kindly donated by Wako Specialty Chemicals and AIBN initiator (2,2′-azobis(2-methylpropionitrile)) was purchased from VWR International, both used as supplied. Oil soluble dye (2,4-dihydroxy-4’-nitroazobenzol and hostasol) and water soluble dye (rhodamine B) were purchased from Aldrich. NaCl (Laboratory reagent grade, Fisher Scientific) and deionised water were used. Dialysis tubing cellulose membranes (33 mm flat diameter), purchased from Aldrich, were washed for few minutes under running water and rinsed with deionised water before use.

III.2.2. Equipment

Emulsification of the dispersed phase was created using either an homogeniser (IKA WERKA, Ultra Turrax, T25 basic with an 1.0 cm head set at speed 6 [24,000 rpm] or a Heidolph Silent Crusher M equipped with a dispersing tool 18DF/M) or a sonifier (Branson 450 W digital sonifier set at 70% amplitude). Monomer conversions were measured by gravimetry or, in the case of vinyl laurate monomer, by ^{1}H NMR analyses on a Bruker AC400 in deuterated chloroform (see Appendix B, Section B.2). Dynamic light scattering measurements to determine particle size distributions and zeta potential measurements were performed on a Malvern DTS Nano. pH measurements were recorded using a Knick pH meter 765 Calimetic. Photographs of emulsions were taken with a Canon digital IXUS 80 IS camera. Scanning electron microscopy was performed on a ZEISS supra 55VP FEGSEM and optical microscopy on an Olympus BH2-HLSH microscope equipped with an Olympus IC 20 lens. Size measurements on micrographs were performed using Image J software.

III.2.3. Preparation and stability of solids-stabilised emulsions

Ludox colloidal silica sols were diluted with deionised water. pH was modified as appropriate and the zeta potential was measured. Various vinyl monomers (oil) were added at different volume fractions and emulsified by either (i) hand-shaking, (ii) using an Ultra-Turrax T25 homogeniser (24,000 rpm) or (iii) a sonifier (Branon 450 W digital sonifier, 6 cycles of 1 minute at 70% amplitude with intervals of 30 seconds to leave the latex cooling down and so to prevent early polymerisation). Emulsion type was inferred by addition of an oil or water dye to the corresponding phase prior emulsification.

The emulsions were stored in closed vials at ambient temperature. In most cases either complete stable-emulsification or de-emulsification of the two liquid phases was observed (see photographs in Appendix C, section C.2). Limited droplet coalescence was assessed by the position of the emulsion-oil boundary for o/w emulsions or the position of the emulsion-water boundary for w/o emulsions.

Formulations of solids-stabilised o/w emulsions with a high fraction of oil (monomers such as styrene, vinyl laurate and vinyl neodecanoate (VEOVA-10)) are reported in section III.3.5.1, Table III-8.

Fumed silica powders were tested for the preparation of solids-stabilised o/w and/or w/o emulsions of vinyl acetate monomer (refer to Appendix C, section C.3).

III.2.4. Preparation of Ludox-stabilised polystyrene latexes in miniemulsion polymerisation via liquid-liquid interfacial stabilisation

Typically, a 40 wt% Ludox TM-40 silica sol (5.0 g) was diluted with deoxygenated H_2O (50.0 g). The pH of this sol was decreased by adding an aqueous solution of HCl (0.1010 N, dropwise to reach pH 3.0-3.5). The oil phase containing styrene monomer (5.0 g, 8.3 wt% overall), hexadecane (4.0 wt% based on monomer) and initiator (0.03 g, 0.6 wt% based on monomer, V-65, 2,2'-azobis(2,4-dimethyl valeronitrile)) was then added. The mixture was homogenised using an Ultra Turrax (24,000 rpm) and then the miniemulsion was formed using an ultrasonic probe (Branson 450 W digital sonifier, 6 cycles of 1 minute at 70% amplitude with intervals of 30 seconds to leave the latex cooling down) under strong stirring and in an ice bath to prevent early polymerisation. After transfer of the miniemulsion to a round bottom flask,

polymerisation was performed overnight without stirring at 51 ºC in an oil-filled bath after having purged the latex under nitrogen for 20 minutes. Final monomer conversions were measured by gravimetry and particle size distributions by dynamic light scattering. Electron microscopy analysis of the dried samples was performed. Formulations of all samples, monomer conversion X_m, average particle diameters d_z, and dispersity indices D_I, are reported in Table III-1. Exact masses of reagents are reported in Table C.1 (Appendix C).

Table III-1. Overall silica and oil contents, hydrodynamic diameters d_z and dispersity indices D_I of the different Ludox-stabilised polystyrene latexes prepared in miniemulsion polymerisation (pH ~3).

Experiment	***Ludox grade***	***Silica content/ wt%***	***Oil content/ wt%***	***X_m (18 h)/ %***	***d_z (DLS)/ nm***	***D_I (DLS)/ -***
CC-1-114 or *batch 1*	TM-40	3.2	8.3	84	218	0.12
CC-1-199 or *batch 2*	TM-40	3.2	8.2	78	231	0.06
CC-1-148	SM-30	3.1	8.2	63	271	0.10
CC-1-147	HS-40	2.8	7.3	55	354	0.05

III.2.5. Preparation of Ludox stabilised poly(styrene-co-vinyl pyridine) latexes in miniemulsion polymerisation via heterocoagulation assembly

The procedure reported in Section III.2.4 was followed at the exception that no hydrochloric acid was added to lower the pH and a 1:5 weight ratio mixture of 4-vinyl pyridine to styrene monomer was used. Formulation of two latexes, average particle diameters d_z, and dispersity indices D_I, are reported in Table III-2. Exact masses of reagents are reported in Table C.2 (Appendix C).

Table III-2. Overall silica and oil contents, hydrodynamic diameters d_z and dispersity indices D_I of the different Ludox-stabilised poly(styrene-*co*-vinyl pyridine) latexes prepared in miniemulsion polymerisation (pH ~10).

Experiment	***Ludox grade***	***Silica content/ wt%***	***Oil content/ wt%***	**d_z *(DLS)/ nm***	***D_I/ -***
CC-1-189	TM-40	11.7	9.7	186.6	0.40
CC-1-191	TM-40	3.3	8.6	347.6	0.51

III.2.6. Solids-stabilised poly(vinyl acetate) latex in suspension polymerisation via liquid-liquid interfacial stabilisation

A double-walled cylindrical glass reactor (~300 mL, Asynt Ltd.) designed to fit an homogeniser (Heidolph Silent Crusher) and equipped with an external circulating heating/cooling bath (Julabo F-25 unit), a condenser, and a four-bladed metal overhead turbine stirrer fitted at approximately 1 cm from the bottom of the reactor vessel (Cowie Ltd.) running at 150 rpm was used.

A 40 wt% Ludox TM-40 silica sol (40 g) was diluted with deoxygenated H_2O (250 g). The pH of this sol was decreased by adding an aqueous solution of HCl (32%) down to pH 3.0-3.5. The system was purged under nitrogen for half an hour and vinyl acetate monomer (57 g), containing AIBN initiator (0.5 g), were added. The mixture was cooled down to 15 ºC while being emulsified with the homogeniser set at 18,000 rpm for 30 min under inert atmosphere. Polymerisation was performed at 65 ºC for 3 hours. Latex solids contents, final monomer conversion X_m, and particle size range d_z from SEM imaging, are reported in Table III-3.

Table III-3. Overall silica and oil contents, final monomer conversion X_m, particle size range d_z from SEM imaging of a Ludox-stabilised poly(vinyl acetate) latex prepared in suspension polymerisation. (See Figure III-17 for SEM images in 'Results and discussion' section III.3.6)

Experiment	*Ludox grade*	*Silica content/ wt%*	*Oil content/ wt%*	X_m/ %	d_z (SEM)/ µm
CC-2-344	TM-40	4.7	16.5	96	~ 0.1 ~ 2-15

III.3. Results and discussion

III.3.1. Energy profile of a spherical particle at a vinyl acetate – water interface

As described in the introduction (Chapter I, section I.4.1), using the Pieranski model,[35] it has been calculated that liquid-liquid interfaces can be used to assemble colloidal particles quasi irreversibly.[36] Herein, we calculated the free energy required to push away one spherical particle trapped at a flat vinyl acetate – water interface using the Clint and Taylor equation:[37]

$$E = \pi R^2 \sigma_{1-2} \left(1 \pm \cos\theta\right)^2 \qquad \textbf{Equation III-1}$$

Where R is the radius of the particle, σ_{1-2} is the interfacial tension between the two liquids and θ is the three-phase contact angle describing the position at which the particle sits at the interface. The sign in the brackets is negative for $\theta < 90$ º, when the particle is removed into the water and positive for $\theta > 90$ º, when the particle is removed into the oil phase.

With given values of R and σ_{1-2}, it already allowed us to draw the energy profile (E) of a colloidal particle adhering to a liquid-liquid interface as a function of θ. We calculated the free energy (E) gained from the adhesion of

one spherical particle of 10, 25 or 100 nm at temperatures of 20 ºC and 60 ºC, with vinyl acetate/water interfacial tensions $\sigma_{1\text{-}2}$ of 24.0 and 19.5 dyne cm^{-1} respectively. We accounted for the thermal energy (Brownian motion) by dividing the free energy by [k_BT], which is plotted in Figure III-1 as a function of the contact angle θ. High values in the range of 10^2 to $10^3 \times k_BT$ predicted a promising route for the stabilisation of o/w emulsion of vinyl acetate by solid particles.

At this stage we are ignoring the line tension force acting at the contact of the spherical particle and the two liquid phases. Its importance and effect on the emulsion droplet size using building blocks of different sizes are described in Section III.3.4.1.

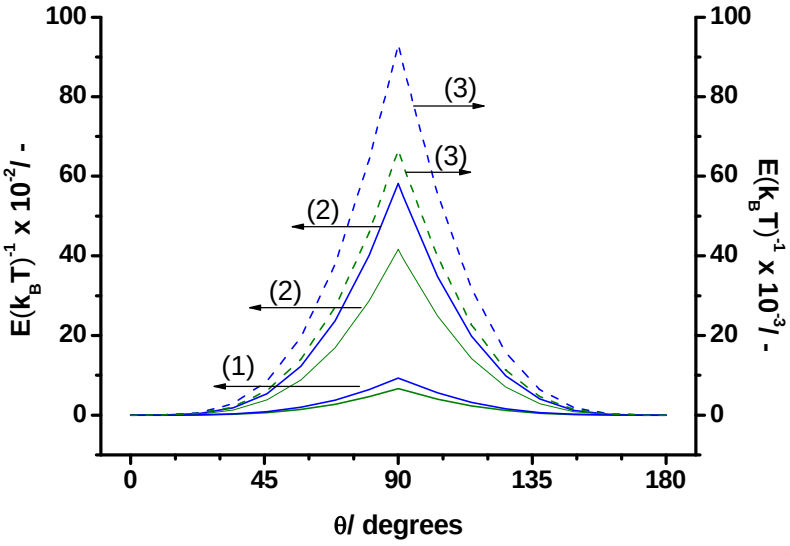

Figure III-1. Dependence of the free energy E, required to force one particle to leave a vinyl acetate – water interface when pushed in the most wettable phase, divided by its thermal energy (Brownian motion k_BT), on contact angle θ. Particle of (1) 10 nm in diameter, (2) 25 nm in diameter and (3) 100 nm in diameter. Blue and green curves at T = 20 ºC ($\sigma_{1\text{-}2}$ = 24.0 dyne cm^{-1}) and 60 ºC ($\sigma_{1\text{-}2}$ = 19.5 dyne cm^{-1}), respectively.

III.3.2. Wetting of silica particles at oil – water interfaces for the stabilisation of emulsion droplets

Partial wetting of the solids particles by the two liquid phases is necessary to stabilise the interface. The position (three-phase contact angle) at which the particle sits at the interface depends on the interfacial tensions (wetting) of the particle with both liquid phases, as well as the interfacial tension between the two liquids. Preliminary studies consisted in adjusting the pH and ionic strength of the water phase for the formation of solids-stabilised emulsions for colloidal particles under investigation.

III.3.2.1. Effect of pH

Ludox silica sols used in this work are commercial aqueous dispersions of silica nanoparticles of 30 or 40 wt% solids contents. Those silica nanoparticles are electrostatically stabilised from the deprotonation of hydroxyl surface groups upon addition of sodium hydroxide (pH ~9-10). Herein, we detail the use of Ludox TM-40 sol, nanoparticles of about 24 nm in diameter. Similar results were obtained with smaller colloidal silica nanoparticles (Ludox HS-40 and SM-30 sols, with diameters of ~14 nm and ~7 nm, respectively). The influence of the pH on their colloidal stability and therefore their stabilising effect for the preparation of oil-in-water emulsions was studied. Samples containing *ca.* 0.5 mL of Ludox TM-40 silica sol (40 wt% solids content), diluted in about 10 mL of deionised water, and *ca.* 1 mL of monomer were prepared. The pH of the aqueous phase (containing the silica nanoparticles) was adjusted to a range of values, from pH ~9-10 down to pH ~3, by adding HCl 0.1 M. The mixtures were hand-shook to form emulsions. Stable o/w emulsions of various monomers (oil) were obtained when the pH was decreased down to 3.5-3.0. Table III-4

summarises the stability of emulsions of styrene, vinyl acetate, vinyl laurate and methyl methacrylate monomers at pH ~10, 8.0, 6.0, 5.0 and 3.5-3.0.

Table III-4. Stability of oil-in-water emulsions formed by hand-shacking mixtures of about 1 mL monomer (oil) in 10 mL of water containing *ca.* 0.5 mL of Ludox TM-40 colloidal silica sol at different values of pH (✓= stable emulsion, ~ = limited coalescence and, × = coalescence).

Monomer \ pH	***~10***	***8.0***	***6.0***	***5.0***	***3.5-3.0***
Styrene	×	×	×	~	✓
Vinyl acetate	×	×	×	✓	✓
Vinyl laurate	✓	✓	×	×	✓
Methyl Methacrylate	×	×	×	~	✓

By dropping the pH, the colloidal silica nanoparticles were rendered colloidally unstable. Lowering their surface charge increased their wettability with the oil phase so that they adhered at the monomer – water interface. The system followed the Bancroft rule so that stable droplets of monomer were formed in the water phase (dispersed phase for the colloidal silica nanoparticles).

O/w emulsions of vinyl laurate monomer were also stable at high values of pH (8-10). This stabilisation effect was attributed to the partial hydrolysis of the monomer producing in situ surfactant thereby stabilising the monomer droplets (as observed in Chapter II using Laponite clay platelets as stabiliser). A difference in the creaming behaviour of the emulsion droplets was also observed. Those emulsions creamed lesser than when prepared at pH 3 which confirmed a different mechanism of stabilisation implying the presence of repulsive electrostatic charges between silica nanoparticles and surface of the monomer droplets, see photographs in Appendix C (section C.1).

Zeta potential measurements of dispersions of Ludox TM-40 silica nanoparticles were performed at 25 ºC and at different values of pH, see plot in Figure III-2. The decrease of the zeta potential (in absolute value), as the pH was dropped, confirmed the progressive loss of their colloidal stability. Commonly, electrostatically stabilised colloidal dispersions are considered to be stable with zeta potentials higher than 30 mV or lower than -30 mV.

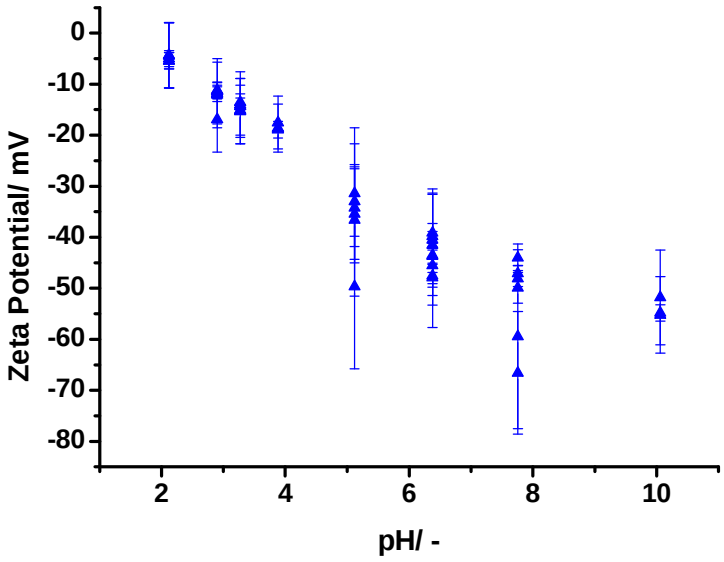

Figure III-2. Graph of the zeta potential as a function of the pH of Ludox TM-40 colloidal silica dispersions.

Another way to control the wetting properties of particles is by surface treatment. A range of fumed silica powders chemically modified at diverse degree (hydrophobised by methylation of the residual hydroxyl groups) was tested and led to the formation of o/w or w/o emulsions (see Appendix C, Section C.2).

III.3.2.2. Effect of ionic strength and concentration in silica nanoparticles

At high weight fraction in colloidal silica, such as 20 wt% in our experiments, the pH-dependent formation of gels over time was observed at room temperature; see photographs in Figure III-3 and Table III-5.

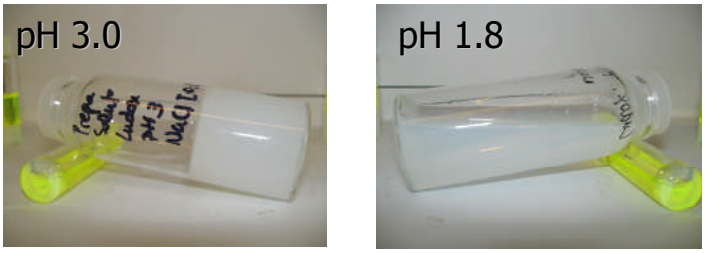

Figure III-3. Photographs of a 20 wt% Ludox TM-40 colloidal silica sol, gelled at pH 3.0 and not gelled at pH 1.8.

The addition of HCl not only reduced the pH, inducing partial suppression of the ionisation of the surface hydroxyl groups, but also increased the ionic strength of the dispersed medium initially containing Na^+ as counterion. The presence of ions compressed the electrical double layer of the silica nanoparticles which resulted in the competition between van der Waals attractive forces and electrical repulsive forces. A physical gel was formed when a reversible equilibrium of the inter-particle interactions was reached.[38] At low value of pH (1.8 in our experimental conditions) the inter-particle bonds decreased and no gel was formed for a 20 wt% Ludox sol.

Table III-5. Gel formation of a dispersion of Ludox TM-40 colloidal silica (20 wt%) over time and at different pH (adjusted with addition of HCl).

Time \ pH	***3.9***	***3.5***	***2.6***	***1.8***
After 2 days	fluid	fluid	fluid	fluid
After 5 days	gel	gel	fluid	fluid
After 9 days	gel	gel	gel	fluid

As previously described (Section III.3.2.1), Ludox TM-40 stabilised o/w emulsions of diverse monomers were obtained at pH of about 3.5-3.0. When high weight ratios (20 wt%) of colloidal silica was used, the formation of silica gel entrapped the monomer droplets, see Figure III-4.

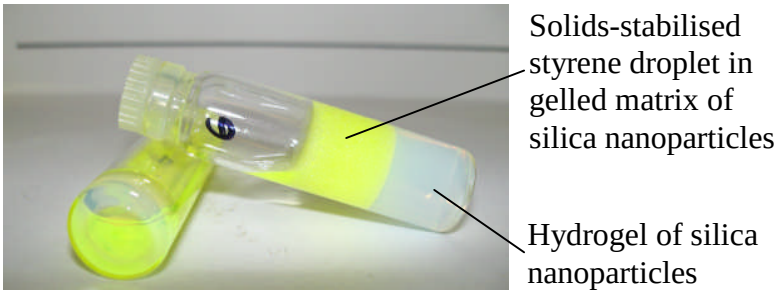

Figure III-4. Photograph of a gelled solids-stabilised o/w emulsion of styrene monomer (40 wt%, oil soluble dye hostasol) using Ludox TM-40 as stabiliser (40 wt%) at pH 3.0.

Unlike the case of clay platelets dispersions forming weak gels upon addition of salt which contributed to the stabilisation of o/w emulsion droplets,[39] in this case the formation of colloidal gels is to be avoided for the preparation of solids-stabilised emulsions. Moreover, as the inter-particle interactions supporting the colloidal gel were (partially) disrupted upon hand-shaking, the solids-stabilised emulsion droplets were also destabilised. This meant that the assembled silica particles at the liquid-liquid interface were involved in stronger inter-particle interactions forming the gel. The shear energy provided was not enough to disrupt all the inter-particle bonds at the microscopic level and the remaining fractals did not stabilise the oil – water interface, so that droplet coalescence occurred. For this, the concentration in colloidal silica in the dispersed medium after the emulsification process has to be kept low. Coverage calculations allowed us to determine the amounts of silica required for the stabilisation of monomer droplets of certain sizes, see Section III.3.5.2.

III.3.3. Stability of solids-stabilised droplets against creaming or sedimentation

Suppressing the surface charge of the colloidal silica induced their assembly at oil – water interfaces, and can lead to successful stabilisation of o/w or w/o emulsions. However, we also observed creaming or sedimentation of the dispersed phase. This was attributed to the difference in densities between the continuous phase and the droplets. As a result of the lack of electrostatic charges and difference in densities, droplet motion occurred with gravity which led to creaming of o/w droplets and sedimentation of w/o droplets.

III.3.4. Well defined armoured latexes in miniemulsion polymerisation

III.3.4.1. Control of the latex particle size by the diameter of the colloidal stabilisers

Waterborne armoured latex particles were successfully prepared using miniemulsion polymerisation. We present a series of experiments conducted with styrene monomer as the dispersed oil. The stabilisation of submicron-sized droplets created by ultra-sonication was obtained by using smaller building blocs of about one length scale in difference, or more, to the monomer droplets. For this purpose we used the three following grades of Ludox colloidal silica: TM-40, HS-40 and SM-30. Their respective average diameters d_{part} (SEM), measured from analysis of SEM micrographs (of at least 50 particles using Image J software), were 24.06 nm, 13.66 nm and 7.39 nm, with standard deviations of 3.36, 2.39 and 1.53, respectively (see SEM images in Figure III-5).

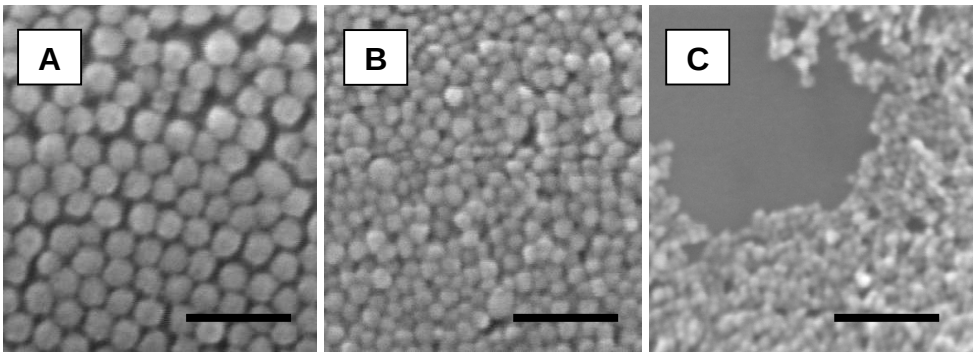

Figure III-5. SEM images of Ludox colloidal silica grades (A) TM-40 ($d_{TM\text{-}40}$ (SEM) = 24.06 nm), (B) HS-40 ($d_{HS\text{-}40}$ (SEM) = 13.66 nm), and (C) SM-30 ($d_{SM\text{-}30}$ (SEM) = 7.39 nm). Scale bars 100 nm.

The pH was dropped to 3.0-3.5 (for reasons previously detailed, see section III.3.2.1) using concentrated hydrochloric acid. The irreversible anchorage of the silica nanoparticles onto the droplet interface was one factor enhancing the stability of the submicron-size droplets. Jamming of the colloidal particles was predicted to limit inter-droplets monomer diffusion thereby minimising broadening of the droplet size distribution. Hexadecane (4 wt% based on styrene monomer) was also used, as hydrophobe, to minimise the phenomenon of Ostwald ripening. Oil and silica contents (wt%) of the prepared latexes were kept close to constant (see Table III-1).

Relatively monodisperse latexes (dispersities D_I < 0.15 from dynamic light scattering measurements) with overall solids content of ~11 wt% were obtained with the different grades of Ludox colloidal silica, see SEM images Figure III-6.

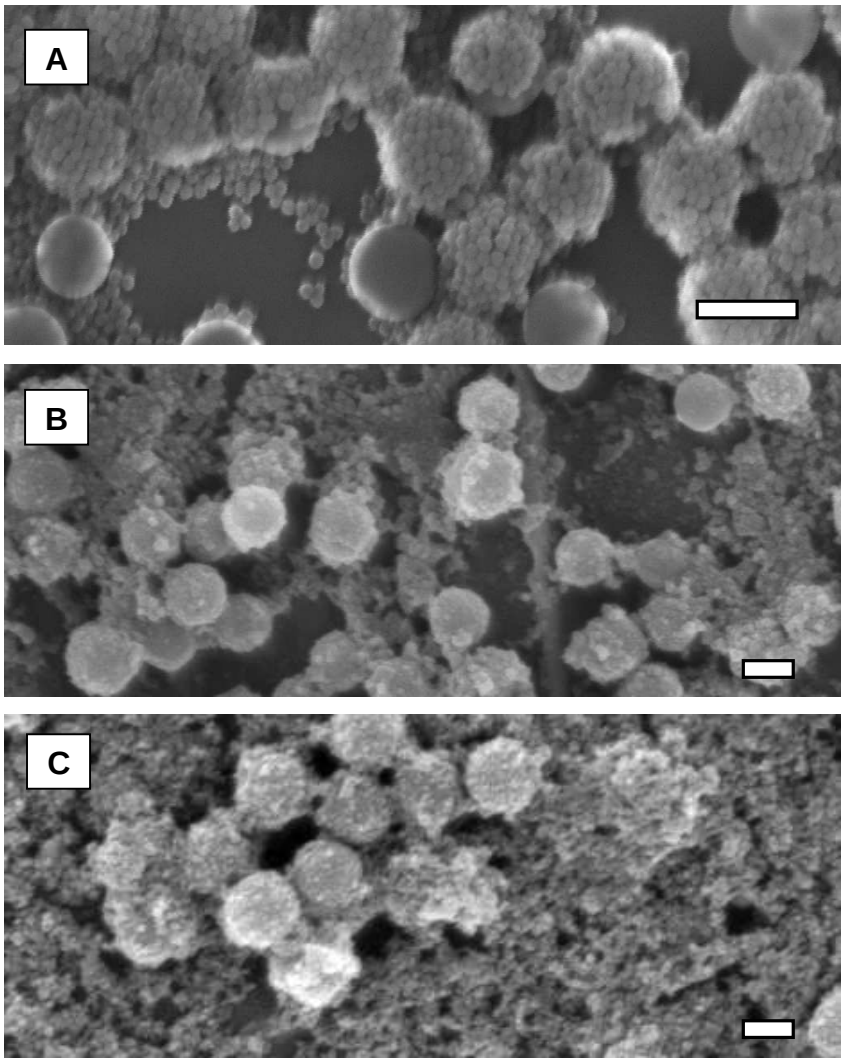

Figure III-6. SEM images of Ludox-polystyrene latexes prepared *via* solids-stabilised miniemulsion polymerisation: (A) Ludox TM-40 (CC-1-199), (B) Ludox HS-40 (CC-1-148), (C) Ludox SM-30 (CC-1-147). All scale bars 200 nm.

Particle size distributions from dynamic light scattering measurements and from the analysis of SEM images are also reported in Table III-6. The partial disintegration of the colloidal silica-armoured shell, observed by SEM imaging (Figure III-6), is discussed in Section III.3.4.2.

Table III-6. Series of Ludox-stabilised polystyrene latexes prepared in miniemulsion polymerisation. d_{part} are the average diameters of Ludox silica nanoparticles (from SEM micrograph analyses). d_z (DLS) and d (SEM) are the average diameters of the armoured latex particles measured by dynamic light scattering and from analysis of SEM micrographs (with the standard deviations), respectively.

Exp.	***Ludox silica grade***	***d_{part}/ nm***	***d_z (DLS)/ nm***	***d (SEM)/ nm***
cc-1-114	TM-40	24.06 +/- 3.36	218	209.70 +/- 21.75
cc-1-199	TM-40	24.06 +/- 3.36	231	211.91 +/- 31.11
cc-1-148	HS-40	13.66 +/- 2.39	271	242.98 +/- 25.75
cc-1-147	SM-30	7.39 +/- 3.36	354	307.35 +/- 31.51

A clear dependence between the average diameter of the latex particles/monomer droplets and the size of the solid stabiliser was observed. Smaller colloidal silica stabiliser ($d_{TM-40} > d_{HS-40} > d_{SM-30}$) led to the formation of bigger latex particles. The explanation for this is lying in the energy profiles of solids particles assembled at liquid-liquid interfaces. The model developed by Clint and Taylor in 1992 described the critical surface pressure to be independent of the nanoparticle radius;[37] this was however, not accounting for the line tension force τ. This force acts along the contact perimeter [$2\pi R_{part} \sin\theta$] of the three phases for a particle of radius R_{part} sitting at the interface with a contact angle θ (see Figure III-7), as described in the 90s by Aveyard *et al.*[40-42] and Widom.[43] Conventionally, a positive line tension indicates a contractile line pushing the particle to the phase which is the most wettable (*e.g.* phase 2 in Figure III-7).

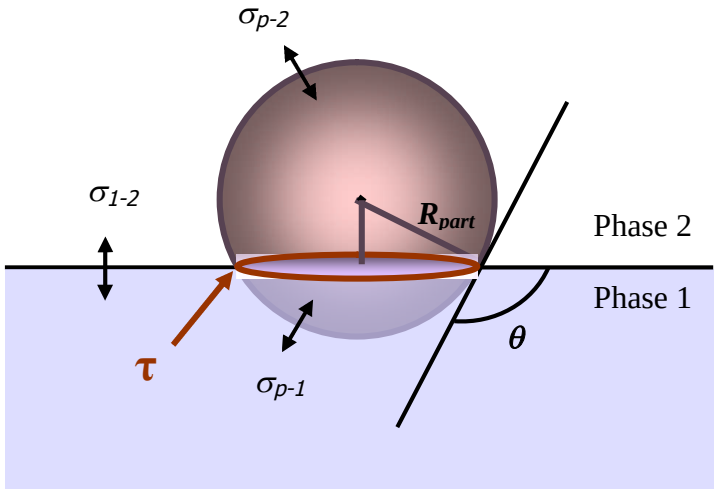

Figure III-7. Spherical particle of radius R_{part} resting at a liquid-liquid interface with a contact angle θ. Tensions $\sigma_{1\text{-}2}$, $\sigma_{p\text{-}1}$, $\sigma_{p\text{-}2}$ correspond to the tensions between phase 1 – 2, particle – phase 1, and particle – phase 2; τ is the line tension acting along the particle – phase 1 – phase 2 contact line.

Aveyard and Clint developed a method for the measurement of line tensions at the solid/liquid/air three-phase contact line showing the influence of the particle diameter on their adherence to the interface.[41] For a hexagonally close-packed monolayer of spherical particles at the interface, the energy required to expel particles in unit area of interface, EN, with $N = 1/\left[2\sqrt{3}R_{part}{}^2\right]$, was given by:

$$EN = \frac{\pi}{\sqrt{3}}\left[\frac{\sigma_{1-2}}{2}(1 \pm \cos\theta)^2 - \frac{\tau}{R_{part}}\sin\theta\right] = \Pi_c \qquad \textbf{Equation III-2}$$

$$i.e.\ \ \Pi_c \propto -\frac{1}{R_{part}}$$

Where σ_{1-2} is the interfacial tension between the two liquid phases and Π_c is called the critical surface pressure.

Although contact angle and line tension are interdependent, they showed for a series of particles with different radii but similar surface properties, such as the

contact angle with water, that a plot of the critical surface pressure versus ($1/R_{part}$) was linear and inversely proportional.

We extend this model to the stabilisation of emulsion droplets. The Laplace pressure is defined as the pressure difference between the inside and the outside of a droplet of radius $R_{droplet}$:

$$\Delta P \equiv P_{inside} - P_{outside} = \frac{2\sigma_{armoured}}{R_{droplet}} \qquad \textbf{Equation III-3}$$

Where $\sigma_{armoured}$ refers in our case the interfacial tension of the solids-stabilised system at equilibrium. This resulting interfacial tension can be related to the critical surface pressure gained from the stabilisation with the solids particles to the initial interfacial tension of the non-stabilised liquid-liquid interface σ_{1-2}:

$$\sigma_{armoured} \equiv \sigma_{1-2} - \Pi_c \qquad \textbf{Equation III-4}$$

In other words, for a given Laplace pressure, with Equations III-1 to III-3 we have $\sigma_{armoured}$ proportional to the radius of the droplet $R_{droplet}$, and should be inversely proportional to the critical surface pressure Π_c.

$$\begin{aligned} R_{droplet}\,(or\ d) &\propto \sigma_{armoured} \\ &\propto -\Pi_c \\ &\propto \left(R_{part}\right)^{-1} \end{aligned} \qquad \textbf{Equation III-5}$$

Therefore, a directly proportional linear trend should be observed by plotting the radius of the droplets $R_{droplet}$ or the average diameter of the armoured latex particles (d_z *(DLS)* from dynamic light scattering measurements or *d (SEM)* determined by SEM analyses, see Table III-6) as a function of

($1/R_{part}$). As displayed in the graph of Figure III-8, we were able to successfully describe the size difference of the polymer particles in terms of interfacial energies of the adhesion of colloidal particles at liquid-liquid interfaces.

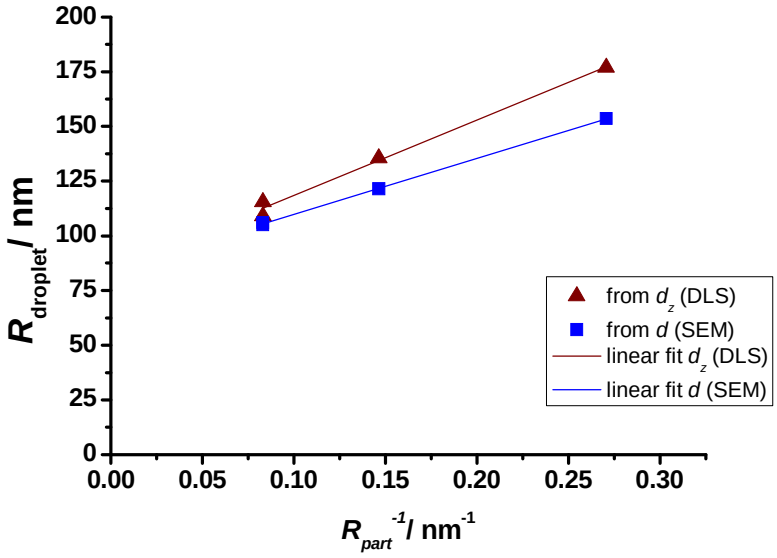

Figure III-8. Graph of the average diameters of the armoured polymer particles (d_z (DLS) from dynamic light scattering measurements and d (SEM) from SEM image analyses) versus one over the average radius of the Ludox stabiliser used, R_{part} (determined by SEM image analyses). Equations of linear fits are: d_z (DLS) = 345.35 R^{-1} + 83.89 and d (SEM) = 255.98 R^{-1} + 84.17 with R^2 of 0.988 and 0.999 respectively.

All polymerisation reactions were conducted for 18 hours at 65 ºC and using the same concentration in initiator (5×10^{-3} g per g of monomer). Lower monomer conversions (at 18 h reaction) were obtained as the diameter of the droplets /latex particles increased. This was due to compartmentalisation of the system as described by Bon and Colver.[39] Smaller droplets result in higher rate of polymerisation as two growing polymer chains cannot undergo termination if they are in two separate particles.

III.3.4.2. Stability of the layer of nano-silica around the polystyrene particles

No imprint on the polystyrene spheres

As previously observed by SEM analysis in Figure III-6, the partial loss of silica nanoparticles from the surface of the polystyrene beads was attributed to drying effects due to the capillary forces and the small interaction between the polymer and silica particles (see also Figure III-9). The reason why the latex particles were smooth, rather than like a golf ball, could potentially be a quite complex problem, *i.e.* surface tension properties.

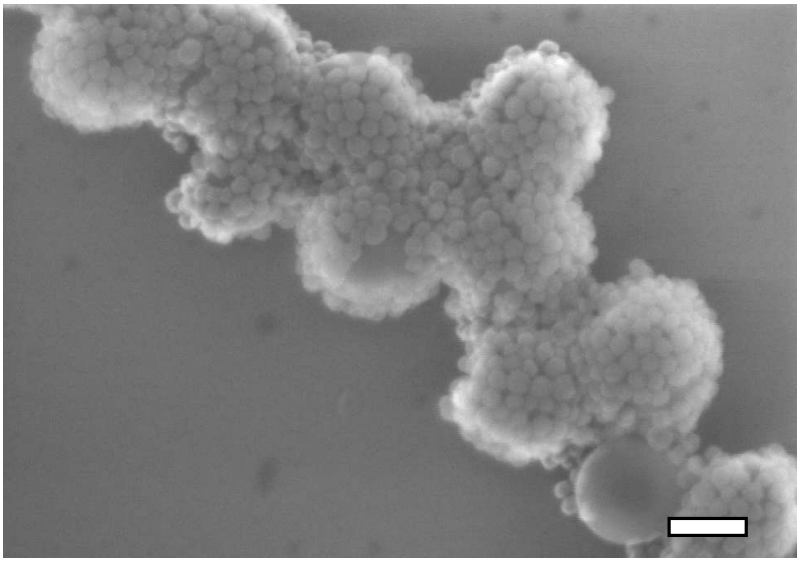

Figure III-9. SEM image of Ludox(TM-40)-polystyrene latex prepared *via* solids-stabilised miniemulsion polymerisation (CC-1-114). Scale bar 100 nm.

The silica nanoparticles having a zeta potential of about -15 mV in the experimental conditions of pH ~3 (refer to Figure III-2) and following the Bancroft rule by forming o/w emulsions, we also supposed the Ludox nanoparticles sat at the monomer – water interface with clear preferential wetting with the aqueous phase than the monomer phase. The Ludox nanoparticles may therefore not be anchored deeply enough to leave an "imprint" on the polymer surface. A part of the explanation may also be found

in the shrinking during the polymerisation process. Indeed, a styrene bead of 150 nm in diameter for instance measures 143 nm after polymerisation (considering full monomer conversion) knowing that the densities of styrene and polystyrene are 0.909 g cm^{-3} at 25 °C and 1.050 g cm^{-3}, respectively.

Addition of surfactant

The weak interactions between the polystyrene particles and the silica nanoparticles were also easily disrupted upon addition of surfactant, such as sodium dodecyl sulfate which was added in excess at a concentration of 5 times the critical micelle concentration (CMC) (Figure III-10).

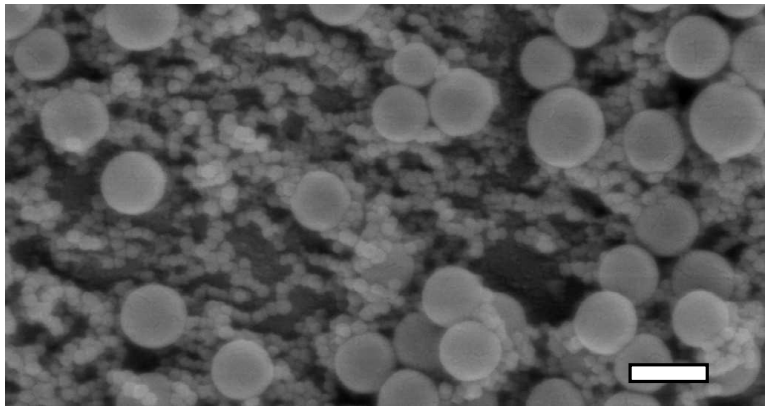

Figure III-10. SEM image of polystyrene latex particles, prepared in miniemulsion polymerisation using Ludox TM-40 as stabiliser, after disintegration of the armoured shell by addition of SDS surfactant (at a concentration of 5 times the CMC). Scale bar 200 nm.

Addition of co-stabiliser/co-monomer

Hedgehog morphologies where the silica nanoparticles act as Pickering stabilisers using a basic co-monomer as a coupler were reported by Landfester *et al.* using a surfactant free miniemulsion process.[27] This strategy enhances the affinity between the polymer particles and the silica nanoparticles. In our experimental of monomer and silica concentrations (silica-to-monomer weight

ratio of 0.38), it can be seen by SEM imaging (Figure III-11) that upon addition of 4-vinyl pyridine as co-monomer and working at high pH (~10, exp. CC-1-191, Table III-2), the silica nanoparticles were quite embedded into the polymer particles. In this case, the nanoparticles were not closely packed as a result of their high repelling surface charge which provided good colloidal stability to the latex so that no sedimentation was observed. However, broad particle size distributions were obtained (dispersities of 0.4 – 0.5) even at increased contents in Ludox colloidal silica with monomer to silica ratio of 1.2 (exp. CC-1-189, Table III-2).

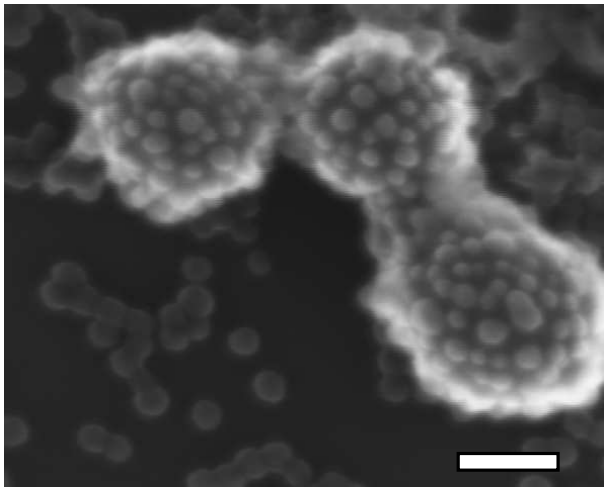

Figure III-11. SEM image showing the hedgehog morphology of hybrid poly(styrene-*co*-4-vinyl pyridine) latex particles prepared in miniemulsion polymerisation using Ludox TM-40 at high pH (CC-1-191). Scale bar 100 nm.

III.3.4.3. Packing patterns of silica nanoparticles on a spherical surface

Electron microscopy investigation of armoured polymer latexes prepared *via* driven assembly of nanoparticles at liquid-liquid interfaces showed that the layer of silica nanoparticles (Ludox TM-40), packed around the polystyrene latex spheres, were in close proximity on the surface. This showed that surface

charges were indeed minimal (see SEM image in Figure III-9 and TEM images in Figure III-12).

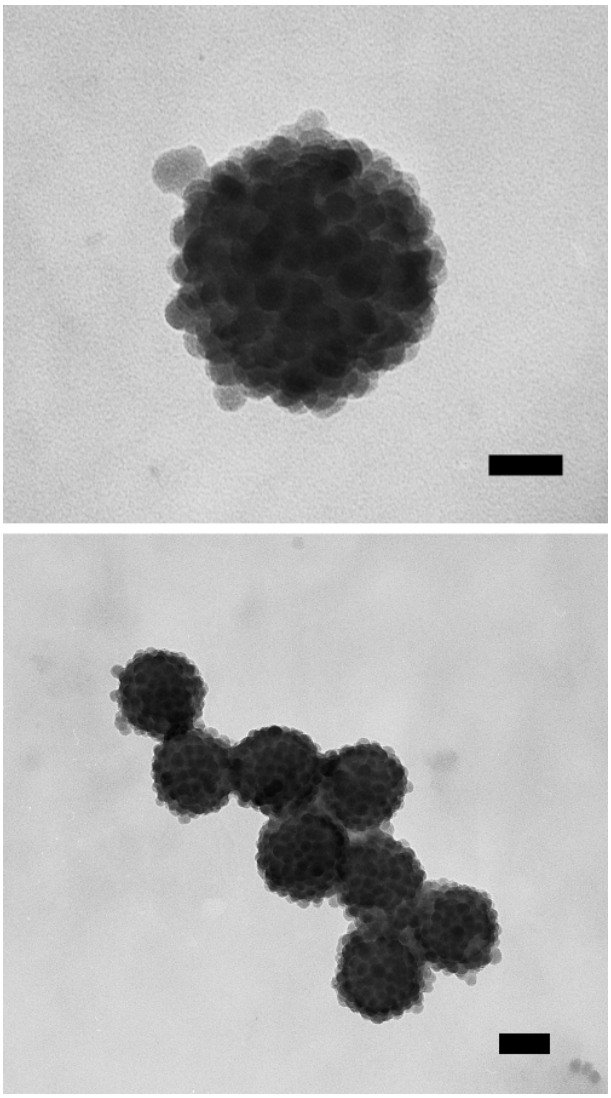

Figure III-12. TEM images of colloidal silica (Ludox TM-40) armoured polystyrene latex particles (batch 1) prepared in miniemulsion polymerisation at pH ~3. Scale bars: (A) 50 nm and (B) 100 nm.

Due to constrain of assembly on curved surfaces and variation in the Ludox TM-40 silica particle size, interesting packing patterns emerged. We analysed those patterns for two batches of armoured polystyrene latexes using the same recipe were prepared (batch 1: CC-1-114 and batch 2: CC-1-199). Their packing patterns are reported in Table III-7.

Table III-7. Analysis of the packing patterns of the silica nanoparticles on the surface of the polystyrene particles. Average ratios of nanoparticles having 4, 5, 6 or 7 neighbours, with their standard deviation, are reported for each batch, 1 (cc-1-114) and 2 (cc-1-199), and the average over the two batches.

		Ratios of nanoparticles with the following number of neighbours			
		4	**5**	**6**	**7**
Batch 1	**average**	0.123	0.473	0.375	0.029
	st. dev.	0.034	0.082	0.102	0.020
Batch 2	**average**	0.081	0.496	0.372	0.051
	st. dev.	0.035	0.066	0.085	0.031
Average	**average**	0.094	0.489	0.373	0.044
	st. dev.	0.038	0.067	0.084	0.029

SEM analysis (see Figure III-13) of approximately 25 armoured polymer latex particles showed that the silica particles were arranged in patterns with either 4, 5, 6, or 7 neighbours, at percentages of 12, 47, 37, or 2.9, respectively for batch 1 for instance. This clearly deviates from the ideal 12-point dislocations seen in 13-atom cuboctahedral clusters, in which the 12 outer atoms each have 5 neighbours. It also deviates from the large assemblies of particles on large droplets investigated by Bausch *et al.*, where exclusively 5- and 7-neighbour grain boundary dislocations were found.[33-34]

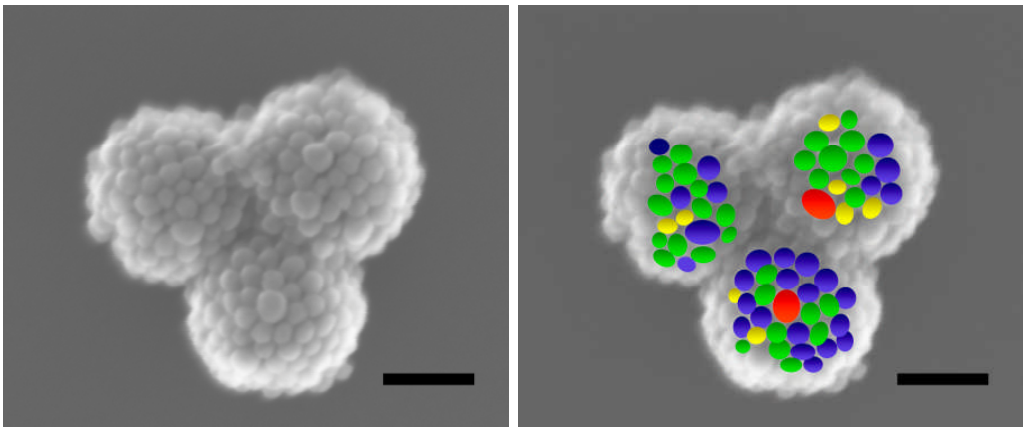

Figure III-13. Example of analysis of packing geometries from an SEM image of a Ludox TM-40 armoured polystyrene latex: yellow, green, blue, and red coloured particles having 4, 5, 6 and 7 neighbours, respectively. Scale bar 100 nm.

Patterns with 4 and 7 neighbours appeared as a result of the dispersity of the silica nanoparticles. This was proven by Fortuna *et al.*[1] who performed Monte Carlo simulations of the arrangement of nanospheres on a spherical surface. They showed that by broadening the particle size distribution of the nanoparticles the packing geometry was no longer described in terms of a 12-points dislocation or grain boundary scars. Simulations using a 12-24 Lennard-Jones potential for the arrangement of nanospheres with dimensions and dispersity of the Ludox TM-40 colloidal silica (24.06 +/- 3.36 nm) around a sphere (polymer particle) of diameter 161.58 nm (calculated from the average size of our armoured particles of batch 2: 209.70 +/- 21.75 nm) found packing patterns in great agreement with our SEM micrograph analyses.

III.3.5. Towards high emulsified contents

III.3.5.1. Effect of the dispersing tool

Emulsification by hand-shaking

To prepare high solids content hybrid polymer latexes, the amount of emulsified monomer (oil) was increased. Series of hand-shaking tests as described in Section III.3.2 were performed using Ludox colloidal silica (TM-40) as solid stabiliser. The solid particles are in the dispersion medium (water) at a concentration of 20 wt% for Ludox colloidal silica particles. The monomer phase (such as styrene, vinyl laurate or vinyl acetate) was added to this aqueous dispersion of increased ratios: from 10/90, 20/80, etc up to 90/10 in volume respectively. (Refer to Appendix C for photographs). By hand-shaking the mixtures sub-millimetre size droplets were formed. Stable o/w silica-stabilised

emulsions were obtained with monomer contents up to 40 – 50% in volume. At higher monomer contents, coalescence of the monomer droplets was observed leading to de-emulsification of the two liquid phases.

Emulsification using a homogeniser

The emulsification of mixtures containing increasing amounts in monomers (styrene, vinyl laurate, VEOVA-10) and Ludox TM-40 colloidal silica sol at pH 3 was performed using an Ultra-Turrax (24,000 rpm). Overall contents in monomer up to 65 wt% or overall contents of monomer plus silica nanoparticles up to 79 wt% conducted to stable oil-in-water emulsions (see Table III-8).

Table III-8. Composition of highly stable o/w emulsions of styrene, vinyl laurate or VEOVA-10 monomers using Ludox TM-40 (pH ~3) as solid stabiliser and an Ultra-Turrax T25 (24,000 rpm) to blend the mixtures.

Exp.	***Monomer***	***Monomer content/ wt%***	***Silica content/ wt%***	***Silica-to-monomer ratio/ $g \times g^{-1}$***
CC-2-243	Styrene			
CC-2-247a	Vinyl laurate	50	20	0.40
CC-2-248a	VEOVA-10			
CC-2-244	Styrene			
CC-2-247b	Vinyl laurate	57	17	0.30
CC-2-248b	VEOVA-10			
CC-2-245	Styrene			
CC-2-247c	Vinyl laurate	65	14	0.22
CC-2-248c	VEOVA-10			

Emulsion droplets in the range of 5 to 30 µm in diameter were observed by optical microscopy (Figure III-14). The calculated volumes occupied by styrene monomer and silica nanoparticles in exp cc-2-245 were 72% and 8% respectively (with densities of 0.873 g cm^{-3} for styrene and 1.75 g cm^{-3} for silica

(calculated from the density of a 40 wt% sol of 1.3 g cm^{-3}). In this system only 20% in volume is occupied by water (dispersion medium). Such high volume fractions demonstrate a very strong stability of the droplets against coalescence. Close-packing of uniform spheres, *i.e.* in HCP or FCC lattices, occupies 74% of the total volume. The achievement of higher volume fractions of the dispersed phase in our samples was due to both the disparity in size between the emulsion droplets and the solids nanoparticles (any excess in the latest can remain in the gaps between close-packed emulsion droplets) and the non-monodispersity of the droplets (see optical micrograph in Figure III-14).

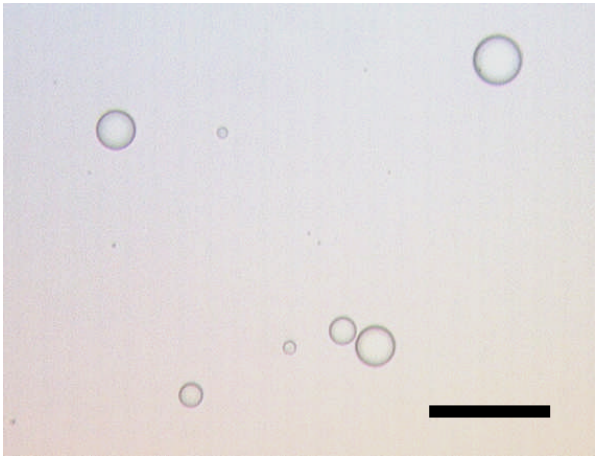

Figure III-14. Optical microscopy picture of a diluted emulsion of styrene in water stabilised with Ludox TM-40 nanoparticles prepared with an Ultra-Turrax T-25. Scale bar 50 μm.

Emulsification by ultra-sonication

A stable Ludox(TM-40) stabilised o/w emulsion prepared with a blender (Ultra-Turrax, 24,000 rpm), containing overall 20 wt% in Ludox nanoparticles and 50 wt% in styrene monomer, was successively ultra-sonicated to form submicron sized droplets of monomer (miniemulsion droplets). Partial demixing occurred as a layer of monomer was observed on the top of the miniemulsion.

By deducting the monomer lost, the effective emulsion contents were estimated to 24 wt% in Ludox nanoparticles and 37 wt% in styrene, see Table III-9.

Table III-9. Composition of Ludox(TM-40) stabilised o/w emulsions of styrene monomer subsequently prepared by blending and ultra-sonicating the mixture (after the sonication process part of the monomer demixed and was not taken into account into those contents).

Exp.	***Emulsification process***	***Monomer content/ wt%***	***Ludox content/ wt%***	***Silica to monomer ratio/ $g \times g^{-1}$***
cc-2-246	Ultra-Turrax	50	20	0.40
	Sonifier	37	24	0.66

This phenomenon was in agreement with the non-reversible adherence of nanoparticles at liquid-liquid interfaces. Combined with the large surface area created for the formation of submicron size monomer droplets, a lack in solids-stabilisers to cover this interface would lead to partial demixing. Coverage calculations described in the next section verified this hypothesis.

III.3.5.2. Coverage calculations

Coverage calculations of the armoured monomer droplets by the silica nanoparticles were performed in a similar way to the case using Laponite clay platelets (see Chapter II, Section II.3.2.3 and Appendix B, Section B.5.2). We assumed (i) full coverage of the droplets by a mono-layer of silica nanoparticles which are arranged in a 2-D square packing (see Figure III-15.A), (ii) silica nanoparticles uniform in size, (iii) monomer droplets uniform in size, and (iv) adherence of the silica nanoparticles to a flat interface with a contact angle of 90 °.

In order to calculate the relative amounts in silica nanoparticles and monomer/oil phase, the effective area covered by one silica nanoparticle in a square geometry (Figure III-15.A) was calculated from:

$$a_{part} = d_{part}^{2} \qquad \textbf{Equation III-6}$$

Where d_{part} is the diameter of a silica nanoparticle (*i.e.* 25 nm was used for Ludox TM-40).

The effective surface area a_{drop} of one monomer droplet/polymer particle on which the silica nanoparticles are arranged was calculated from the surface crossing the centre of the silica nanoparticles. This sphere has a diameter of (d_z – d_{part}) (see Figure III-15.B), so that we have:

$$a_{drop} = \pi (d_z - d_{part})^2 \qquad \textbf{Equation III-7}$$

Where d_z is the diameter of the core-shell structure which can be measured by dynamic light scattering.

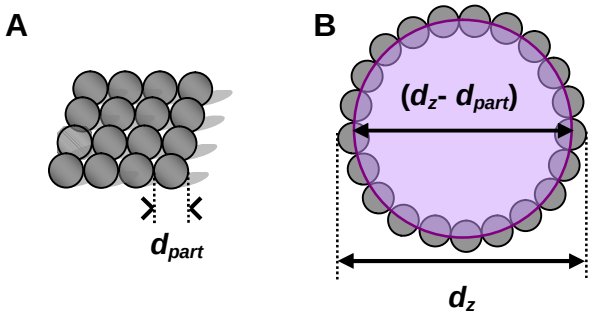

Figure III-15. Schematic of the 2-D arrangement of the silica nanoparticles in a square geometry (A), and representation of solids-stabilised o/w droplets: adherence of the silica nanoparticles at the oil – water interface with a contact angle of 90 º (B).

Assuming full coverage, the number of silica nanoparticles, N_{part}, per monomer droplet equals:

$$N_{part} = \frac{a_{oil}}{a_{part}} = \frac{\pi (d_z - d_{part})^2}{d_{part}^2} \qquad \textbf{Equation III-8}$$

The volume of one silica nanoparticle, V_{part}, is simply calculated from:

$$V_{part} = \frac{\pi}{6} d_{part}^3 \qquad \textbf{Equation III-9}$$

The volume of one monomer droplet, V_{drop}, was evaluated from the volume of a sphere of diameter between ($d_z - d_{part}$), see Figure III-15.B:

$$V_{drop} = \frac{\pi}{6} (d_z - d_{part})^3 \qquad \textbf{Equation III-10}$$

Considering no excess/ free silica nanoparticles in the dispersed phase, the weight ratio of solids-stabilisers to oil (monomer), [m_{part}/m_{oil}], was combined with Equations III-8 to III-10:

$$\frac{m_{part}}{m_{oil}} = \frac{N_{part} V_{part} \rho_{part}}{V_{drop} \rho_{oil}} = \pi \frac{d_{part}}{(d_z - d_{part})} \frac{\rho_{part}}{\rho_{oil}} \qquad \textbf{Equation III-11}$$

Where m_{part}, m_{oil} represent the masses of colloidal silica and oil, respectively. ρ_{part} and ρ_{oil} are the densities of the silica nanoparticles and the oil. ρ_{part} of Ludox TM-40 was considered to be 1.75 g cm^{-3} and ρ_{oil} was given a representative value of 0.9 g cm^{-3} for the calculations. The results are presented in the graph of Figure III-16. Silica-to-oil weight ratios are plotted as a function of the oil droplet diameter for silica nanoparticles of 25 nm, 15 nm or 8 nm in diameter.

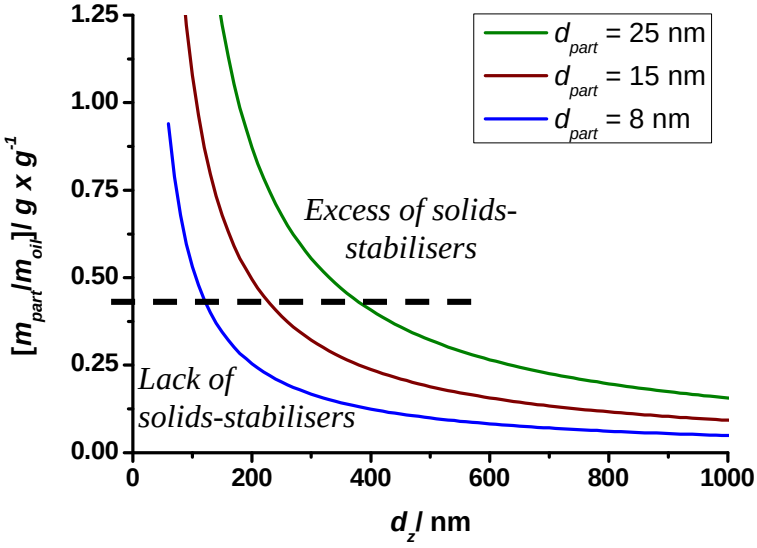

Figure III-16. Graph of the solids-stabilisers-to-oil weight ratio versus the droplet diameter for spherical stabilisers of diameter of 25 nm (green curve), 15 nm (brown curve) and 8 nm (blue curve).

This graph verifies the experimental observation given in the previous section. It can be read that for a weight ratio in silica-to-monomer of 0.40, silica can fully cover (stabilise) uniform droplets with a diameter of not smaller than ~370 nm. In our experiments, when enough energy was provided (*i.e.* ultra-sonication) thereby creating droplets as small as ~200 nm in diameter, partial droplet coalescence/demixing of the monomer (oil) occurred due to a lack in silica nanoparticles.

III.3.6. Solids-stabilised latexes of poly(vinyl acetate) in suspension polymerisation

Poly(vinyl acetate) (PVAc) latexes armoured with a layer of silica nanoparticles were prepared in a suspension polymerisation process. The obtained solids-stabilised emulsion of VAc with overall contents of 4.7 and 16.5

wt% in silica nanoparticles and monomer, respectively, was polymerised solidified upon polymerisation. Interestingly, two particle size distributions were obtained. From SEM analysis not only armoured polymer particles of about 2 to 15 µm in diameter were observed but also submicron (< 200 nm in diameter) hybrid particles were formed (see Figure III-17). The latest were attributed to the phenomenon of secondary nucleation due to the high water solubility of vinyl acetate monomer. We therefore developed further the emulsion polymerisation process as a route for the synthesis of armoured poly(vinyl acetate) latexes, Chapter IV.

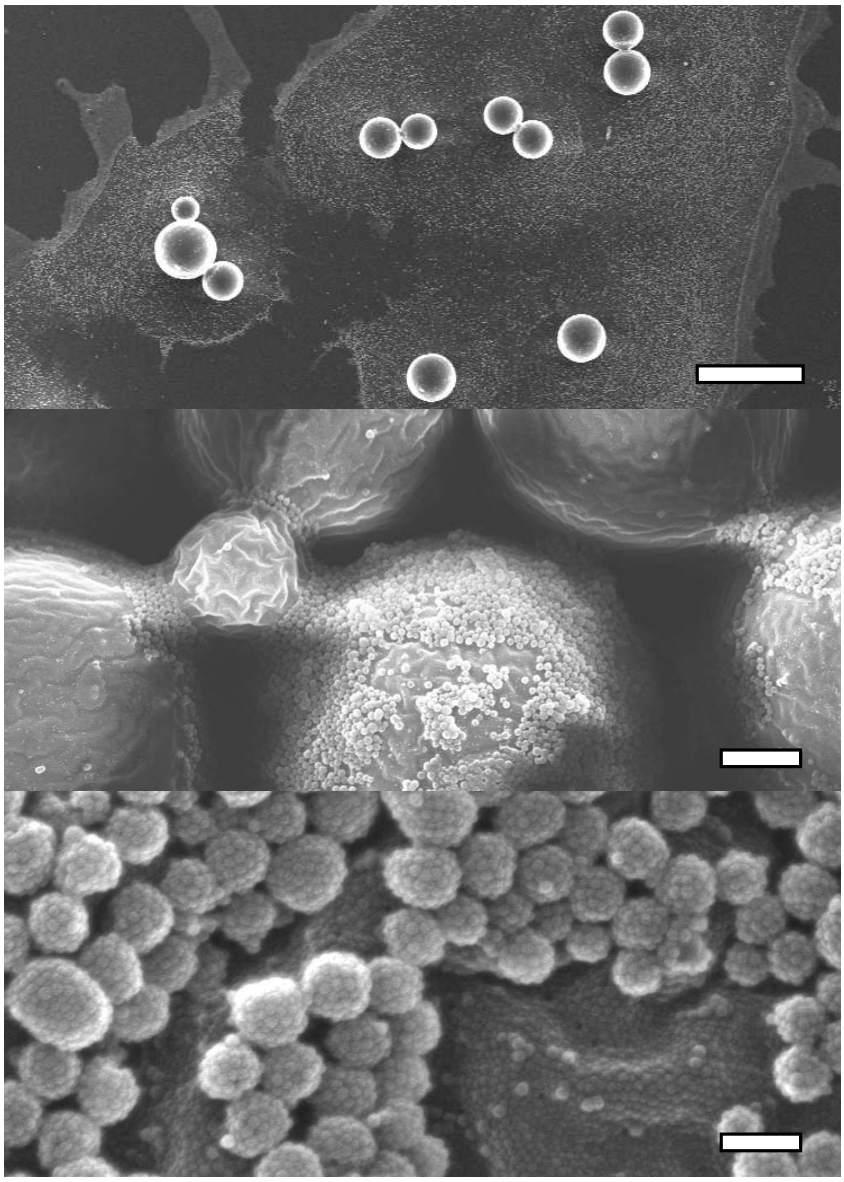

Figure III-17. SEM micrographs of Ludox(TM-40)-poly(vinyl acetate) latex prepared via solids-stabilised suspension polymerisation (CC-2-344). Scale bars (A) 20 µm, (B) 2 µm and (C) 200 nm.

III.4. Conclusions

We investigated the assembly of solids particles of silica at liquid-liquid interfaces for the preparation of armoured polymer latexes. Surface properties of the Ludox silica nanoparticles were tuned by modifying pH of the aqueous phase for the stabilisation of emulsion droplets. Ludox-armoured polystyrene latex particles were successfully prepared using a minimemulsion

polymerisation process. The size of the polymer particles was found to be inversely proportional to the size of the stabilising Ludox blocks and this was described from the interfacial and line tensions of a solids-stabilised system of emulsion droplets. High volume fraction emulsions (up to 80 vol%) were obtained with droplets in the micronsize range, whereas, in agreement with coverage calculations, limitations were found for the preparation of miniemulsion (submicron-size) droplets due to the very high surface area created. Finally, upon solidification of the monomer droplet in a suspension polymerisation process, poly(vinyl acetate) latexes armoured with a layer of silica nanoparticles were synthesised. A bimodal distribution of latex particles was obtained; not only micronsized particles were formed but secondary nucleation also led to the formation of sub-micronsized armoured polymer particles. This route is developed further in the next chapter, where we investigated the formation of Ludox(TM-40) armoured polymer particles.

III.5. References

1. Fortuna, S.; Colard, C. A. L.; Troisi, A.; Bon, S. A. F., *Langmuir* **2009,** *25* (21), 12399-12403.
2. Binks, B. P.; Lumsdon, S. O., *Phys. Chem. Chem. Phys.* **1999,** *1* (12), 3007-3016.
3. Binks, B. P.; Lumsdon, S. O., *Phys. Chem. Chem. Phys.* **2000,** *2* (13), 2959-2967.
4. Binks, B. P.; Lumsdon, S. O., *Langmuir* **2000,** *16* (23), 8622-8631.
5. Binks, B. P.; Lumsdon, S. O., *Langmuir* **2000,** *16* (6), 2539-2547.
6. Horozov, T. S.; Binks, B. P.; Aveyard, R.; Clint, J. H., *Colloid Surface A* **2006,** *282+283*, 377-386.
7. Binks, B. P.; Liu, W.; Rodrigues, J. A., *Langmuir* **2008,** *24* (9), 4443-4446.
8. Binks, B. P.; Whitby, C. P., *Langmuir* **2004,** *20* (4), 1130-1137.
9. Choi, J. Y.; Kim, C. H.; Kim, D. K., *J. Am. Ceram. Soc.* **1998,** *81* (5), 1184-1188.
10. Wu, Z.; Han, H.; Han, W.; Kim, B.; Ahn, K. H.; Lee, K., *Langmuir* **2007,** *23* (14), 7799-7803.
11. Finkle, P.; Draper, H. D.; Hildebrand, J. H., *J. Am. Chem. Soc.* **1923,** *45*, 2780-8.
12. Golemanov, K.; Tcholakova, S.; Kralchevsky, P. A.; Ananthapadmanabhan, K. P.; Lips, A., *Langmuir* **2006,** *22* (11), 4968-4977.
13. Binks, B. P., *Curr. Opin. Colloid In.* **2002,** *7* (1,2), 21-41.
14. Aveyard, R.; Binks, B. P.; Clint, J. H., *Adv. Colloid. Interfac.* **2003,** *100-102*, 503-546.
15. Hassander, H.; Johansson, B.; Törnell, B., *Colloid Surface* **1989,** *40*, 93-105.
16. Midmore, B. R., *Colloid Surface A* **1998,** *132* (2-3), 257-265.
17. Prestidge, C. A.; Barnes, T.; Simovic, S., *Adv. Colloid Interfac.* **2004,** *108-109*, 105-118.
18. Binks, B. P.; Whitby, C. P., *Colloid Surface A* **2005,** *253* (1-3), 105-115.
19. Binks, B. P.; Rodrigues, J. A.; Frith, W. J., *Langmuir* **2007,** *23* (7), 3626-3636.
20. Ghouchi Eskandar, N.; Simovic, S.; Prestidge, C. A., *Phys. Chem. Chem. Phys* **2007,** *9* (48), 6426-6434.
21. Cummins, P. G.; Staples, E.; Penfold, J., *J. Phys. Chem.* **1990,** *94* (9), 3740-5.
22. Frelichowska, J.; Bolzinger, M.-A.; Chevalier, Y., *Colloid Surface A* **2009,** *343* (1-3), 70-74.
23. Hohenstein, W. P.; Mark, H., *J. Polym. Sci.* **1946,** *1*, 127-45.
24. Hohenstein, W. P.; Mark, H., *J. Polym. Sci.* **1946,** *1*, 549-80.
25. Wiley, R. M. Clay-thickened suspension-polymerization of vinyl compounds. U.S. Patent 2,886,559, 1959.
26. Wiley, R. M. Suspension polymerization. U.S. Patent 2,932,629, 1960.
27. Tiarks, F.; Landfester, K.; Antonietti, M., *Langmuir* **2001,** *17* (19), 5775-5780.
28. Zhang, K.; Wu, W.; Meng, H.; Guo, K.; Chen, J. F., *Powder Technol.* **2009,** *190* (3), 393-400.

29. Zhang, Y.; Chen, H.; Shu, X.; Zou, Q.; Chen, M., *Colloid Surface A* **2009,** *350* (1-3), 26-32.
30. Thomson, J. J., *Philos. Mag.* **1904,** *7* (39), 237-265.
31. Curl, R. F.; Smalley, R. E., *Science* **1988,** *242* (4881), 1017-22.
32. Guo, Y.; Karasawa, N.; Goddard, W. A., III, *Nature* **1991,** *351* (6326), 464-7.
33. Bausch, A. R.; Bowick, M. J.; Cacciuto, A.; Dinsmore, A. D.; Hsu, M. F.; Nelson, D. R.; Nikolaides, M. G.; Travesset, A.; Weitz, D. A., *Science* **2003,** *299* (5613), 1716-8.
34. Lipowsky, P.; Bowick, M. J.; Meinke, J. H.; Nelson, D. R.; Bausch, A. R., *Nat. Mater.* **2005,** *4* (5), 407-411.
35. Pieranski, P., *Phys. Rev. Lett.* **1980,** *45* (7), 569-72.
36. Colver, P. J.; Chen, T.; Bon, S. A. F., *Macromol. Symp.* **2006,** *245-246*, 34-41.
37. Clint, J. H.; Taylor, S. E., *Colloid Surface* **1992,** *65* (1), 61-67.
38. Zaccarelli, E., *J. Phys. Condens. Mat.* **2007,** *19* (32), 323101/1-323101/50.
39. Bon, S. A. F.; Colver, P. J., *Langmuir* **2007,** *23* (16), 8316-8322.
40. Aveyard, R.; Beake, B. D.; Clint, J. H., *J. Chem. Soc. Faraday T.* **1996,** *92* (21), 4271-4277.
41. Aveyard, R.; Clint, J. H., *J. Chem. Soc. Faraday T.* **1995,** *91* (1), 175-6.
42. Aveyard, R.; Clint, J. H., *J. Chem. Soc. Faraday T.* **1996,** *92* (1), 85-9.
43. Widom, B., *J. Phys. Chem.-US* **1995,** *99* (9), 2803-6.

Chapter IV.

Silica-armoured poly(vinyl acetate) latexes made using solids-stabilised emulsion polymerisation[a]

A versatile emulsion polymerisation process is developed in which solid nanoparticles are used as stabiliser, thereby replacing the role of surfactants, allowing the simple fabrication of armoured nanocomposite of poly(vinyl acetate) latexes. Key mechanistic events of solids-stabilised emulsion polymerisations are described and we demonstrate the use of disc centrifugation as a quantitative tool to determine the fate of nanoparticles in their use as solids-stabilisers.

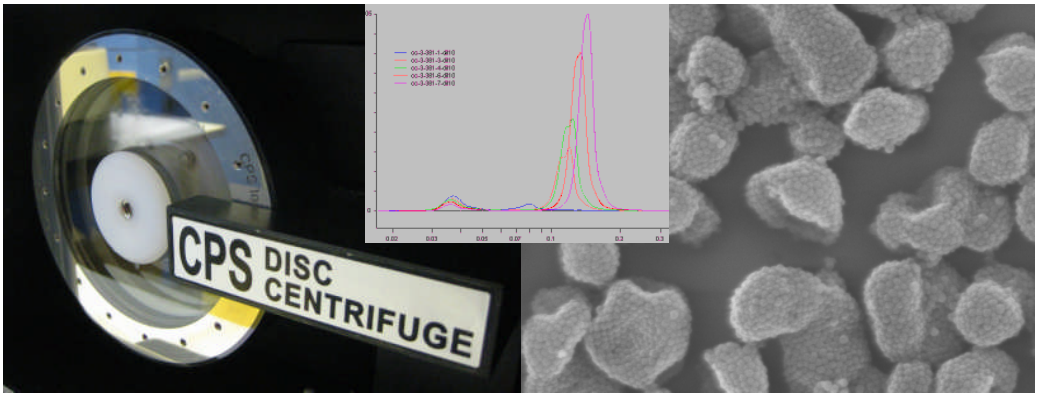

[a] Part of this work was published

1. Colard, C. A. L.; Teixeira, R. F. A.; Bon, S. A. F., *Langmuir* **2010,** *26* (11), 7915-7921.

2. Colver, P. J.; Colard, C. A. L.; Bon, S. A. F., *J. Am. Chem. Soc.* **2008,** *130* (50), 16850-16851.

IV.1. Introduction

A considerable number of research groups have reported on the preparation of inorganic armoured polymer latexes using a single step heterogeneous polymerisation process.[2-12] Armes *et al.* described the synthesis of hybrid polymer latexes armoured with silica nanoparticles using heterocoagulation based on electrostatic attraction with the aid of auxiliary monomers/initiators as assembly tool to produce the raspberry-like morphologies.[2-5] They extended their work using commercial alcoholic silica sols in dispersion polymerisation for the preparation of submicron-sized armoured polystyrene latexes[4-5] and recently reported a simple route to synthesise armoured polystyrene latex particles in emulsion polymerisation using glycerol-functionalised silica.[3] Armoured polystyrene latexes involving acid-base interactions between a co-monomer, 4-vinyl pyridine, and highly charged silica particles were prepared by Antonietti *et al.*.[6] Song *et al.*[7] recently reported the use of titania as solid stabiliser and photocatalyst and found that the stability of the dispersion was improved by electrostatic interactions upon use of the anionic co-monomer sodium (styrene sulfonate).[8] Chen and co-workers reported an emulsion polymerisation process using an auxiliary cationic co-monomer, 2-(methacryloyl)ethyltrimethylammonium chloride, to promote adsorption of nanosilica onto growing latex particles of poly(styrene) and poly(*n*-butyl acrylate).[9] Sheibat-Othman and Bourgeat-Lami studied the synthesis of polystyrene/silica (PS/SiO_2) and poly(styrene-co-methyl methacrylate)/SiO_2 composite latex particles by surfactant-free solids-stabilised emulsion polymerisation in the presence of small amounts of poly(ethylene glycol)

monomethylether methacrylate (PEGMA) macromonomer to promote nanoparticle adhesion to the surface of the latex particles.[11] We recently reported on the fabrication of waterborne hybrid polymer latexes armoured with silica nanoparticles *via* emulsion polymerisation without addition of any surfactant or co-monomer.[12]

The preparation of silica nanoparticle armoured poly(vinyl acetate) latexes *via* emulsion polymerisation which will be developed in this chapter was also recently investigated by Wu *et al.* who ascribed adhesion of the silica nanoparticles onto the surface of the latex particles to hydrogen bond interactions.[10]

In all of these heterogeneous polymerisation processes the presence of the inorganic nanoparticles not only has a marked influence on the final mechanical and physical properties of the polymer dispersions, but also plays a key role in the kinetic events throughout the polymerisation reaction. The armoured layer of inorganic nanoparticles on the surface of latex particles has a pronounced effect on radical entry and exit events in (mini)emulsion polymerisations.[11, 13-14] The relative amounts of nanoparticles with respect to both water and monomer used in the polymerisation processes are critical parameters. The surface chemistry of the nanoparticles dictates their affinity between the water phase and their adsorbed state at the surfaces of the latex particles which determines whether the synthesis of the nanocomposite armoured polymer colloids is successful. Note that we make the assumption here that nanoparticles do not get fully encapsulated, which potentially is possible for certain systems. The presence of the nanoparticles not only influences the colloidal stability of the system but also can show a profound effect on the number of armoured particles formed

and thus on the average particle size and the particle size distribution of the hybrid polymer dispersion.

A method to follow the concentration of nanoparticles in the water phase throughout the polymerisation process would therefore be of great help to shine a light on the complex interplay of mechanistic events. Monitoring the amount of nanoparticles however is not that trivial, especially not when there is no large size difference (approximately one order of magnitude between their diameter) between the nanoparticles and the armoured supracolloidal structures. Atomic force and electron microscopic techniques are labour intensive, particle tracking using dark field microscopy is complicated by difference in scattering intensities, dynamic light scattering suffers from its light intensity scaling with the radius of colloids to the power six, and hydrodynamic chromatography commonly uses a surfactant containing eluent phase which upon analysis would lead to detachment of nanoparticles that were adhered to the surface of the polymer latex.

Herein, we report an emulsion polymerisation process of vinyl acetate in which colloidal stability was provided by nanosized solid particles of silica that adhered to the surface of the polymer colloids, thereby replacing the role of surfactants. This resulted in polymer latexes which were armoured with a layer of nanoparticles. The mechanism of particle formation in our solids-stabilised system is described and discussed in terms of overall solid content and silica-to-monomer ratio. We demonstrated that a disc centrifuge brought outcome and could be used as a quantitative monitoring tool to measure the concentration of nanoparticles in the water phase throughout solids-stabilised emulsion polymerisations. We performed series of emulsion polymerisations in presence

of silica nanoparticles (Ludox TM-40, *ca.* 25 nm in diameter) and showed that our developed method to quantify the amount of silica nanoparticles in the water phase throughout the polymerisation process is an invaluable tool to explain features such as the packing densities of the nanoparticles on the surface of the latex particles and occasional limited coalescence of armoured particles, observed in the solids-stabilised emulsion polymerisations.

IV.2. Experimental

IV.2.1. Materials

Monomers, vinyl acetate (VAc) and vinyl pivalate (VPiv), were purchased from Aldrich at 99% or greater purity and used as received. Ludox TM-40 sol (colloidal silica, 40 wt% in water) was purchased from Aldrich. HCl (aq. 37 wt%, reagent grade) was supplied by BDH. Potassium persulfate (KPS, 99+% p.a) was obtained from Fluka. Deionised water was used in all experiments. Poly(vinyl chloride) (PVC) standard latex (0.377 μm particle diameter) and *n*-dodecane were provided by Analytik Ltd. Sucrose (analytical reagent grade) was purchased from Aldrich and used as received.

IV.2.2. Equipment

Emulsion polymerisations were carried out in round bottom flasks or in a double-walled cylindrical glass reactor (250 mL, Asynt Ltd.) equipped with an external circulating heating bath (Julabo F-25 unit), a condenser, and a four-bladed metal overhead turbine stirrer fitted at approximately 2 cm from the bottom of the reactor vessel (Cowie Ltd.) typically running at 300 rpm. pH measurements were performed on a pH-Meter (765 calimatic, Knick). A disc centrifugation particle sizer (CPS Disc Centrifuge, Model DC24000, CPS

Instruments Inc.) was used to develop our quantitative method to monitor and determine the amount of silica nanoparticles in the water phase throughout the solids-stabilised emulsion polymerisations. Average particle sizes and dispersities of the armoured latexes were measured by dynamic light scattering using a Malvern Zetasizer Nano. SEM analyses were performed using a Zeiss Supra55VP FEGSEM with an EBSD camera and the samples were prepared on silicon wafers (kindly donated by Wacker Chemie AG) to be analysed uncoated. TEM analyses were performed on a 1200EXII TEM with a 1K Gatan camera using Formvar-Film grids (200 Mesh Cu, Agar Sc. S138). An Analytical Balance (Precisa XT 220A) and micropipettes Pipetman P200 (20 – 200 μL) and P1000 (200 – 1000 μL) were used for accurate measurements.

IV.2.3. Typical solids-stabilised emulsion polymerisation

A 40.0 wt% solution of Ludox TM-40 silica sol (33.0 g, 5.7 wt% overall, or 44.0 wt% based on monomer) was diluted and dispersed in 167.0 g of deionised water. The pH of the dispersion was adjusted with concentrated HCl (aq) to pH ~4.5 and was placed under a nitrogen atmosphere in a 250 mL double-walled glass reactor by purging. Monomer, 30.0 g (13.0 wt%), was added and the reaction mixture was heated to 65 ºC, whilst stirring at 300 rpm. The emulsion polymerisation was started upon addition of 0.13 g KPS dissolved in 3.0 g of water. Monomer conversion was monitored *via* gravimetry by taking typically samples of ~2 g by syringe. All final monomer conversions were >95%. Contents and ratios of all experiments can be found in Table IV-1 to V-5. Refer to Appendix D for exact amounts of all experiments (section D.1).

Table IV-1. Composition (overall weight contents and weight ratios) of the Ludox(TM-40) stabilised poly(vinyl acetate) latexes prepared by emulsion polymerisation. Reactions conducted at 65 ºC and different values of pH.

Exp.	*Monomer content/ wt%*	*Silica content/ wt%*	*Silica: monomer/ g×g^{-1}*	*KPS: monomer/ g×g^{-1}*	*pH of Ludox sol/ -*
cc-2-342	7.6	4.2	0.56	0.0060	3.0
cc-3-354	7.6	4.2	0.56	0.0055	4.5
cc-3-355	7.6	4.4	0.58	0.0056	5.5

Table IV-2. Composition (overall weight contents and weight ratios) of the Ludox(TM-40) stabilised poly(vinyl acetate) latexes prepared by emulsion polymerisation. Reactions conducted with various solids contents at pH ~4.5 and 65 ºC.

Exp.	*Monomer content/ wt%*	*Silica content/ wt%*	*Overall solids/ wt%*	*Silica: monomer/ g×g^{-1}*	*KPS: monomer/ g×g^{-1}*
cc-3-367	11.3	5.0	16.3	0.45	0.0038
cc-3-377	19.8	8.7	28.5	0.44	0.0042

Table IV-3. Composition (overall weight contents and weight ratios) of the Ludox(TM-40) stabilised poly(vinyl acetate) latexes prepared by emulsion polymerisation. Reactions conducted with various silica-to-monomer ratios at pH ~4.5 and 65 ºC.

Exp.	*Monomer content/ wt%*	*Silica content/ wt%*	*Overall solids/ wt%*	*Silica: monomer/ g×g^{-1}*	*KPS: monomer/ g×g^{-1}*
cc-2-345B	7.3	12.1	19.4	1.67	0.0162
cc-2-342	7.6	4.2	11.9	0.56	0.0060
cc-3-379	19.9	4.3	24.2	0.22	0.0042
cc-3-369	20.0	10.0	29.9	0.50	0.0050

Table IV-4. Ludox(TM-40)-stabilised poly(vinyl acetate) latexes prepared by emulsion polymerisation at 65 ºC in a semi-batch process by feeding vinyl acetate until coagulation occurred (see text, section IV.3.4.1).

Exp.	*Monomer feed/ mL×min^{-1}*	*Water/ mL*	*Silica: water ratio/ g×g^{-1}*	*KPS: water ratio/ g×g^{-1}*
cc-3-357	0.35	228	2.2	0.00023
cc-3-371	2.25	175	12.5	0.00143

Table IV-5. Composition (overall weight contents and weight ratios) of the polymer latexes prepared by emulsion polymerisation in presence of Ludox(TM-40) silica nanoparticles. Reactions conducted with vinyl acetate (VAc) and vinyl pivalate (VPiv) monomers at pH ~4.5 and sampled for disc centrifuge measurements.

Exp. *(Monomer)*	*Monomer content/ wt%*	*Silica content/ wt%*	*Silica content in water phase/ wt%*	*Silica: monomer ratio/ g×g^{-1}*	*KPS: monomer ratio/ g×g^{-1}*
cc-3-390 (VPiv)	13.1	5.8	6.6	0.44	0.0043
cc-3-381 (VAc)	13.0	5.7	6.5	0.44	0.0043
cc-2-345E (VAc)	11.1	11.6	13.1	1.04	0.0081

IV.2.4. Typical procedure of disc centrifugation measurements

We operated the disc centrifuge at maximum speed (24,000 rpm). A density gradient was built from 24.0 wt% to 8.0 wt% sucrose solutions in deionised water. The gradient was prepared by the subsequent injections of mixtures of a 24.0 wt% and an 8.0 wt% sucrose solution in water: (1.6 + 0) mL, (1.4 + 0.2) mL, (1.2 + 0.4) mL, (1.0 + 0.6) mL, (0.8 + 0.8) mL, (0.6 + 1.0) mL, (0.4 + 1.2) mL, (0.2 + 1.4) mL, (0 + 1.6) mL, respectively. Next we injected 0.5 mL of

dodecane to extend the life time of the gradient by limiting evaporation. A waiting period of 15 minutes was essential for the gradient to become linear, consistent and stable. After this, samples could be analysed. Typically the gradient remained stable for a period of 5-6 h. A typical run to determine the concentration of silica nanoparticles took approximately 20-30 min. After this a new gradient had to be built. As calibration standard a waterborne poly(vinyl chloride) latex with average particle diameter of 377 nm was used. The settings of the software procedure were, for the sample parameters: maximum diameter = 1 μm, minimum diameter = 0.017 μm, particle density = 1.75 $g.mL^{-1}$, particle refractive index = 1.45, particle absorption = 0.001 K, for the calibration standard parameters: peak diameter = 0.377 μm, half height peak width = 0.1 μm, particle density = 1.385 $g.mL^{-1}$ and for the fluid parameters:[15] fluid density = 1.064 $g.mL^{-1}$, fluid refractive index = 1.357, fluid viscosity = 1.3 cP.

Each analysis consisted of the injection of about 0.05 mL of PVC standard followed by the injection of about 0.1 mL of sample. The syringe was systematically weighed before and after injection of the sample to determine accurately the amount injected. Colloidal silica nanoparticles solutions of 0.39 wt%, 0.33 wt%, 0.28 wt%, 0.22 wt%, 0.21 wt%, 0.15 wt% and 0.11 wt% were prepared by weight from the commercial Ludox TM-40 sol of 40.0 wt% and were used as quantitative calibration standards. Samples taken throughout the solids-stabilised emulsion polymerisations were diluted 10 times with deionised water, using micropipettes, before injection into the disc centrifuge.

The analysis of the traces, signal intensity, corresponding to the colloidal silica nanoparticles on the CPS traces, is discussed in Appendix D, Section D.3.

IV.3. Results and discussion

Armoured poly(vinyl acetate) (PVAc) particles were successfully prepared using a soap-free emulsion polymerisation process. We performed various series of emulsion polymerisations of vinyl acetate in the presence of silica nanoparticles of about 25 nm in diameter (Ludox TM-40). A monolayer of silica nanoparticles adhered on the surface of the polymer particles. By transmission electron microscopy analyses, it was verified that no silica nanoparticles were encapsulated (see for instance Appendix D, Figure D.1).

IV.3.1. Optimisation of the pH for the synthesis of poly(vinyl acetate) latex particles armoured with silica nanoparticles

In our first series, we used vinyl acetate monomer at monomer-to-water ratios of 7 – 8 wt% and silica nanoparticles-to-water ratio of 4 – 5 wt% (see Table IV-1.), thereby keeping the silica-to-monomer ratio constant at a relatively high value, *ca.* 0.57. In order to minimise hydrolysis of vinyl acetate monomer/polymer a pH of about 4.5 is suitable.[16] Herein we varied the pH of the water phase (3.0, 4.5 and 5.5) to verify the influence of the surface charge density of the silica nanoparticles for the formation of armoured composite latexes. The charge density bared by the obtained armoured polymer particles was evaluated *via* zeta potential measurements of the latexes (Table IV-6).

Table IV-6. pH of the Ludox sol, average particle sizes d_z and dispersity indices D_I (DLS), pH and zeta potentials of Ludox(TM-40) stabilised PVAc latexes.

Exp.	*pH Ludox sol/ -*	*d_z (DLS)/ nm*	*D_I (DLS)/ -*	*pH final latex/ -*	*Zeta potential/ mV*
cc-2-342	3.0	377.0	0.100	2.9	-28.0
cc-3-354	4.5	387.7	0.085	3.4	-35.6
cc-3-355	5.5	286.3	0.018	4.7	-44.1

All emulsion polymerisation reactions carried out at initial value of pH of 3.0, 4.5 and 5.5 led to the formation of armoured latex particles with low dispersity indices (D_I ~ 0.1 or lower), see Figure IV-1.A. As the pH increased more hydroxyl group on the silica nanoparticle surface were deprotonated. Zeta potentials of the obtained latexes ranged from -28.0 down to -35.6 and -44.1 mV at corresponding pH of 2.9, 3.4 and 4.7 respectively (see Chapter III, Section III.3.6 and Figure III.2 for the graph of the zeta potential as a function of the pH of Ludox TM-40 colloidal silica dispersions). The monolayer of silica nanoparticles arranged around the polymer particles in closely-packed patterns independently from the pH, see SEM images in Figure IV-1.B and C. This was different from the case of poly(methyl methacrylate) nanocomposite particles prepared at a pH of about 5.5 for which an inter-particle distance of about 10 nm between the silica nanoparticles was observed.[1, 12] The reason for this was probably a strong adherence of the silica nanoparticles onto the surface of the polymer colloids thereby overcoming the inter-particle electrostatic repulsions. Although the particles were dispersed in aqueous medium, we postulated the presence of hydrogen bonding interactions between the hydroxyl group of the silanol and the carbonyl groups of the PVAc for such composite latexes which was confirmed by Wen *et al*. who performed infrared spectroscopy.[10]

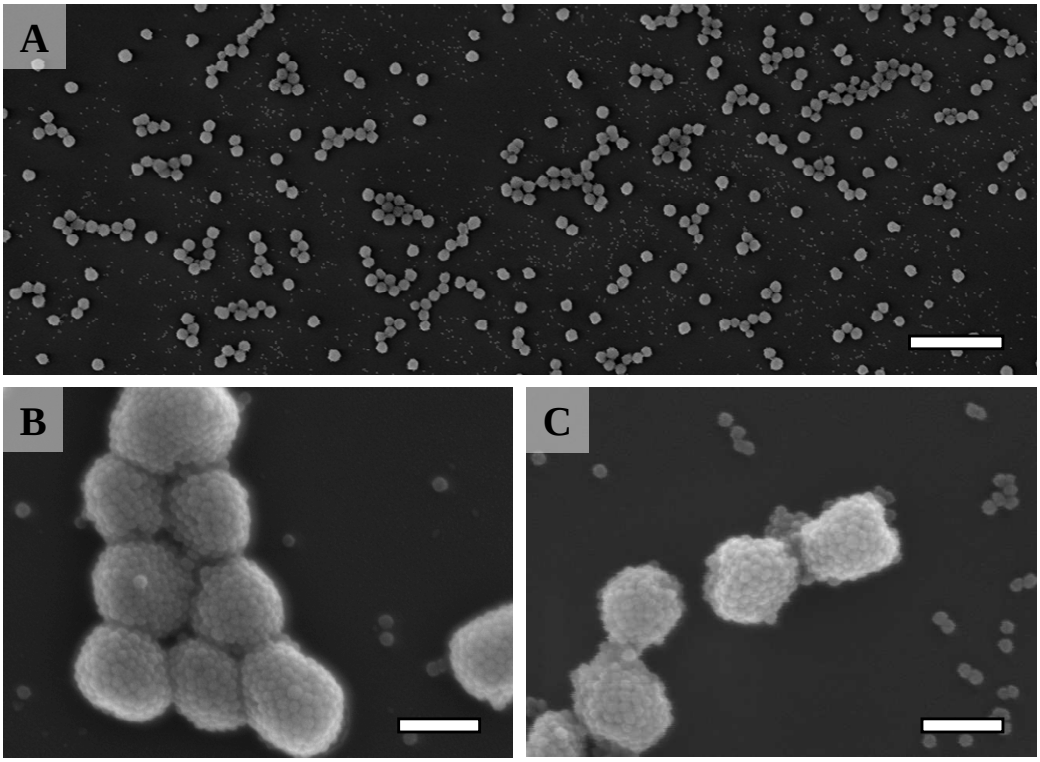

Figure IV-1. SEM images of Ludox TM-40 stabilised PVAc latexes prepared in emulsion polymerisation. (A) lower magnification showing relatively narrow particle size distribution (latex CC-2-342, scale bar: 2 μm). (B) and (C) zoom-in showing the close-packing of the silica nanoparticles on the surface at both pH 3.0 (latex CC-2-342) and 5.5 (latex CC-3-355), respectively (scale bars: 200 nm).

The surface charge density logically also had an influence on the latex stability towards flocculation and sedimentation. This is further developed in Chapter V, Section V.3.1.1.

IV.3.2. Silica-stabilised poly(vinyl acetate) latexes with increased overall solids-content

Latexes with high solids content can be required for commercial application; commonly 50 – 60 wt% dispersions. By increasing the overall solids content of our solids-stabilised latexes, both monomer and silica nanoparticles in same proportions (see Table IV-2) thereby keeping the silica-to-monomer ratio constant at about 0.45, latexes with similar particle size

distributions were obtained. That is to say armoured particles of poly(vinyl acetate) of about 350 nm with dispersity indices lower than 0.05 were obtained, see Table IV-7. Latexes with higher solids contents were obtained by feeding monomer to the reaction vessel (refer to Section IV.3.4).

Table IV-7. Composition (overall weight content and silica-to-monomer ratio) of Ludox(TM-40) stabilised PVAc latexes prepared by emulsion polymerisation. Reactions conducted at 65 ºC and pH ~4.5.

Exp.	*Overall solids/ wt%*	*Silica: monomer/ g×g^{-1}*	*d_z (DLS)/ nm*	*D_I (DLS)/ -*
cc-3-367	16.3	0.45	334.5	0.026
cc-3-377	28.5	0.44	364.7	0.007

IV.3.3. Influence of the silica-to-monomer ratio in our solids-stabilised system

As expected the silica-to-monomer ratio was found to have an influence on the particle size distribution of the prepared armoured latexes. A series of latexes synthesised in batch reactions is reported in Table IV-8.

Table IV-8. Recipes for the synthesis of Ludox TM-40 stabilised PVAc latexes prepared by emulsion polymerisation at 65 ºC and initial pH 4.0. By decreasing the ratio silica to monomer, larger particles with broader distributions were obtained in batch reactions.

Exp.	*Monomer content/ wt%*	*Silica content/ wt%*	*Silica: monomer/ g×g^{-1}*	*d_z (DLS)/ nm*	*D_I (DLS)/ -*
cc-2-345B	7.3	12.1	1.67	235.3	0.032
cc-2-342	7.6	4.2	0.56	480.4	0.119
cc-3-379	19.9	4.3	0.22	604.4	0.123

By decreasing the silica-to-monomer ratio from 1.67 to 0.22 g g^{-1}, *i.e.* the relative amount of solids-stabiliser, larger poly(vinyl acetate) particles were obtained with hydrodynamic diameter ranging from about 230 nm up to about 600 nm. However, broadening of the particle size distribution occurred as observed by SEM analysis (see Figure IV-2) and by DLS measurements with dispersity indices increasing from 0.03 to 0.12 (see Table IV-8).

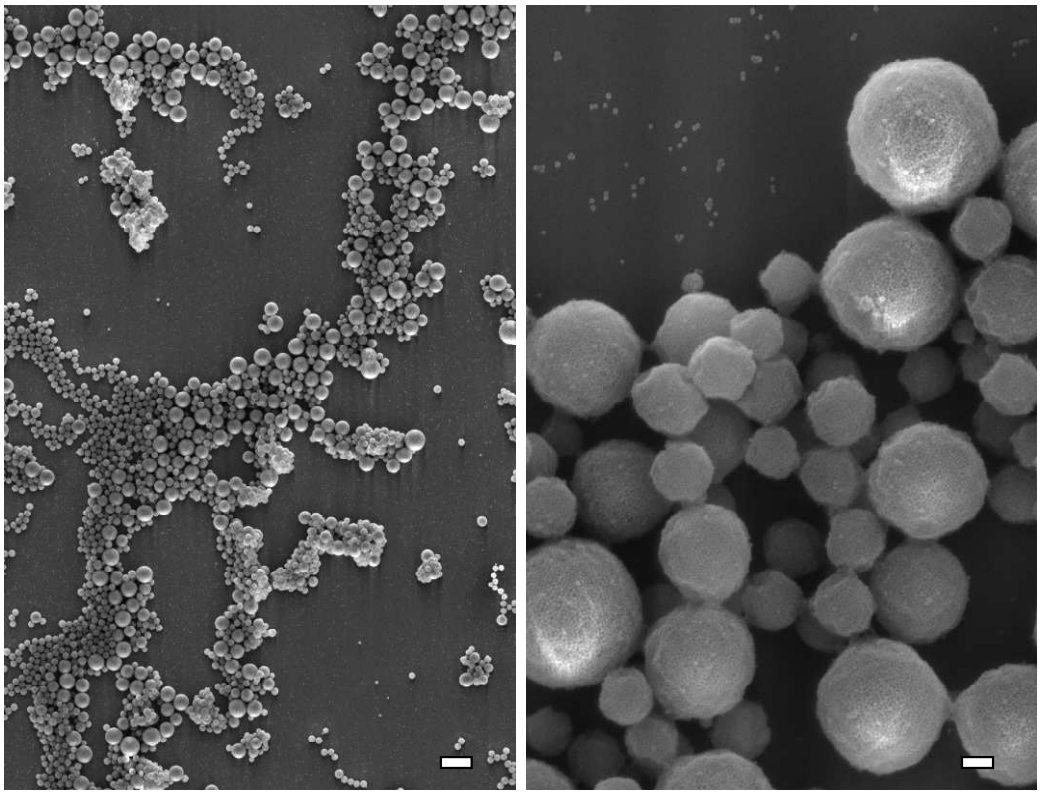

Figure IV-2. SEM images of Ludox TM-40 stabilised PVAc latex prepared in batch emulsion polymerisation for a low silica-to-monomer ration of 0.22 (cc-3-379). Scale bars 2 μm and 200 nm, left and right respectively.

This suggested that broadening of the particle size distribution was due to either the event of secondary nucleation or the inter-combination/coalescence of polymer particles due to a lack of silica nanoparticles (stabiliser). Further investigations were conducted to understand the key steps of the mechanistic of our solids-stabilised emulsion polymerisation process. It will be understood in

the following section that in this system coalescence of polymer particles was responsible for broadening particle distributions.

IV.3.4. Unravelling the mechanistic of the solids-stabilised emulsion polymerisation process

Vinyl acetate is known for its high water solubility (42.7 g L^{-1} at 60 ºC)[17], which favours polymerisation in the water phase in comparison to more hydrophobic monomers.[16] Formation of poly(vinyl acetate) particles in emulsion polymerisation has received considerable interest over the last century. Before describing our solids-stabilised system, it is to note that the mechanism of formation of poly(vinyl acetate) particles – (i) nucleation, (ii) growth and (iii) coalescence – appears to be heavily dependant on the quantity and efficiency of the employed stabiliser. For instance, French reported in 1958 on the emulsion polymerisation process of vinyl acetate using block copolymers of ethylene and propylene oxides as emulsifying agents.[18] It was found in this case that the number of polymer particles remained constant during the reaction and that by the time 13.5% conversion was reached all the monomer had diffused into the polymer particles but at 7.7% conversion vinyl acetate was largely in separate droplets. In 1995, Sangster *et al.* described the reversible swelling of poly(vinyl acetate) latex particles in sodium dodecyl sulphate (SDS) solutions.[19] They found that swelling increased from 0 to about 50% in volume with amounts of SDS ranging from 5.0 to 12.0 mM. This meant that swelling already occurred at SDS concentrations lower than its critical micelle concentration (CMC) of 8.0 mM. They also observed that in the presence of salt (sodium chloride 135 mM) which decreases the CMC of SDS, swelling occurred at lower concentrations in

SDS, around 2.0 to 4.0 mM, and was limited to 15% in volume even at a SDS concentration up to 10 mM.

In order to design silica-armoured poly(vinyl acetate) latexes, we needed to understand the key mechanistic steps of their formation. Herein we investigated the size distribution and the structure of the latex particles of our solids-stabilised system throughout the emulsion polymerisation process. Particle growth, under monomer starved and non-starved conditions, was first investigated. We then used disc centrifugation as a tool to measure the concentration of 'free' stabiliser (silica nanoparticles) in the aqueous phase throughout the polymerisation process.

IV.3.4.1. Preparation of solids-stabilised latexes under monomer starved and non-starved regimes

Semi-batch emulsion polymerisation reactions were performed by feeding vinyl acetate monomer to the reactor vessel throughout the process and samples were taken for analysis. Two sets of reactions were conducted and feeding rates ensured starved and non-starved conditions throughout the polymerisation process (exp. cc-3-357 with feeding rate of 0.35 mL min^{-1} and exp. cc-3-371, monomer feed of 2.25 mL min^{-1}, respectively (see Table IV-4)). Details on the instantaneous monomer conversion as a function of the amount of VAc added can be found in Figure D.1, Appendix D. The silica-armoured poly(vinyl acetate) latexes of both experiments had similar particle size distributions throughout the emulsion polymerisation process. Samples were analysed by scanning electron microscopy and by dynamic light scattering. For adequate comparison between experiments, the average particle diameter and the dispersity index were plotted as a function of the silica-to-polymer ratio rather

than the monomer conversion (see Figure IV-3). Note that consequently the graph reads from right to left as the polymerisation process occurred and the silica-to-polymer ratio decreased.

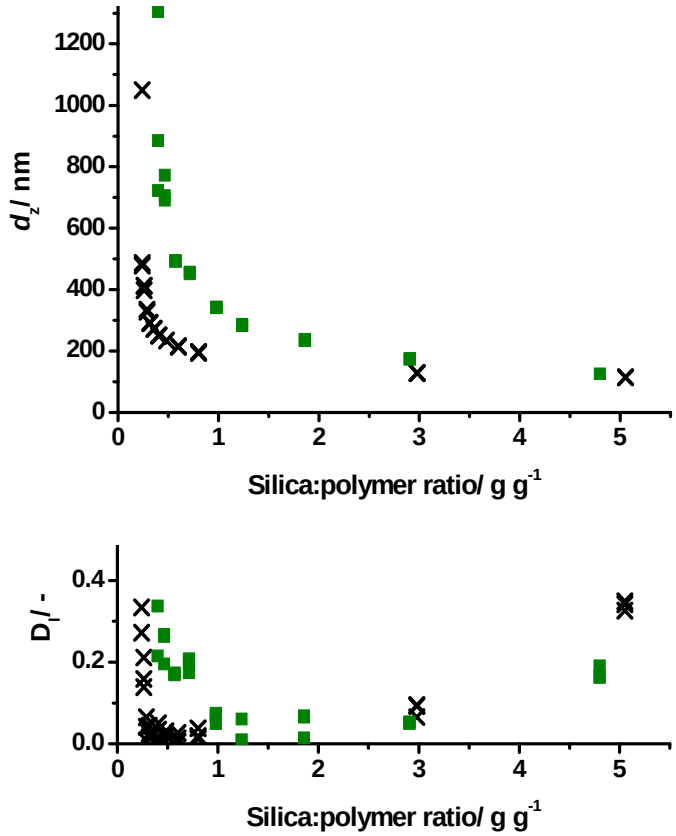

Figure IV-3. Average particle diameter, d_z (top), and dispersity, D_I, (bottom) versus the silica-to-polymer ratio throughout the (Ludox TM-40)-stabilised emulsion polymerisation of vinyl acetate. VAc fed for [✕] starved conditions (exp. cc-3-357) and [■] non-starved conditions (exp. cc-3-371).

The little shift in average particle diameter and dispersity indices observed in Figure IV-3 between the two processes of emulsion polymerisation are believed to be potentially due to the difference in solids contents and/or the overall rate of the polymerisation. In both cases, starved and non-starved monomer regimes, the data suggested the following mechanism for polymer particle formation. A short nucleation period was observed as dispersity indices decreased which was followed by particle growth (constant number in polymer

particles) characterised by low dispersity indices for silica-to-polymer ratios from 3 down to 1. At silica-to-polymer ratios around 0.5, the formation of doublet and triplet particles was observed. Those shapes formed by limited coalescence were attributed specifically to solids-stabilised systems due to the surface-to-volume excess in silica nanoparticles jamming onto the surfaces (see framed image in Figure IV-4, exp. cc-3-357). Upon addition of more monomer those shapes were lost and broad particle size distributions were obtained (see Figure IV-4, exp. cc-3-357). We observed by SEM imaging random density coverage amongst particles of diverse particle sizes. However, no small and smooth poly(vinyl acetate) particles were observed. We believe this confirmes the absence of secondary nucleation in our solids-stabilised system.

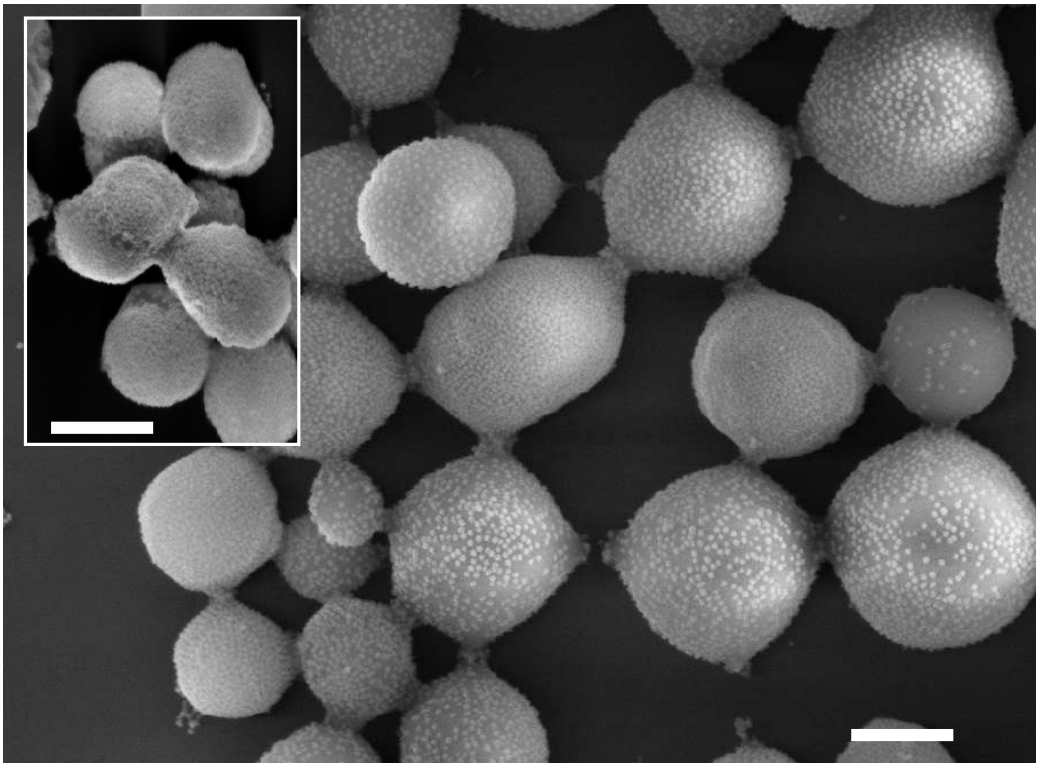

Figure IV-4. SEM images of a Ludox(TM-40)-stabilised poly(vinyl acetate) latex prepared in semi-batch emulsion polymerisation in starving condition of monomer (exp. cc-3-357): silica-to-polymer ratios of 0.22 (framed micrograph) and 0.07. Scale bars 500 nm.

IV.3.4.2. Investigation on the mechanism of particle formation in solids-stabilised latexes using disc centrifugation

To unravel the mechanistic role of the nanoparticles in these polymerisation processes and the related polymerisation kinetics a method to measure the concentration of the nanoparticles in the water phase at a given time, or extent of monomer conversion, in the nanoparticle-stabilised emulsion polymerisation process would be very useful. For reasons mentioned in the introduction of this chapter, we decided to explore disc centrifugation as a quantitative tool in the silica nanoparticle (Ludox TM-40, diameter approx. 24 nm)-stabilised emulsion polymerisations of vinyl acetate (VAc), or in the case of vinyl pivalate (VPiv) where no solids-stabilisation occurred. We will first discuss quantitative disc centrifugation, after which we highlight a simple approach to calculate the concentration of nanoparticles in the water phase throughout the particle growth period in solids-stabilised emulsion polymerisations, which was based on a model for the packing of nanoparticles onto the surface of the polymer latex particles. We then correlate the quantitative disc centrifugation data on the concentration of nanoparticles in the water phase throughout solids-stabilised emulsion polymerisations with our model and discuss the experimental observations that particle packing and thus nanoparticle partitioning showed monomer dependence, and that limited coalescence could occur leading to armoured non-spherical clusters.

Disc centrifugation for quantitative analysis

As a direct result of a difference in density, the application of a centrifugal force on a colloidal dispersion allows either sedimentation or creaming of

particles that under the normal gravitational force would remain dispersed. The disc centrifugation technique is based on this principle and is commonly used to measure particle size distributions of colloids.[11] A combination of particle mass and shape allows separation which is detected typically using turbidity as a measure, hereby employing a laser. Turbidity can be used quantitatively in order to determine the concentration of nanoparticles present in the water phase. In the disc centrifugation analysis of waterborne dispersions often a sucrose gradient of the aqueous spinning fluid is used to minimise peak broadening. We found that in order to get reliable and reproducible quantitative data good accuracy had to be taken in preparation of this sucrose gradient. The underlying reason was that variation in the sucrose concentration influences the differential refractive index, the turbidity and hence the signal intensity. Details on the technique and experimental procedure to build the sucrose gradient in the rotating disc can be found in the experimental section IV.2.4 and in the Appendix D, section D.3. The maximum sucrose molality used was 0.70 mol kg^{-1} of water with a corresponding density of ~ 1.064 g ml^{-1} and viscosity of ~ 1.3 cP.[32] This is less than the density of the nanocomposite polymer latexes and the Ludox silica, and therefore allowed sedimentation upon imposing the centrifugal force by rotation of the disc.[33]

In order to correlate the intensity of the detection signal to the concentration of the nanoparticles we injected a series of calibration standards of known concentration of Ludox(TM-40) silica nanoparticles dispersed in water. Note that it was important to accurately know the injected mass of the sample, as detection and thus signal intensity obviously correlated with the number of nanoparticles.

The calibration data for the signal intensity of the detector versus the concentration of the silica nanoparticles dispersed in water could be fitted with a linear expression for the range of concentrations investigated (linear fit: $R^2 > 0.95$)., that is up to *ca*. 0.40 wt% of silica nanoparticles in water. To correlate the detector signal to concentration we used three different methods of data analysis: (i) full area of the peak, (ii) lower half-area of the peak, and (iii) base-line corrected peak height (see Appendix D, section D.3.2 for details). The peak shape of the Ludox(TM-40) was constant throughout the series of calibration standards. The method measuring the height of the peak was most straightforward and accurate; the base-line corrected height measurements were not as sensitive to noise observed at small diameters on the left hand side of the peak. All further data was analysed using this method.

Theoretical model to determine the concentration of nanoparticles in the water phase

Our model was based on the assembly of the nanoparticles initially free in the water phase onto the surface of the growing latex particles. The total surface area provided by the monomer droplets was small in emulsion polymerisations, which allowed us to neglect the amount of nanoparticles adhered to the surface of the monomer droplets. The amount of nanoparticles in the water phase, C, expressed in number per gram of water, depended on the initial concentration of silica nanoparticles, C_0, and correlated with the amount of silica nanoparticles that adhered to the surface of the latex particles, C_S, expressed in the same dimensions:

$$C = C_0 - C_S \qquad \textbf{Equation IV-1}$$

In line with the cover calculations developed in Chapter III (section III.3.5.2), we assumed that no nanoparticles were encapsulated fully into the polymer particles, and also that colloidal silica and polymer particles were monodisperse in size, and both of spherical shape. When we knew the number of latex particles, and size, we could calculate their total surface area. Once we knew the adhesion behaviour of the nanoparticles and thus their packing patterns we were able to calculate the total amount of nanoparticles adhered, and thus C_S. The diameter of Ludox TM-40, d_{silica}, was measured to be 24.06 nm (+/- 3.36 nm) from TEM micrographs.[18] Values for the area which was covered by nanoparticles from the armoured polymer latex particle, A_{polym}, were obtained from the average hydrodynamic diameter for the armoured-polymer composite latex particles, d_z, as determined by dynamic light scattering, and the diameter of the silica nanoparticles (see Figure IV-5).

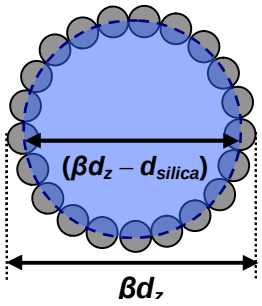

Figure IV-5. Representation of a solids-stabilised particle of hydrodynamic diameter d_z and actual diameter βd_z where β is a correcting factor (see text). The nanoparticles of silica are assembled on sphere of diameter ($\beta d_z - d_{silica}$) and area A_{polym}.

When we used the value for d_z as a measure for calculating the amount of nanoparticles adhered onto the polymer latex particles, we needed to keep in mind that (i) dynamic light scattering provides a hydrodynamic and higher order

mean value for the diameter of the particles, (ii) the nanocomposite armoured particles were of a non-smooth raspberry-type nature, whereby we assumed the formation of a single armoured layer. We therefore introduced a correction factor β. This led to:

$$A_{polym} = \pi\left(\beta d_z - d_{silica}\right)^2 \qquad \textbf{Equation IV-2}$$

To correlate our model to experimental data, different packing patterns and packing densities have been considered. An effective area "occupied" by one silica nanoparticle, A_{silica}, can be calculated with Equation IV-3.

$$A_{silica} = P\, d_{silica}^2 \qquad \textbf{Equation IV-3}$$

We introduce a packing parameter P to allow for correction as a result of different packing geometries and thus packing densities of the nanospheres onto the surface of the latex particle. We define P = 1 for a 2D square packing geometry, $A_{silica-2D}$, in which the silica squares touch each other (negligible thickness of double layer). Hexagonal packing of the nanospheres is more closely packed reducing the effective area occupied by each silica nanosphere, $A_{silica-hex}$, with $P = \sqrt{3}/2$, or 0.866. Both these values of P do not take into account the curvature, finite dimensions, and the non-monodisperse nature of Ludox TM-40 silica nanoparticles. To accommodate for this we therefore considered the packing density obtained from the Monte Carlo simulations that predicted the packing patterns of armoured Ludox TM-40-polystyrene latexes made *via* Pickering miniemulsion polymerisation.[18] The packing parameter P is found to be 0.909 for the assembly of 206 silica nanospheres on a spherical surface of 161.58 nm in diameter.

The total number of polymer particles (N_{polym}) per gram of water, C_{polym}, is found using:

$$C_{polym} = \frac{N_{polym}}{m_{water}} = \frac{m_{m,0} X_m \Big/ \rho_{polym}}{m_{water} \frac{\pi}{6} \left(\beta d_z - d_{silica}\right)^3} \qquad \textbf{Equation IV-4}$$

Where $m_{m,0}$ is the initial mass of monomer, m_{water} is the mass of water, X_m monomer conversion (determined by gravimetry), ρ_{polym} the density of the polymer. Note that we do not account for the particle swelling with a monomer-polymer swelling ratio of up to 7:1 in the case of vinyl acetate.[16]

The concentration of adhered silica particles, C_S, can be calculated from [$C_S A_{silica} = C_{polym} A_{polym}$] (Equations IV-2 to IV-4), which combined with Equations IV-1 leads to a final expression for C:

$$C = \frac{6}{m_{water} d_{silica}^{\ 2}} \left[\frac{m_{silica}}{\pi \rho_{silica} d_{silica}} - \frac{m_{m,0} X_m}{\rho_{polym} P\left(\beta d_z - d_{silica}\right)} \right] \qquad \textbf{Equation IV-5}$$

Where m_{silica} is the initial mass of silica and ρ_{silica} the density of silica.

Emulsion polymerisations carried out in presence of silica nanoparticles

Emulsion polymerisations were carried out using vinyl acetate (VAc) and vinyl pivalate (VPiv) as monomers in the presence of Ludox TM-40 silica nanoparticles. We carried out Ludox(TM-40)-stabilised emulsion polymerisations of vinyl acetate and vinyl pivalate at monomer contents of about 13 wt%, silica:monomer ratios of 0.44, using potassium persulfate as radical initiator at 0.13 g in 187.55 g of water (Table IV-5, exp. cc-3-381 and cc-3-390). In a third emulsion polymerisation batch of vinyl acetate, the content of

solid-stabiliser was doubled (silica:monomer ratio of 1.04), (Table IV-5, exp. cc-2-345E). Monomer conversion was followed with gravimetry, and the concentration of silica nanoparticles was monitored throughout the emulsion polymerisation process with our quantitative disc centrifugation method. The final polymer latexes were analysed by SEM (see Figure IV-6). From Figure IV-6(a), it can be seen that the emulsion polymerisation of vinyl pivalate in presence of Ludox(TM-40)-silica nanoparticles did not result in a nanocomposite armoured polymer latex. A reason for this might be the hydrophobicity of poly(vinyl pivalate). In comparison to poly(vinyl acetate) particles, the potential adhesion of the silica nanoparticles onto the particle surface *via* hydrogen bonding would be weakened as less hydroxyl groups are present. This behaviour for hydrophobic monomers has previously been observed[11-12] and the lack of adhesion could be overcome by either using small amounts of hydrophilic co-monomer, such as 4-vinylpyridine (4-VP),[6] 2-(methacryloyl)ethyltrimethyl-ammonium chloride,[9] poly(ethylene glycol) monomethylether methacrylate (PEGMA) macromonomer,[11] or by modifying the hydrophilicity of the nanoparticles, such as glycerol-functionalised silica.[3]

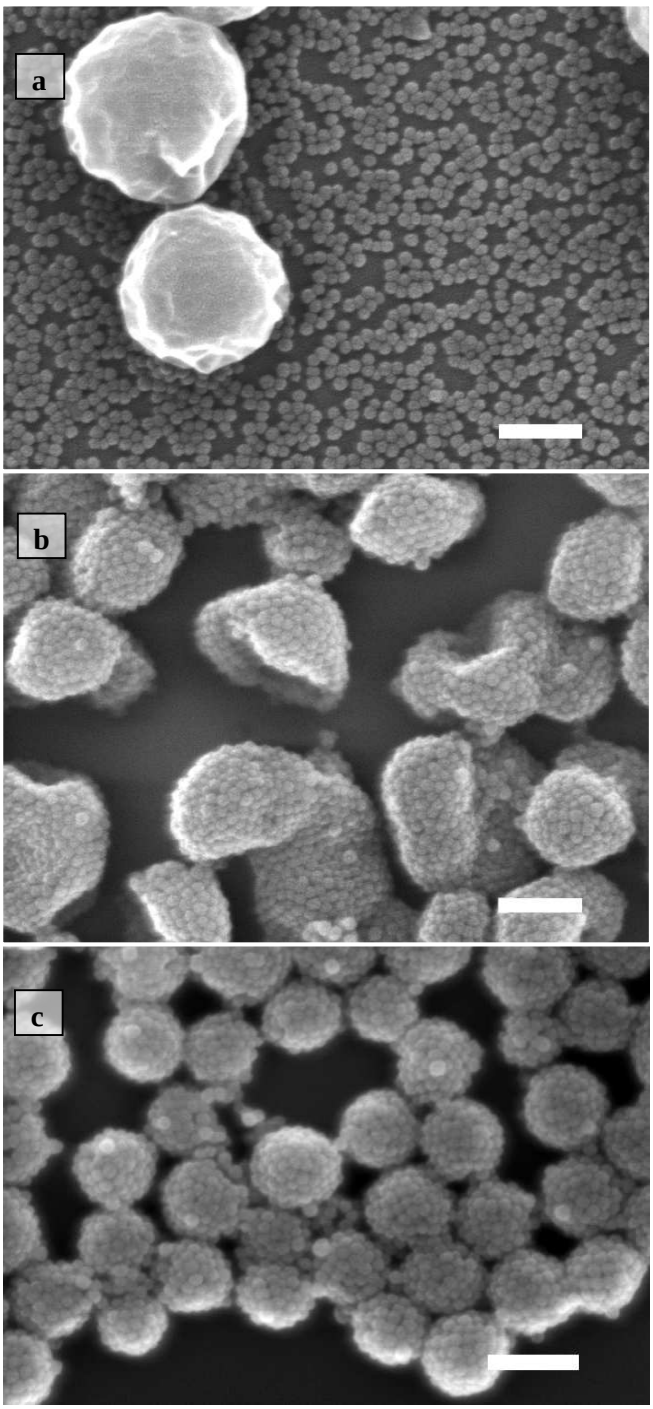

Figure IV-6. SEM images of latexes prepared in batch emulsion polymerisation in presence of Ludox TM-40 colloidal silica. [a] PVPiv latex with a silica:monomer ratio of 0.44 (exp. cc-3-390). [b] PVAc latex with a silica:monomer ratio of 0.44 (exp. cc-3-381) and [c] PVAc latex with a silica:monomer ratio of 1.04 (exp. cc-2-345E). Scale bars 200 nm.

The emulsion polymerisation of vinyl acetate in presence of silica nanoparticles yielded in armoured polymer latexes, as can be seen from Figure

IV-6(b) and (c). Intriguingly, the final nanocomposite latex in Figure IV-6(b) was of non-spherical shape. When silica nanoparticle stabilised emulsion polymerisations of vinyl acetate were carried out at higher loadings of nanoparticles, this effect of limited coalescence was overcome, Figure IV-6(c). A reaction in which we used, 11.1 wt% of vinyl acetate, and 11.6 wt% of silica nanoparticles afforded nearly spherical armoured latex particles. We increased the silica:VAc weight ratio used from the original 0.44 to 1.04.

Figure IV-7 shows the concentration of silica nanoparticles, *C*, as function of monomer conversion, X_m, as determined by quantitative disc centrifugation for the PVAc and PVPiv reactions with a silica:monomer weight ratio of 0.44 (or 5.8 wt% silica nanoparticles). The data obtained from the emulsion polymerisation of vinyl pivalate shows no relevant drop in nanoparticle concentration in the water phase. This is in agreement with the SEM analysis of the final polymer latex (see Figure IV-6(a)). Measured values exceed the value of C_0, an effect which we attribute to the non-homogeneity of the sample taken from the emulsion polymerisation reactor. The data obtained for vinyl acetate shows that indeed throughout the emulsion polymerisation process the silica nanoparticles concentration in the water phase, *C*, drops and thus that they adhere to the surface of the growing latex particles, as previously suggested by us.[12] The ability of silica nanoparticles to stick to poly(vinyl acetate) latex particles was previously demonstrated by Wen *et al.*[10] and by Uricanu *et al.*, the latter elegantly studied the adsorption behaviour of silica nanoparticles onto the surface of pre-fabricated latex spheres dispersed in water.[20]

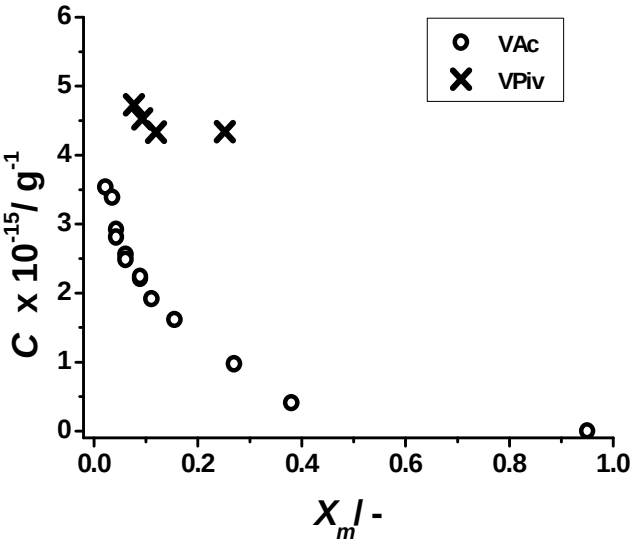

Figure IV-7. The measured concentration of silica nanoparticles in the water phase, *C*, versus monomer conversion, X_m, as measured by quantitative disc centrifugation. [○] Solids-stabilised emulsion polymerisation of vinyl acetate (13.0 wt%) at 5.8 wt% of silica nanoparticles. [×] Emulsion polymerisation of vinyl pivalate (13.1 wt%) in presence of 5.8 wt% silica nanoparticles. (Exp cc-3-381 and cc-3-390 in Table IV-5, respectively)

For the silica nanoparticle stabilised emulsion polymerisation of vinyl acetate we measured the average particle diameter, d_z, and the dispersity, D_I, of the particle size distribution by dynamic light scattering (see Figure IV-8). Note that no difference in particle size was found when performing dynamic light scattering measurements on the latex diluted in pure water or in water saturated with monomer.

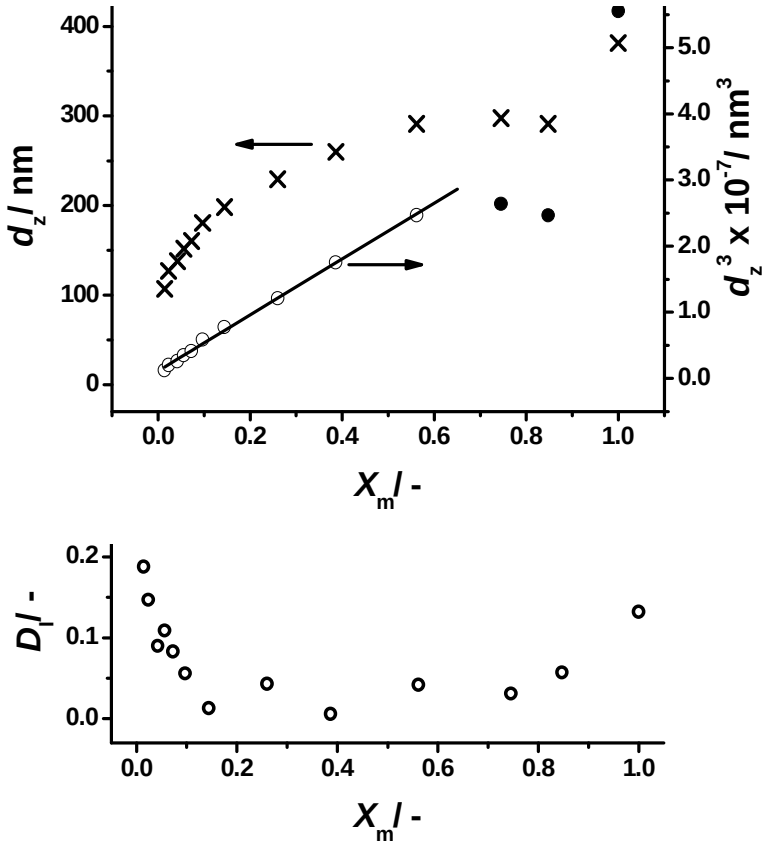

Figure IV-8. Average particle diameter, d_z, and d_z^3 (top), and dispersity, D_I, (bottom) versus monomer conversion, X_m, of (Ludox TM-40)-stabilised emulsion polymerisation of vinyl acetate (cc-3-381 in Table IV-5). Linear fit yields: $d_z^3 = 1.13\ (\pm\ 0.16) \times 10^6 + 4.23\ (\pm\ 0.07) \times 10^7\ X_m$ ($r^2 = 0.998$). Closed symbols were excluded in linear fit.

From experimental observations we found that solids-stabilised emulsion polymerisations often have a relatively narrow particle size distribution, which meant that particle formation was fast comparatively to particle growth. When we assumed that throughout the particle growth period the number of polymer latex particles, N_{polym}, stayed constant, the average particle size, d_z, versus monomer conversion should show a 3rd order dependence (hereby ignoring monomer-swelling), as conversion scales to mass, which scales to volume, and volume scales to d_z^3. Such behaviour was indeed observed from Figure IV-8 (top), up to approximately 70% monomer conversion. Noteworthy was that the

dispersity of the particle size distribution went up considerably at the later stages of the emulsion polymerisation process. This coincided with undetectable low levels of remaining silica nanoparticles in the water phase (see Figure IV-7). The lack of solid stabilisers resulted in coalescence of not fully covered poly(vinyl acetate) latex particles. We believed that since the coalescing particles were swollen and thus in a "soft" state, especially in the outer regions near the surface, the silica particles could migrate and rearrange. This agreed with the SEM analysis (see Figure IV-6(b)) in which fused armoured agglomerates of non-spherical shape were observed and was held up by TEM analysis in which the fused regions of the agglomerates do lack presence of silica nanoparticles (see Appendix D, Figure D.1).

Since d_z scales with $X_m^{1/3}$ for this solids-stabilised emulsion polymerisation, C should scale with $X_m^{2/3}$, as could be derived using Equation IV-5. This under the condition that partitioning of the silica nanoparticles remained the same throughout the particle growth period, uninfluenced by diffusion limitations of the heterocoagulation process and the nanoparticle occupancy of the surface of the armoured polymer latex particle. Indeed such behaviour can be observed from Figure IV-9. The measured values at low conversion were omitted as a result of inhomogeneous sampling which might have been also taken during the period of particle nucleation.

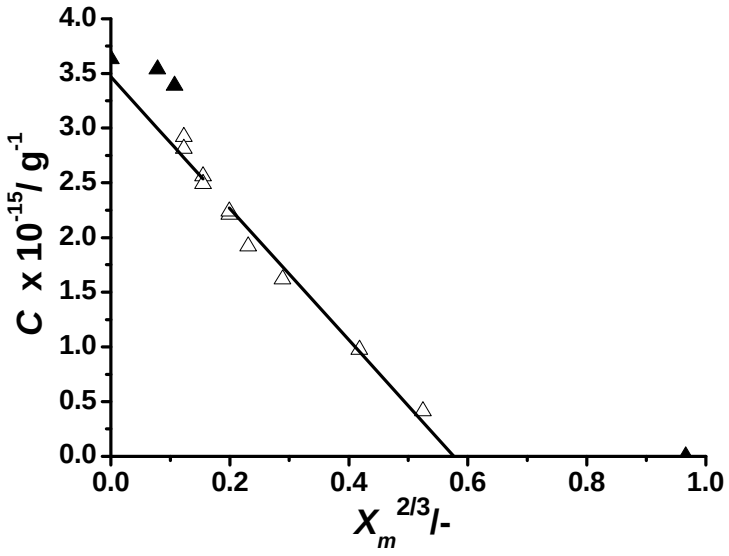

Figure IV-9. The measured concentration of silica nanoparticles in the water phase, C, versus $X_m^{2/3}$ for the solids-stabilised emulsion polymerisation of vinyl acetate (13.0 wt%) at 5.8 wt% of silica nanoparticles (cc-3-381, Table IV-5). Linear fit yields: $C = 3.46\ (\pm 0.07) \times 10^{15} - 6.01\ (\pm 0.28) \times 10^{15}\ X_m^{2/3}$ ($r^2 = 0.98$). Closed symbols were excluded in linear fit.

Using the two linear correlations obtained for $C \propto -6.01 \times 10^{15}\ X_m^{2/3}$ and $d_z \propto \sqrt[3]{4.23 \times 10^7}\ X_m^{1/3}$ and with the aid of Equation IV-5 we could find a value for $P\beta$ of 0.67 (using ρ_{polym} = 1.19 g cm^{-3}). For close-packed systems (the nanoparticles are in close proximity on the surface) we stated values for P of approximately 0.9. This meant that the average values for the diameter of the particles, d_z obtained from dynamic light scattering for the armoured latex particles needed to be corrected with a factor β of 0.73. This was plausible when compensating for the combined effects of the non-spherical geometry of the particle, the thickness of the double layer, and the dispersity of the particle size distribution (see Figure IV-8).

IV.4. Conclusions

We investigated the fate of nanoparticles used as stabilisers in solids-stabilised emulsion polymerisation for the formation of armoured hybrid polymer latexes. Although vinyl acetate is known for its high water solubility, we found that this solids-stabilised system was characterised by a short particle nucleation period, followed by an interval for particle growth and finally the occurrence of inter-particle combination thereby reducing the surface-to-volume ratio due to a lack of stabiliser. We showed that disc centrifugation could be used as a powerful tool to analyse and determine the concentration of nanoparticles in the water phase throughout the polymerisation process. The obtained concentration profiles versus monomer conversion unravelled the key mechanistic features in the formation of the raspberry-like armoured polymer colloids, such as potential limited coalescence of armoured particles in the later stages of the solids-stabilised emulsion polymerisation process leading to non-spherical structures. A good correlation was obtained between the measured concentration profiles and our theoretical model, which required a value for the average particle size of the armoured latex, experimentally obtained *via* dynamic light scattering measurements.

IV.5. References

1. Colard, C. A. L.; Teixeira, R. F. A.; Bon, S. A. F., *Langmuir* **2010,** *26* (11), 7915-7921.
2. Balmer, J. A.; Schmid, A.; Armes, S. P., *J. Mater. Chem.* **2008,** *18* (47), 5722-5730.
3. Schmid, A.; Armes, S. P.; Leite, C. A. P.; Galembeck, F., *Langmuir* **2009,** *25* (4), 2486-2494.
4. Schmid, A.; Fujii, S.; Armes, S. P., *Langmuir* **2005,** *21* (18), 8103-8105.
5. Schmid, A.; Fujii, S.; Armes, S. P., *Langmuir* **2006,** *22* (11), 4923-7.
6. Tiarks, F.; Landfester, K.; Antonietti, M., *Langmuir* **2001,** *17* (19), 5775-5780.
7. Song, X.; Zhao, Y.; Wang, H.; Du, Q., *Langmuir* **2009,** *25* (8), 4443-4449.
8. Song, X.; Yin, G.; Zhao, Y.; Wang, H.; Du, Q., *J. Polym. Sci. Part A* **2009,** *47* (21), 5728-5736.
9. Zhang, Y.; Zou, Q.; Shu, X.; Tang, Q.; Chen, M.; Wu, L., *J. Colloid Interf. Sci.* **2009,** *336* (2), 544-550.
10. Wen, N.; Tang, Q.; Chen, M.; Wu, L., *J. Colloid Interf. Sci.* **2008,** *320* (1), 152-158.
11. Sheibat-Othman, N.; Bourgeat-Lami, E., *Langmuir* **2009,** *25* (17), 10121-10133.
12. Colver, P. J.; Colard, C. A. L.; Bon, S. A. F., *J. Am. Chem. Soc.* **2008,** *130* (50), 16850-16851.
13. Bon, S. A. F.; Colver, P. J., *Langmuir* **2007,** *23* (16), 8316-8322.
14. Yu, C.-L.; Kang, J.-S.; Zhang, F.-A., *J. Macromol. Sci. A* **2009,** *46* (9), 870-875.
15. Analytik Ltd analytical solutions, C. I. E., *CPS Disc Centrifuge DC24000, System Documentation* **2009**.
16. Erbil, H. Y., *Vinyl Acetate Emulsion Polymerization and Copolymerization with Acrylic Monomers*. CRC Press: 2000; 324.
17. Chai, X. S.; Schork, F. J.; DeCinque, A.; Wilson, K., *Ind. Eng. Chem. Res.* **2005,** *44* (14), 5256-5258.
18. French, D. M., *J. Polym. Sci.* **1958,** *32* (125), 395-411.
19. Hidi, P.; Napper, D. H.; Sangster, D. F., *Macromolecules* **1995,** *28* (18), 6042-6054.
20. Uricanu, V.; Eastman, J. R.; Vincent, B., *J. Colloid Interf. Sci.* **2001,** *233* (1), 1-11.

Chapter V.

Stability of silica-armoured poly(vinyl esters) latexes, production of powders and their application in tile adhesive formulations

The role of the silica nanoparticles armouring the polymer latexes was investigated. By increasing the pH better colloidal stability was obtained until coalescence occurred at high ionic strength. In the spray-drying process the thickness of the silica shell had an important role in limiting polymer inter-diffusion upon film formation. A series of powders made through spray-drying of the armoured polymer latexes were tested as additives in cement-based formulations for tile adhesives. Desired performance characteristics, however, were not obtained in comparison to standard formulations.

V.1. Introduction

Polymer latexes made from vinyl acetate and co-monomers such as ethylene, are attractive for a great variety of dispersion formulations in industry. An essential physico-chemical characteristic of these polymers is their wettability and adherence to a great variety of surfaces such as wood, glass, metal, minerals and polymers. Applications using poly(vinyl acetate) based latexes include coatings, paints, adhesives and mechanical reinforcing additives in construction materials such as cement, mortar and concrete.[1-2] These polymer binders tend to have a plasticising effect in the formulation of cementitious mortars.

Cement is a hydraulic binder made of finely ground inorganic material, mainly calcium silicates. Upon addition of water, the paste hardens as the reaction of hydration occurs. New compounds formed are calcium hydroxide and calcium silicate hydrate. The latter develops the strength and stability of the cementitious material. Minimisation of the quantity of added water results in fewer capillary pores, lower porosity and stronger cements. The role of additives is to enhance good workability of the cement paste for an appropriate time scale and also provide good cohesion/strength to the material prepared.

The need of improving material performance has already motivated the investigation of synergistic combinations. It is common to formulate a blend of polymers and inorganic dispersions to improve the properties of individual systems. Conventionally, poly(vinyl alcohol) (PVOH) is used as protective colloids and redispersable agent for the production of redispersible powders of poly(vinyl acetate-co-ethylene), which are added to cementitious formulations. The aim of this chapter is to evaluate if the armour of silica nanoparticles on our

polymer latexes made *via* solids-stabilised emulsion polymerisation could (partially) replace poly(vinyl alcohol). For this purpose, the stability of these inorganic-polymer dispersions was investigated at increased contents in calcium hydroxide. Spray-drying of those latexes was then performed and the produced redispersible powders were tested as binders in tile adhesive formulations.

V.2. Experimental

V.2.1. Materials

Various polymer latexes of vinyl acetate (co-vinyl neodecanoate) stabilised by silica nanoparticles (Ludox TM-40 or Ludox SM-30) were prepared using a solids-stabilised emulsion polymerisation process. Refer to chapters IV for details on the emulsion polymerisation process used. Vinyl neodecanoate monomer (mixture of isomers) was purchased from Aldrich. The compositions of the latexes further investigated in this chapter are given in Table V-1 of the results and discussion part (V.3.1) and exact amounts can be found in Appendix E, Table E.1. Sodium hydroxide (laboratory reagent grade) and calcium hydroxide (95%) were purchased from Aldrich and used as received.

V.2.2. Equipment

The 100 mL sedimentation tube was donated by Wacker Chemie AG. pH measurements were performed on a pH-Meter (765 calimatic, Knick). SEM analyses of the dried latexes were performed using a Zeiss Supra55VP FEGSEM with an EBSD camera or equivalent apparatus was used at Wacker Chemie AG (Burghausen, Germany) to image the powders. Particle size distributions of dispersions were measured on a Malvern Zetasizer Nano. Particle size distributions of powders were measured on a Beckman Coulter –

LS 13 320 Laser Diffraction Particle Analyser equipped with a Tornado – dry powder module. Differential scanning calorimetry analyses were performed on a Metler-Toledo DSC 821e.

V.2.3. Typical procedure for the sedimentation tube

A portion of latex containing 0.5 g of the solids (*i.e.* polymer and silica) was weighed in a 100 mL beaker (3.17 g of latex cc-3-367). This was diluted with 50 mL of deionised water and mixed thoroughly. The diluted latex was poured into the sedimentation tube. The beaker was rinsed with water (of modified pH with NaOH or $Ca(OH)_2$ as specified) which was filled into the tube up to the 100 mL mark of the tube. The tube was closed and shaken to homogenise again the dispersion and gas bubbles were avoided at the bottom of the tube. The tube was held vertically and sedimentation was read after some time (typically 1 and 24 hours).

V.2.4. Standard conditions of spray-drying

A laboratory spray-drier apparatus (Büchi 190 Mini Spray Dryer) was used (see description in section V.3.2). Spray-drying was performed at a speed of 1 L of latex in 1 to 3 hours. In order to get the spray-drier running, the water flow (cool down unit), the aspirator (flow indicator 600) and the heating were subsequently switched on. Injection of the sample could start when the inlet temperature was about 180 ºC and the outlet temperature *ca.* 70 ºC.

V.2.5. Standard test for tile adhesive application

The workability, slip and glue properties of the formulated adhesive paste were determined according to EN 12004 using the prepared redispersible powders as one of the ingredients in comparison to standards using poly(vinyl

alcohol) as protective colloids (redispersible powders 4 TL 'Powder A' and 4 TL 'Powder B'). For a detailed formulation refer to Table E.2 in Appendix E. Typically, all components (cement, sand, various inorganic powders, the previously obtained poly(vinyl acetate)-based powder, and water) were mixed roughly by hand and then blended for 1 minute. The mixture was then left for 5 minutes and after the viscosity was measured (workability check). The amount of water was adjusted to obtain a viscosity between 500,000 – 600,000 cP. The material was spread on a concrete support and a visual checking was done against bubbles. A tile of 415 g was placed on it with a weight of 5 Kg for 30 seconds than left without the weight for 30 more seconds. The tile on its support was then placed vertically and the slip was measured after 5 minutes. The hardness of the excess of material was checked over time (workability check after 1 hour).

The tensile adhesion strengths were measured by performing pull off tests at a speed of 250 N s^{-1} following procedures PML-543 (20 min open time) and PML-505 (wet storage conditions: 7 days SC/21 days in water, and high temperature storage conditions: 14 days SC/14 days TS+70 ºC/1 day SC) according to EN1348 with SC being the standard climate of 23 ºC and 65% humidity.

V.3. Results and Discussion

V.3.1. Product properties

A series of poly(vinyl acetate) (PVAc)-based latexes armoured with a monolayer of silica nanoparticles were prepared in emulsion polymerisation. The composition of the latexes further used in this chapter is reported in Table

V-1. Variables were the overall solids content, the silica-to-monomer ratio to trigger the formation of larger polymer particles, the polymer composition by introducing vinyl neodecanoate as co-monomer and the size of the colloidal silica.

Table V-1. Composition (overall weight contents and weight ratios) of the solids-stabilised poly(vinyl esters) latexes prepared by emulsion polymerisation using Ludox TM-40 silica (*ca.* 24 nm in diameter) unless indicated. Main criterion, changed from one sample to another, is shown in bold.

Exp.	***VAc content/ wt%***	***VEOVA-10 content/ wt%***	***Silica content/ wt%***	***Overall solids/ wt%***	***Silica: monomer/ g×g^{-1}***
cc-3-367	11.3	-	5.1	**16.4**	0.45
cc-3-377	19.8	-	8.7	**28.5**	**0.44**
cc-3-379	19.9	-	4.3	24.2	**0.22**
cc-3-383	**17.8**	**2.0**	8.7	28.5	0.44
cc-3-384	**15.9**	**4.0**	8.7	28.5	0.44
cc-3-410	19.7	-	2.2 **(*)**	21.9	0.11

(*) Ludox SM-30 (*ca.* 7 nm in diameter)

Information on the particle size distributions of the latexes was obtained from dynamic light scattering measurements (Malvern DTS Nano), see Table V-2, and confirmed by SEM analyses. Aging of the latexes led to the formation of micronsized flocs and sedimentation (see next section). However this was reversible as sediments were easily redispersed upon hand-shaking and the initial particle size distributions were recovered after sonicating the samples for about 10 minutes.

Table V-2. Average particle sizes d_z and dispersity indices D_I (DTS nano) of the solids-stabilised poly(vinyl esters) latexes prepared by emulsion polymerisation using Ludox TM-40 silica (*ca.* 24 nm in diameter) in all cases excepted in exp. cc-3-410 where Ludox SM-30 (*ca.* 7 nm in diameter) was used.

Exp.	***d_z (DTS nano)/ nm***	***D_I (DTS nano)/ -***	***Figure***
cc-3-367	334.5	0.026	
cc-3-377	364.7	0.007	
cc-3-379	604.4	0.123	V-1.A
cc-3-383	372.9	0.153	
cc-3-384	617.6	0.077	
cc-3-410	724.4	0.54	V-1.B

By using smaller silica nanoparticles (Ludox SM-30, *ca.* 7 nm in diameter), in comparison to Ludox TM-40 (*ca.* 24 nm in diameter), the armoured PVAc particles formed had a thinner shell which gave more flexibility to the particles to deform. This was observed when performing scanning electron microscopy (SEM) under vacuum and using an acceleration voltage of 5 kV (see Figure V-1).

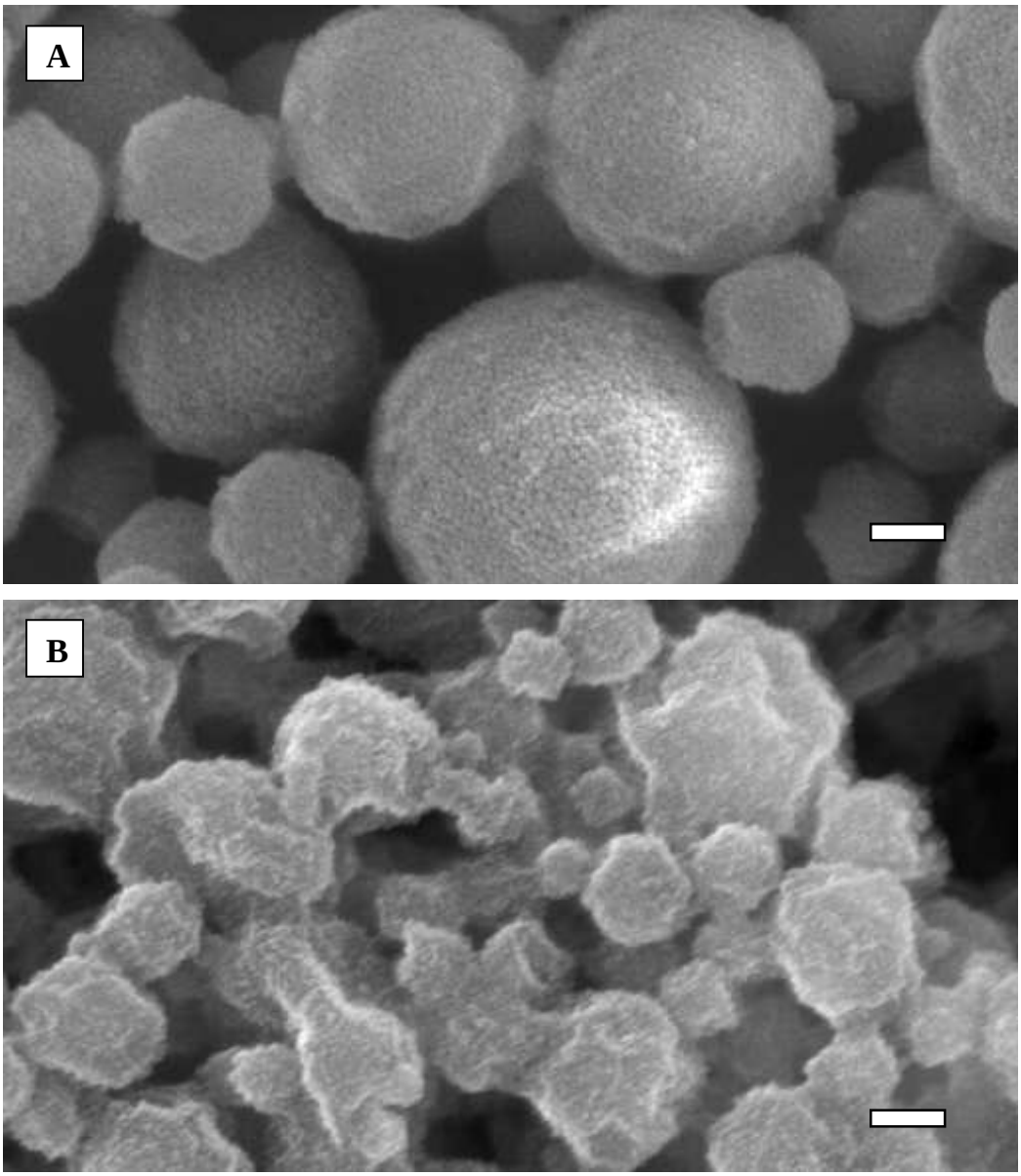

Figure V-1. SEM images of silica-stabilised PVAc latexes prepared in emulsion polymerisation: (A) using Ludox TM-40 silica (exp. cc-3-379), (B) using Ludox SM-30 silica (exp. cc-3-410). Both scale bars 200 nm.

V.3.1.1. Study of the colloidal stability via a sedimentation method

The colloidal stability of the silica-armoured polymer dispersions was investigated using the procedure and a sedimentation tube (see Figure V-2) provided by Wacker Chemie AG (Burghausen, Germany). The ionic strength in calcium cations and the pH were increased to mimic the conditions in cementitious application when hydration of the silicates occurs.

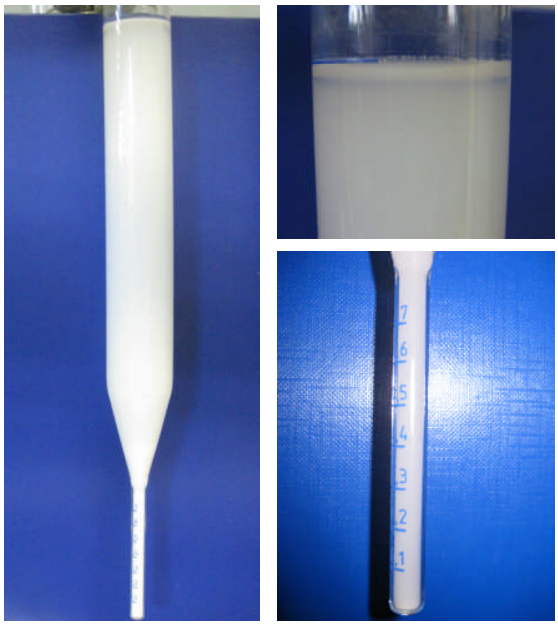

Figure V-2. Photographs of the sedimentation tube for experiment cc-3-413 after 24 hours.

The experiments were conducted with a latex of 16.4 wt% overall solids content (cc-3-367). Results are summarised in Table V-3 and understood in terms of diffuse electrical double layer. At low pH (pH 3.5, exp. cc-3-373A) when diluting the original latex with deionised water, slow sedimentation was observed due to a lack in surface charges. By increasing the pH better colloidal stability was obtained from the ionisation of the surface hydroxyl groups bared by the silica nanoparticles (exp. cc-3-373B/412/413). This enhanced stability and potentially the partial hydrolysis of PVAc into PVOH led to desorption of the Ludox colloidal silica from the polymeric surface, as observed by scanning electron microscopy (Figure V-3). At higher ionic strength (exp. cc-3-373C), coalescence of the latex particles was induced as the electrical double layer was compressed by the calcium cations.

Table V-3. Sedimentation studies of silica-stabilised poly(vinyl acetate) latexes at increased ionic strength and pH.

Exp.	*Aqueous base*	*Dispersion pH/ -*	*Macro-coagulation*	*Sedimentation*	
				After 1 h	*After 24 h*
cc-3-373 A	-	3.5	None	None	~0.07
cc-3-373 B	NaOH	11.0	None	None	None
cc-3-412	$Ca(OH)_2$	7.1	None	None	None
cc-3-413	$Ca(OH)_2$	10.3	Very little coagulation	None	*
cc-3-373 C	$Ca(OH)_2$	12.7	Completely coagulated	n.a.	n.a.

* Slight sedimentation/concentration was observed, see Figure V-2.

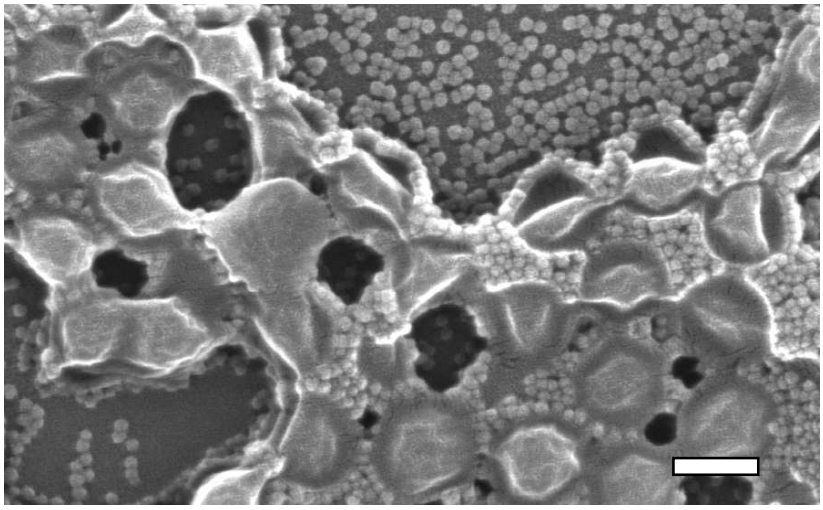

Figure V-3. SEM image showing the destruction of the armouring layer of silica nanoparticles around the PVAc latex particles by increasing the pH (exp. cc-3-373B, after 20 days at pH 11.0). Scale bar 200 nm.

V.3.1.2. Thermal analysis

The glass transition temperatures (T_g) of our sample series of silica-armoured poly(vinyl esters) latexes were measured by differential scanning calorimetry (DSC) at a standard heating rate of 10 ºC min^{-1} from -70 to 160 ºC. An example of DSC trace is displayed in Figure V-4 and T_g values of all samples are summarised in Table V-4.

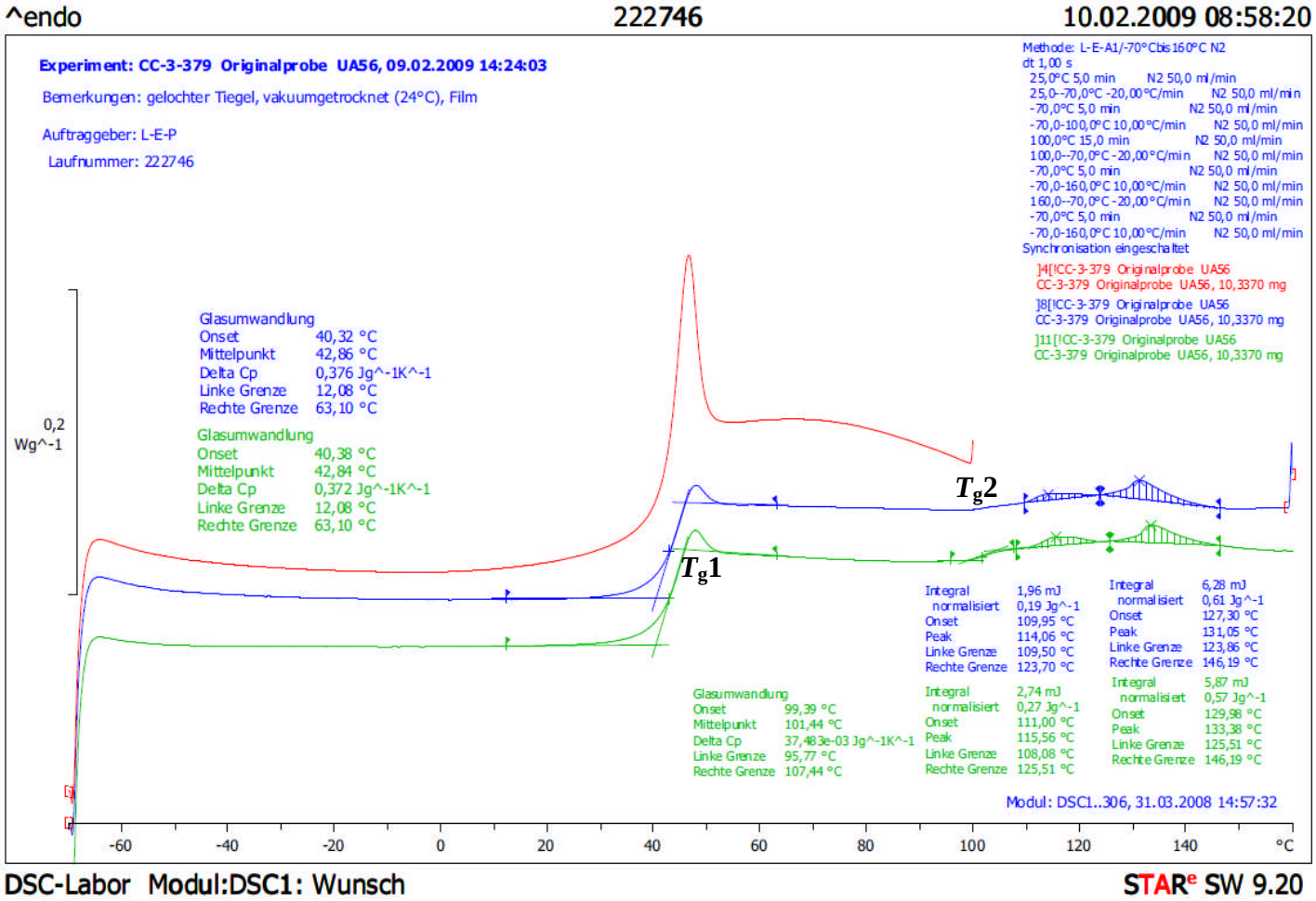

Figure V-4. DSC analysis of latex cc-3-379.

Table V-4. Glass transition temperatures (T_g) of the solids-stabilised poly(vinyl esters) latexes measured by DSC at a standard heating rate of 10 ºC min^{-1} (second heating).

Exp.	*P(VAc:VEOVA-10) weight ratio*	*T_g1*/ ºC*	*T_g2*/ ºC*	*Endo peaks ºC*
cc-3-367	[100-0]	42	77	-
cc-3-377	[100-0]	41	107	100 – 140
cc-3-379	[100-0]	43	101	110 – 140
cc-3-383	[90-10]	40	77	-
cc-3-384	[80-20]	38	78	-
cc-3-410	[100-0]	44	-	-
***PVAc*[1]**	*[100-0]*	*30*	*n.a.*	
***PVOH*[3]**	-	*n.a.*	*79*	
***PVOH stabilised hybrid particles*[3]**	*[80-20]*	*20*	*79*	

* Temperature at the middle point of the transition. See Appendix for an example of DSC spectrum annotated with the measurement parameters.

Thermal properties of polymer blends,[4] thin films[5-6] and nanocomposites[7-13] have already roused lot of interests. Different effects on the glass transition temperature (T_g) have been observed. In some cases, disappearance of the T_g point occurred when inorganic fillers were present[7-10] and in other cases increases or decreases in the T_g[11] were observed.[10, 12] Percy *et al.* reported that those apparently opposite behaviours might simply reflect the interfacial properties or wettability of the fillers.[13]

Values (T_g1) around 41-44 ºC were measured for our prepared hybrid nanocomposite polymer films. The presence of the silica nanoparticles was found to have a marked effect on the value of the bulk T_g (T_g1) of PVAc which has a known value of about 30 ºC.[1] Vinyl neodecanoate (VEOVA-10) used as co-monomer was expected to give more flexibility to the composite due to the

low T_g of the homopolymer (-3 ºC). However only a small decrease in T_g1 of about 4 ºC was observed for the VAc:VEOVA-10 (80:20) copolymer whereas Bohorquez observed a T_g of 20 ºC for a latex of similar composition at the difference that PVOH was used as stabiliser.[3] The detection of a second glass transition temperature (T_g2) in some samples was probably due to complex adhesion effects of the inorganic fillers [14-19] or might suggest the alcoholisation of a small fraction of PVAc with PVOH having a T_g point at temperatures around 75 – 80.[3] For a couple of samples (cc-3-377/-379), T_g2 appeared to be shifted to higher temperatures around 100 – 110 ºC and endothermic peaks appeared around 100 – 140 ºC. Although no obvious reasons can be given to explain this difference between our samples, it is known that intermolecular interactions such as hydrogen bonding between the silica nanoparticles and the polymer can affect the crystallisation and melting temperatures.[20] Pure PVOH has a melting point at about 230 ºC and partially hydrolysed PVOH around 180 – 190 ºC. Increased contents in silica (up to 59 wt%) lowered gradually the endothermic transition of PVOH fibres to just over 100 ºC[21] or the degree of crosslinking between PVOH and silica had similar effect.[22]

V.3.2. Production of redispersible powders by spray-drying the latexes

Powders are attractive since they offer several advantages for large manufacturing in comparison to dispersions. They have a longer shelf life and there is no concern with respect to freezing. Lower costs for shipping and storage are also important benefits. Spray-drying is an indispensable process for the production of redispersible powders which has been used over few decades by diverse industries such as foodstuffs and pharmaceuticals. Over the last decade, this process also received more attention for better understanding of the

structural and physico-chemical properties of the formed powder particles.[23-25] It consists in evaporating the aqueous phase of the latex dispersion under hot dry air. The spray nozzle forms droplets of the dispersion of controlled size (atomisation). Under a hot air flux the water evaporates and the latex particles are concentrated into a powder particle. To obtain redispersible powders, film formation of the latex particles has to be prevented. When the polymer dispersion is sprayed below its minimum film formation temperature (high glass transition temperature) the particles are not expected to coalesce. PVOH-stabilised dispersions of PVAc are commonly spray-dried in pilot plants. Due to its relatively low glass transition temperature of poly(vinyl acetate) (T_g ~ 40 ºC) inter-particle polymer-polymer diffusion can be avoided by supplementing the system with polymer protective colloids (*i.e.* PVOH, T_g ~ 80 ºC) and inorganic anti-caking agents, such as $CaCO_3$ or SiO_2 particles.

Powders were produced by using a laboratory spray-drier represented in Figure V-5. No protective colloid or anti-caking agents were added for the spray-drying process of our series of silica-armoured polymer dispersions. Monodisperse (TM-40)-armoured PVAc dispersions of particles of about 300 nm in diameter and low solid content (16 w%, cc-3-367) could be spray-dried without any problems. Difficulties in spray-drying our latexes increased as the solid content and the latex particle size increased. The presence of larger flocs tended to film-form and bloc the spray nozzle which is no wider than 200 microns. By diluting twice and sonicating the dispersions, blockage issues were minimised.

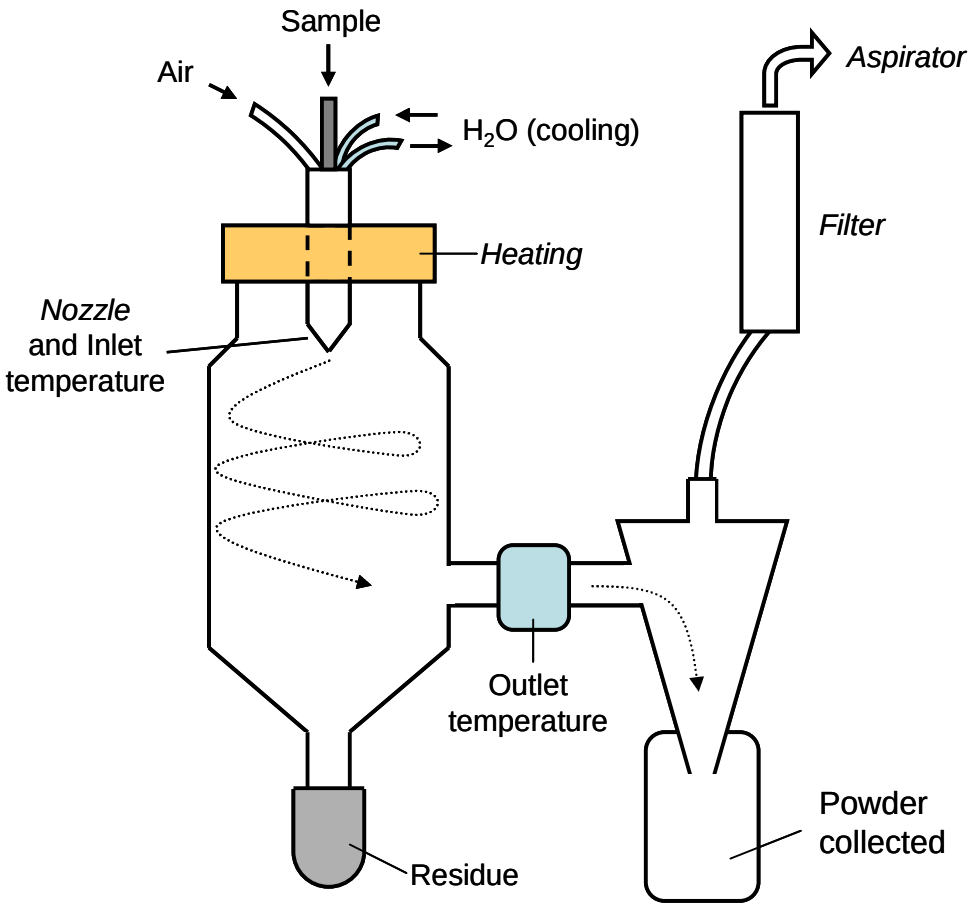

Figure V-5. Scheme showing the different parts of the laboratory spray-drier used and the powder flow.

Imaging of the powders showed a structural difference between samples prepared with different grade of Ludox silica. PVAc particles armoured with silica nanoparticles of ~ 24 nm in diameter (Ludox TM-40) were quite robust and could be observed in the powder particles (see Figure V-6.A) as only little deformation occurred. Whereas PVAc particles armoured with silica of ~ 7 nm in diameter could not be distinguished anymore in the powder particles (Figure V-6.B). They deformed and potentially film-formed during spray-drying which should be avoided for redispersibility purposes.

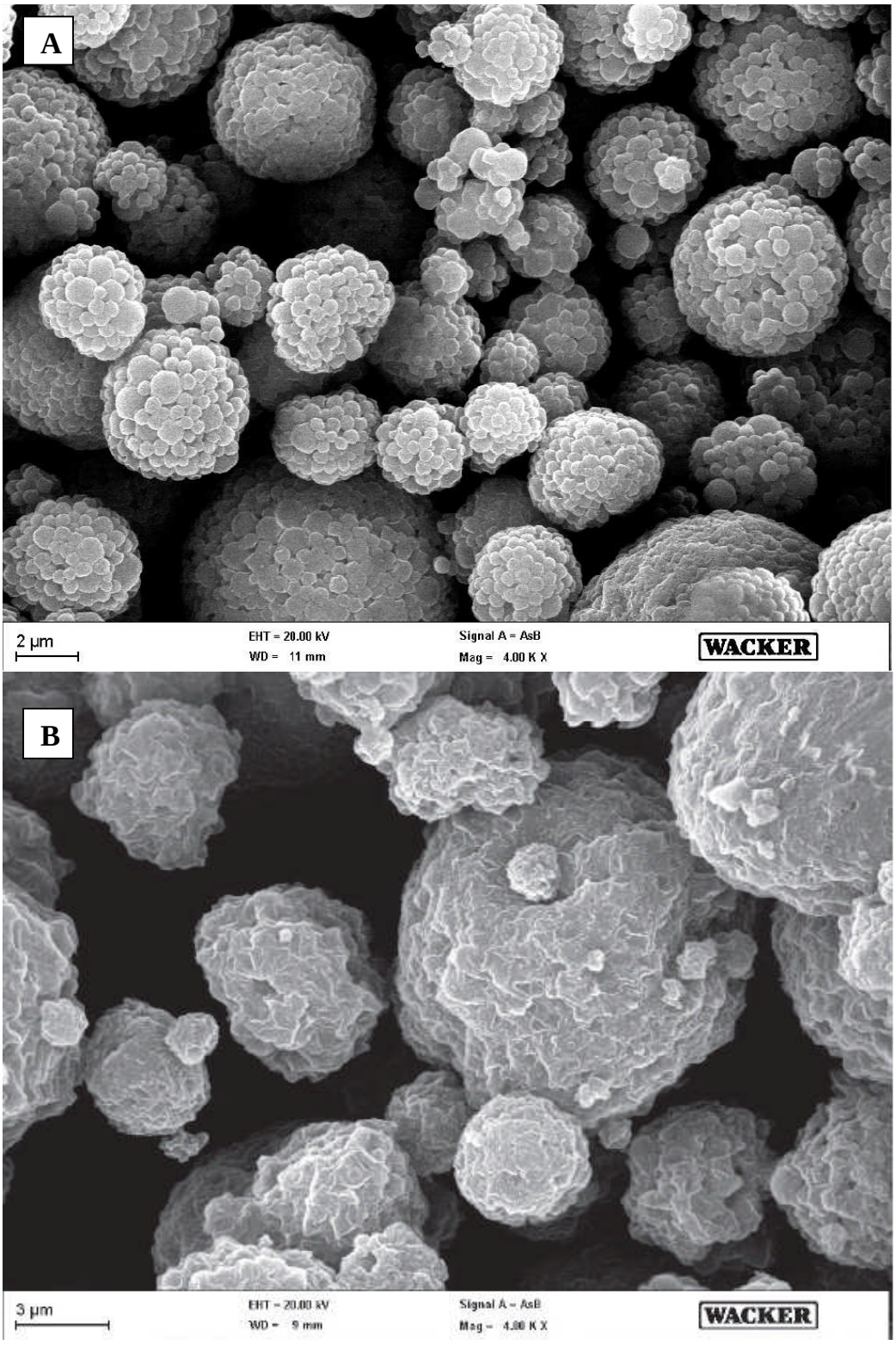

Figure V-6. SEM images of powders obtained from spray-drying silica-stabilised PVAc latexes prepared in emulsion polymerisation: (A) using Ludox TM-40 silica (exp. cc-3-379), (B) using Ludox SM-30 silica (exp. cc-3-410).

Typically powder particles produced should be in the range of 30 – 100 microns in diameter. However, when analysed by light scattering with a tornado unit, an important number of submicron-size particles was observed. This showed the lack in cohesion between the particles constituting the powder particles. Typical particle size distribution spectra, in volume (%) and number (%), of the powder (exp. cc-3-379) are given in Figure V-7. Although this showed their ease to redisperse, the presence of such fine particles in a dry state becomes hazardous and brings issues to handle it (volatile dust).

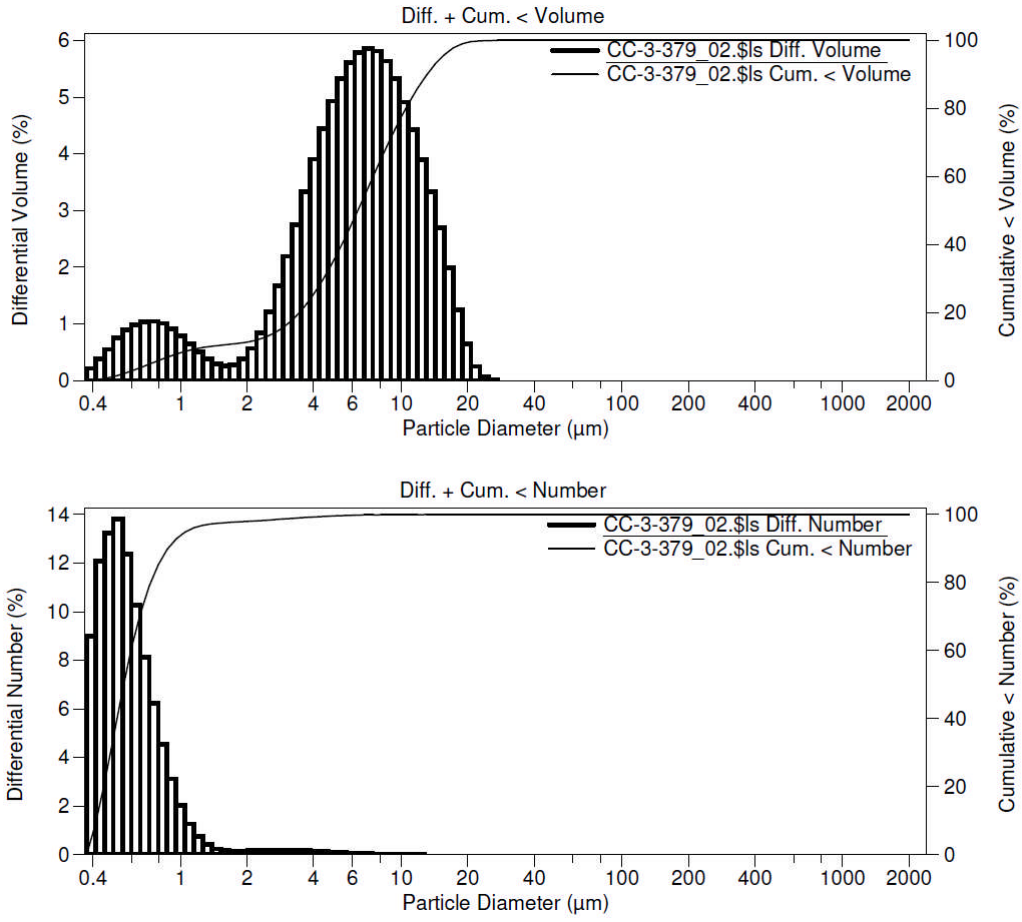

Figure V-7. Laser diffraction analysis of the dry powder obtained from spray-drying latex cc-3-379; particle size distributions in volume (top) and number (bottom).

V.3.3. Testing the redispersible powders in cement-based tile adhesives formulations

These silica/PVAc-based powders were used as additives in formulations for tile adhesives (with sand, cement and various inorganic components, see Table E.2, Appendix E for details). The texture of the paste, its workability over time, and the tensile adhesion strength was studied and compared to pastes obtained with standard additives of poly(vinyl alcohol)-PVAc based powders (4 TL ‘Powder A’ and 4 TL ‘Powder B’). An acceptable workability was only obtained with a strong increased in water demand compared to a standard polymer powders (approx. 25% excess). All sample tests are summarised in Table E.3 and E.4.

Tensile adhesion strength of the material was then measured by performing pull off tests according to EN 1348 after 20 minutes open time and after different storage conditions (see experimental part). The open time after 20 min, which is an important property for cementitious tile adhesives, was for all of our samples zero. This is understandable as it is known that poly(vinyl alcohol), usually used as protective colloid, has a strong positive impact to open time. After critical wet or temperature storage, the tensile adhesion strengths were significantly below the values of the reference samples, especially after high temperature storage. Results of all pull-off tests are plotted in Figures E.1 in Appendix E. The flexibility and shear strength of the system were therefore poor. Powders made from silica-stabilised latexes were not in the same property range as the standard additive powders.

V.4. Conclusions

The stability of poly(vinyl acetate)-based latexes stabilised with silica nanoparticles against sedimentation could be tuned by increasing the pH until desorption of the nanoparticles would occur. When reaching high ionic strength of the dispersion, coagulation was observed. Silica-polymer powders were obtained by spray-drying our latexes. A thick armouring shell was found to prevent film formation of the latex particles during the process which, on the other hand, led to a lack of cohesion within the powder particles. When used as additive in application formulations, our silica-polymer system had a higher water demand to reach good workability of the paste than standard polymer additives. Tensile strength of the material for tile adhesives was much below standards. The presence of silica nanoparticles seemed to limit film forming of the polymer particles in the cementitious paste which gave poor adhesive properties to the material.

V.5. References

1. Erbil, H. Y., *Vinyl Acetate Emulsion Polymerization and Copolymerization with Acrylic Monomers*. CRC Press: 2000; p 324.
2. Hewlett, P. C., *Lea's Chemistry of Cement and Concrete, Fourth Edition*. 2004; p 1092.
3. Bohorquez, S. J. Polymeric surfactants in miniemulsion polymerization: Industrial applications. The University of the Basque Country, 2007.
4. Shultz, A. R.; Young, A. L., *Macromolecules* **1980,** *13* (3), 663-668.
5. Keddie, J. L.; Jones, R. A. L.; Cory, R. A., *Europhys. Lett.* **1994,** *27* (1), 59-64.
6. Keddie, J. L.; Jones, R. A. L.; Cory, R. A., *Faraday Discuss.* **1995,** *98*, 219-30.
7. Motomatsu, M.; Takahashi, T.; Nie, H.-Y.; Mizutani, W.; Tokumoto, H., *Polymer* **1997,** *38* (1), 177-182.
8. Krishnamoorti, R.; Vaia, R. A.; Giannelis, E. P., *Chem. Mater.* **1996,** *8* (8), 1728-1734.
9. Frisch, H. L.; Xue, Y., *J. Polym. Sci. A1* **1995,** *33* (12), 1979-1985.
10. Hajji, P.; David, L.; Gerard, J. F.; Pascault, J. P.; Vigier, G., *J. Polym. Sci. Pol. Phys.* **1999,** *37* (22), 3172-3187.
11. Bhardwaj, P.; Singh, S.; Singh, V.; Aggarwal, S.; Mandal, U. K., *Int. J. Polym. Mater.* **2008,** *57* (4), 404 - 416.
12. Arrighi, V.; McEwen, I. J.; Qian, H.; Serrano Prieto, M. B., *Polymer* **2003,** *44* (20), 6259-6266.
13. Percy, M. J.; Amalvy, J. I.; Randall, D. P.; Armes, S. P.; Greaves, S. J.; Watts, J. F., *Langmuir* **2004,** *20* (6), 2184-2190.
14. Tsagaropoulos, G.; Eisenberg, A., *Macromolecules* **1995,** *28* (18), 6067-77.
15. Tsagaropoulos, G.; Eisenburg, A., *Macromolecules* **1995,** *28* (1), 396-8.
16. Blum, F. D.; Xu, G.; Liang, M.; Wade, C. G., *Macromolecules* **1996,** *29* (27), 8740-8745.
17. Kovacevic, V.; Leskovac, M.; Lu, S.; Blagojevi; Vrsaljko, D., *Macromolecular Symp.* **2005,** *221* (1), 11-22.
18. Chen, L.; Zheng, K.; Tian, X.; Hu, K.; Wang, R.; Liu, C.; Li, Y.; Cui, P., *Macromolecules* **2010,** *43* (2), 1076-1082.
19. Hetayothin, B.; Blum, F. D., *Polym. Prepr. (Am. Chem. Soc., Div. Polym. Chem.)* **2008,** *49* (1), 632-633.
20. Lim, J. S.; Noda, I.; Im, S. S., *Polymer* **2007,** *48* (9), 2745-2754.
21. Shao, C.; Kim, H.-Y.; Gong, J.; Ding, B.; Lee, D.-R.; Park, S.-J., *Mater. Lett.* **2003,** *57* (9-10), 1579-1584.
22. Krumova, M.; López, D.; Benavente, R.; Mijangos, C.; Pereña, J. M., *Polymer* **2000,** *41* (26), 9265-9272.
23. Sen, D.; Mazumder, S.; Melo, J. S.; Khan, A.; Bhattyacharya, S.; D'Souza, S. F., *Langmuir* **2009,** *25* (12), 6690-6695.
24. Tsapis, N.; Bennett, D.; Jackson, B.; Weitz, D. A.; Edwards, D. A., *Proc. Natl. Acad. Sci. USA* **2002,** *99* (19), 12001-12005.
25. Tsapis, N.; Dufresne, E. R.; Sinha, S. S.; Riera, C. S.; Hutchinson, J. W.; Mahadevan, L.; Weitz, D. A., *Phys. Rev. Lett.* **2005,** *94* (1), 018302/1-018302/4.

Chapter VI.

Highly porous nanocomposite reinforced open-cell foams through freeze-drying mixtures of colloids and their application as gas sensors[a]

Nanocomposite reinforced soft polymer foams were built by freeze-drying a mixture of colloids dispersed in water, thereby using ice-crystals as template for the porous structure. “Soft” polymer latex particles film-formed and the cell walls were covered by “hard” nanoparticles which maintained the foam structure by enhancing its robustness. Addition of carbon black as a third colloidal component led to conducting nanocomposite foams which could be used as promising gas sensors.

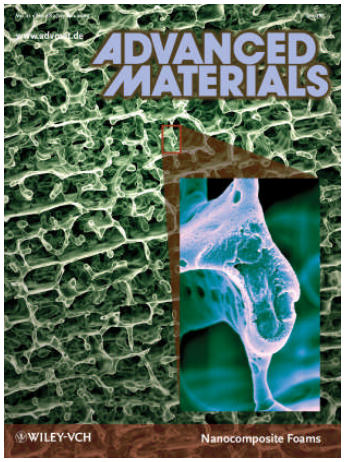

[a] Part of this work was published

1. Colard, C. A. L.; Cave, R. A.; Grossiord, N.; Covington, J. A.; Bon, S. A. F., *Adv. Mater*. **2009,** *21* (28), 2894-2898.

VI.1. Introduction

Low-density solid foams are lightweight materials resulting from an interconnected three-dimensional hollow structure. The scale, geometry and organisation of the hollow compartments within, commonly referred to as cells, determine the key characteristics of these cellular materials. When the cells are completely isolated from their neighbours, the resulting foam is considered closed-celled. Conversely, when the cells are interconnected through open faces, the foam is described as open-celled. The unique properties of cellular materials have led to an increasing interest in synthetic foams, one important class being polymer-based foams. Many applications for these foams exist ranging from insulation materials, supports for catalysts, scaffolds for growth of biological cells and tissues, to 3D-batteries, cheap sensors, antistatic shields, and band-gap materials, among others.[2]

Several routes have been developed to fabricate polymer-based foams. One of the most straightforward methods, so-called 'foaming' or 'expanding' process, consists of introducing small discontinuities (for example by dispersing compressed gas which acts as a blowing agent) into a liquid monomer or polymer melt prior to mechanically reinforcing the cellular structure upon polymerisation or cooling.[3] Hollow materials for photonic applications have been manufactured in which colloidal components assembled into colloidal crystals serve as templates to produce the cellular periodic patterns.[4] Low-density polymeric cellular monoliths have been prepared using molecular porogens[5] or emulsion droplets as templates. An example of the latter is the use of *High Internal Phase Emulsions* (HIPE) where the volume fraction of the internal phase exceeds 74%. These are commonly stabilised by low molar mass

surfactants.[6-7] Upon polymerisation of the continuous monomer phase, cellular monoliths, often referred to as poly(HIPE)s, are formed.

Alternatively, polymeric cellular materials can be constructed from colloidal building blocks, whose assembly can produce a variety of supracolloidal structures. In the case of poly(HIPE)s, Colver and Bon demonstrated that polymeric microgels can be used to stabilise emulsion droplets, thereby opening the pathway to monolithic foams with specific local cellular environments.[8] A different, somewhat random, colloidal assembly strategy is the formation of gels from a dispersion of colloids. This method creates robust and highly porous materials with an open-cell structure in which the colloidal building blocks are coalesced or even "glued" together irreversibly.[9] Particularly elegant are continuous bijels obtained from *in situ* phase separation of liquid mixtures, in which solid particles stabilise the newly created interface, as reported by Clegg *et al.*.[10]

An interesting choice of template to guide and confine the assembly of colloids is ice crystals. Talalay pioneered the formation of rubber foam *via* this route in the 1940s by freezing, coagulating and thawing/heating of a rubber latex.[11-12] Typically, a colloidal dispersion is frozen non-instantaneously thereby creating ice crystals *in situ.* After defrosting or sublimation, the reciprocal porous structure remains. Most recent examples do not employ colloids as base constituents and instead include cryo-gels which are prepared by freeze-thawing an initial water-soluble polymer solution[13] or monomer mixture which is polymerised in the non-frozen liquid of the interstitial regions prior to the thawing step.[14] Hybrid organic-inorganic cryogels were made by an *in situ* sol-gel reaction of tetramethoxysilane in an aqueous solution of poly(vinyl alcohol)

prior to the templating procedure *via* freezing.[15] Zhang *et al.* showed the fabrication of aligned porous polymeric structures by directional freezing of polymer solutions, in a few cases in presence of dispersed nanoparticles.[16-17]

Our approach to fabricate polymer foams differs from the above ice-templating strategies in that we use a multi-component mixture of colloids, with a crucial difference in hardness and size as key building blocks. A blend of larger "soft" (*i.e.* low glass transition temperature) polymer latexes is used (diameters in range of 200 – 500 nm) in conjunction with small "hard" nanoparticles (typical length scale *ca.* ten times smaller than the polymer particles). The difference in diameters of the colloids induces a concentration gradient near the wall of a growing ice crystal, caused by an excluded hydrodynamic volume effect, with the smaller "hard" nanoparticles creating an excess closer to the wall. This creates an armoured composite self-supporting cellular structure with a soft polymer composite matrix. By changing several experimental parameters, *e.g.* the nanoparticle-polymer latex ratios and individual concentrations, as well as the nanoparticle type, it is possible to control to a certain extent the pore structure and the overall porosity of the polymer foams. The latter is directly linked to the amount of water used. Moreover, our approach proved to be versatile in composite tunability since it was successfully employed to prepare low-density foams, with porosities easily exceeding 85 vol%, using various types of inorganic nanoparticles, namely silica, Laponite clay, and aluminium oxide, as well as small poly(styrene) (PS) latex particles. We believe our approach of using a mixture of colloids to fabricate foams is extremely versatile for the production of composite cellular materials in a great variety of fields. Here we demonstrate the use of this

strategy to create a conducting nanocomposite soft polymer foam and application of this material as a chemical gas sensor, by using colloidal carbon black as conductive filler. Such a combination of insulating foam dispersed with conducting materials offers numerous advantages for chemoresistive chemical sensor systems. The most important of these are the reversibility of the reaction, which is driven simply by an adsorption/desorption process, the possibility of operating the materials at room temperature, unlike traditional metal-oxide-based sensors and the wide range of available polymers, which offers a spectrum of selectivity values. Furthermore, the foam structure will substantially increase the surface area for chemical adsorption offering increased response magnitude and faster reaction times. Thus, we believe these materials could become a new generation of sensing films.

VI.2. Experimental

VI.2.1. Materials

Vinyl laurate monomer, *n*-hexadecane and sodium hydroxide aqueous solution (NaOH, 0.1 M) were purchased from Aldrich and used without further purification. Azobisisobutyronitrile (AIBN) was kindly donated by Wako, Inc.

For the synthesis of polystyrene nanoparticles: styrene, toluene, sodium styrene sulfonate (NaSS), sodium dodecyl sulfonate (SDS) and potassium persulfate (KPS) were purchased from Sigma-Aldrich and used as received.

Laponite RD clay particles were kindly donated by Rockwood Additives Ltd. The Ludox colloidal silica sol (TM-40) and aluminium oxide (Al_2O_3) nanoparticles were purchased from Aldrich. Silicon wafers (used as sample holders for SEM characterisations) were kindly donated by Wacker Chemie AG.

For the preparation of conducting foams, carbon black (C-black) nanoparticles (Black Pearls 2000) were purchased from Cabot Corporation.

VI.2.2. Equipment

A Branson 450 W digital sonifier (in pulse mode, at 70% amplitude with the following procedure: 6 cycles of 1 minute each, with 40-second intervals in-between) was used to generate submicron-sized emulsion droplets of monomer/hydrophobe in the aqueous phase (referred to as miniemulsion) and to disperse the carbon black particles. The vinyl laurate monomer final conversion was measured by ^{1}H NMR analyses on a Bruker AC400 in deuterated chloroform (see Appendix B, section B.1). Average particle sizes and particle size distributions were measured by dynamic light scattering (DLS) on a Malvern Instruments Zetasizer 3000HSa. The pH measurements were recorded using a Knick pH meter 765 Calimetic. Scanning electron microscopy (SEM) was performed on ZEISS supra 55VP FEG-SEMs with either a Gatan Alto 2500 or a Quorumtech cryo system. All samples characterised by this technique were sputter-coated with platinum (Pt). Conventional SEM samples were sputtered for 40 seconds at 1.5 kV and 25 mA using the auto mode of a Quorum technologies Polaron SC7640 Auto/Manual high resolution sputter coater, and cryo-SEM images were sputtered in the cryo preparation chambers with chromium (Cr). Thermal analysis of the polymer latex was performed using Modulated Temperature Differential Scanning Calorimetry (MTDSC) on a Universal V4.3A TA Instruments.

VI.2.3. Preparation of poly(vinyl laurate) latexes via miniemulsion polymerisation

5.0 g of vinyl laurate was mixed with 0.2 g of *n*-hexadecane and 0.04 g of AIBN. This organic phase was added to 50.0 g of water with a pH of 10-11, adjusted by addition of NaOH (aq, 0.1M). The mixture was emulsified by sonication in an ice bath. The latter is used to prevent early polymerisation. The miniemulsion was degassed by purging with nitrogen gas for 30 minutes, after which the polymerisation was carried out overnight at 65 ºC. Final monomer conversion was typically higher than 90% and average particle sizes were about 200 – 300 nm with dispersities lower than 0.2 (DLS).

VI.2.4. Preparation of polystyrene nanoparticles via emulsion polymerisation

10.0 g of a 1:1 mixture of styrene and toluene was added to 89 g of water, which contained 0.1 g of NaSS and 0.5 g of SDS. This mixture was subsequently degassed through purging with nitrogen gas for 20 minutes, and then pre-heated at 65 ºC for 5 minutes. After injection of 0.05 g of KPS initiator dissolved in 1.0 g of water, the polymerisation was carried overnight at 65 ºC. The final monomer conversion was 99% as measured by gravimetry. The latex was dialysed in deionised water, which was believed to remove the toluene. According to DLS measurement, the average particle size was 37.2 nm, with a polydispersity of 0.15.

VI.2.5. Preparation of composite foams

Various types and quantities of ‘hard’ nanoparticles (Laponite RD clay, Ludox colloidal silica sol and Al_2O_3 nanoparticles) were added to 1.0 g of poly(vinyl laurate) latex. Silicon wafers and custom modified SEM stubs (*i.e.*

SEM stubs in which crosses were carved) were filled with *ca.* 30 µL of the dispersions. The samples were frozen by plunging them into a slush of solid/liquid nitrogen and subsequently freeze-dried under reduced pressure of *ca.* 100 Pa. The compositions of the prepared foams are reported in Table VI-1.

VI.2.6. Calcination of composite foams

Composite foams with a silica-to-PVL ratio of 1.68 were heated at a rate of 5 ºC per minute from room temperature to 600 ºC after which they were kept for 2 hours at 600 ºC.

VI.2.7. Summary of all prepared reinforced polymer foams (non-conductive)

All samples are reported in the following Table VI-1. Overall solids contents were calculated from both masses of PVL and nanoparticles (silica, clay or poly(styrene)) in the initial dispersion prior to freeze-drying. Porosities were calculated from the relative quantity of water in the sample and taking into account the densities of the components.

Table VI-1. Composition of mixtures of colloids used in preparation of nanocomposite reinforced soft polymer foams.

Types of Nanoparticles	***Overall Solids Contents / wt%***	***Ratios Nanoparticles : PVL / g × g^{-1}***	***Calculated porosities * / %***	***Figures***
-	9.3	0.00	-	Figure VI-3.A
Ludox TM-40	12.1	0.22	-	Figure VI-3.B
Ludox TM-40	13.0	0.38	88.6	Figure VI-3.C Figure VI-4
Ludox TM-40	13.5	0.46	88.3	Figure VI-3.D
Ludox TM-40	12.7	0.54	89.2	Figure VI-5
Ludox TM-40	14.4	0.61	87.9	
Ludox TM-40	17.4	1.55	86.9	
	10.6 [#]	*n.a.* [#]	94.1 [#]	Figure VI-6.B [#]
Ludox TM-40	19.7	2.22	85.8	Figure VI-3.E
Ludox TM-40	24.7	4.33	-	Figure VI-1
Ludox TM-40	29.8	8.62	-	
Ludox HS-40	17.4	1.55	86.9	
Ludox SM-30	16.0	1.55	88.0	
Laponite clay	10.7	0.16	-	Figure VI-7.A
Aluminum oxide	16.3	0.90	-	Figure VI-7.B
nano PS [§]	13.5	0.50	-	Figure VI-7.C
Ludox TM-40	40.0	0.00	73.8	
Ludox TM-40	10.0	0.00	94.4	Figure VI-6.A
Ludox TM-40	5.0	0.00	97.3	

* We assumed ideal mixing with densities of 0.94 g cm^{-3} for PVL, of 1.75 g cm^{-3} for Ludox nanoparticles and of 0.931 g cm^{-3} for ice.[18]

[#] Inorganic foam obtained after calcination of the composite material. We considered no volume contraction when calculating the porosity.

[§] Refer to section VI.2.4 for the recipe of the PS nanoparticles synthesis

VI.2.8. Preparation of hybrid carbon black/silica/polymer foams to be used as gas sensors

First, 0.15 g of carbon black (C-black) nanoparticles were dispersed in 3.74 g of a 3 wt% SDS aqueous solution by sonication whilst cooled using an ice-bath. Secondly, 0.62 g of a 40 wt% Ludox silica sol was added to the aqueous C-black suspension. Then, the oil phase composed of 0.5 g of vinyl laurate monomer and 0.025 g of AIBN was added and the whole mixture was emulsified by a second sonication process. After degassing the reaction mixture with nitrogen for 30 minutes, the polymerisation was carried out overnight at 65 ºC. Finally, as aforesaid, the foams were generated by subsequent freezing approximately 30 μL of the polymer/silica/C-black based dispersion in nitrogen slush and freeze-drying.

VI.2.9. Testing hybrid carbon black/silica/polymer foams as gas sensors

To evaluate these materials as gas sensors, three chemoresistive devices were prepared. Our fabricated conducting nanocomposite polymer foams were integrated onto a printed circuit board heater each with two gold terminals (1 mm × 1 mm) using silver paint. These had resistance of 182, 88 and 33 kΩ. The sensors were exposed to ethanol and toluene vapours in air. The sensors were fitted within an automated flow injection analysis system developed within the School of Engineering, at the University of Warwick. This controls the vapour concentration over the sensors and the temperature and humidity of the sensors.[19] The sensors were placed under controlled environmental conditions with a temperature of 30 ^{o}C ± 2 ^{o}C and humidity of 22% ± 2% relative humidity. The sensor resistances were measured by driving the devices at a constant current of 0.1 μA and the voltage drop over the sensors measured using a

custom built interface circuit. The sensors were exposed to five different concentrations of ethanol (2200, 3200, 7000, 10400, 14900 ppm –parts per million) and toluene (1100, 1600, 3600, 5400 and 14900 ppm) vapour in air, each for 600 seconds with 600 seconds recovery period.

VI.3. Results and discussion

VI.3.1. Colloidal dispersion of multi-components

Low glass transition temperature latexes of poly(vinyl laurate) (PVL) were prepared by miniemulsion polymerisation. The surfactant stabilising the polymer particles was produced *in-situ* by the occurrence of partial monomer hydrolysis during the emulsification step, which was carried out by sonication prior to polymerisation. For details on this refer to Chapter II, section II.3.2.3.

This “soft” polymer latex was blended with “small” and “hard” nanoparticles, for instance Ludox TM-40 silica nanoparticles, for the preparation of highly porous composite foams. The next paragraph describes the strategy used to fabricate the porous structure.

VI.3.2. Formation of porous material using the ice-templating strategy

When a waterborne mixture of colloids is frozen, if not entrapped in the ice-crystals, the colloids are confined in the region between them. The ice-crystals can be removed by subsequent freeze-drying. The result is a porous composite network showing the reciprocal structure. In the case of self-supported materials, when the structure does not collapse, the porosity can be estimated from the percentage of solids whereby the structure of the foams mirrors the morphology of the ice-crystals (see Table VI-1). Control on the freezing

temperature, and hence the size and morphology of the ice-crystals, is therefore of crucial importance to template the structured material.

The samples were frozen in a slush of liquid/solid nitrogen (*ca.* -210 °C). Low temperature is employed in order to generate micron-sized ice-crystals. The ice-crystals typically have the shape of columns, dendrites or "ice fingers".[18, 20] Subsequently, the ice-crystals were sublimated by exposing samples to a reduced pressure of 1 mbar (or 100 Pa). The temperature of sublimation was estimated at *ca.* 250 K (or -23 ºC) from the pressure-temperature phase diagram of H_2O.[18] Highly porous materials were obtained and could be imaged at room temperature using scanning electron microscopy, see Figure VI-1 (A and B).

It is interesting to note that, at atmospheric pressure and room temperature, the ice can melt resulting in damage to the foam structure, see Figure VI-1 (C and D). Collapse was logical due to the importance of capillary forces at this length scale; the cohesion of the structured material was not strong enough.[21]

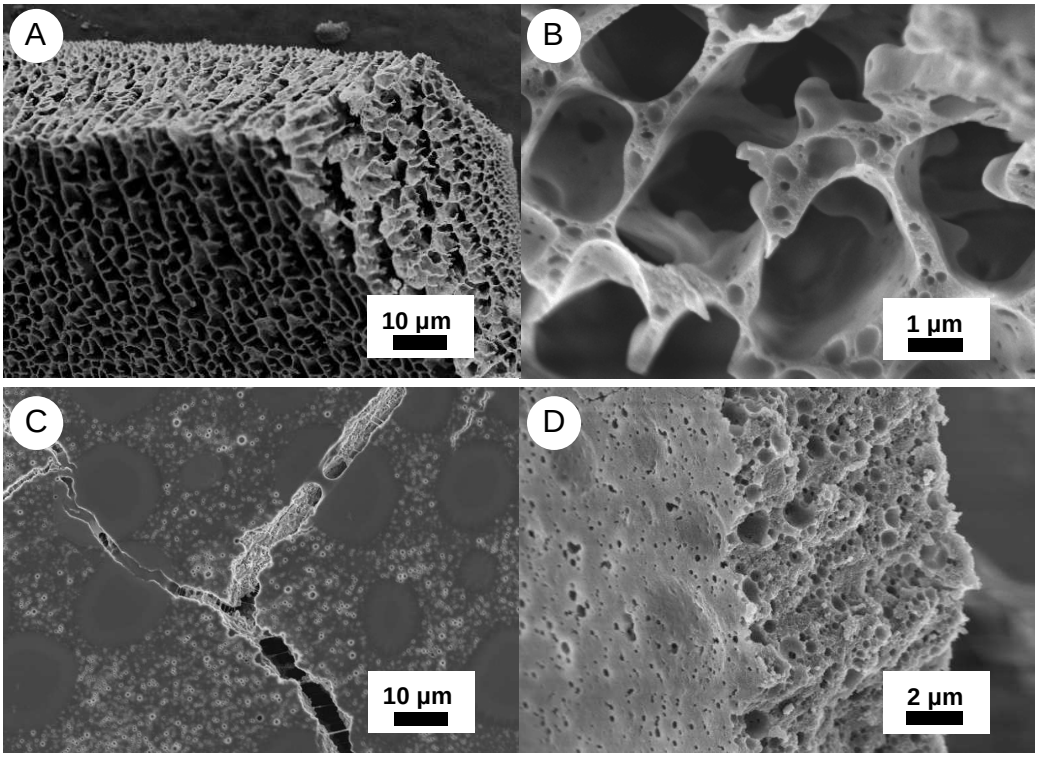

Figure VI-1. SEM images of composite foams obtained after subsequently freezing a waterborne mixture of colloids and, freeze-drying (A and B) or drying (C and D) the sample ("hard" silica nanoparticles (Ludox TM-40) and larger "soft" PVL latex: mass ratio of silica/polymer = 4.33 and overall solid contents of the samples = 24.7 wt%).

Morphology controlled by heat transfer

The porous structure of the foams mirrors the morphology of the formed ice crystals. The obtained cellular structures were clearly affected by heat transfer and mass transfer experienced during the freezing of the water. Notably, for portions of the samples located at sufficient distance from its boundaries, elongated and parallel sheets of foam are observed, while perpendicularly to the elongated-cell axe, a more cellular morphology is found (see *e.g.* Figure VI-2.B). In these zones, equiaxed crystal growth according to an orientation parallel to, or as close as possible to, the main heat flux direction occurred, [18] leading to parallel needle-shaped ice crystals.[22-23] This is in accordance with results obtained from directional freezing experiments carried out by Zhang and

coworkers[16] and the works by Deville *et al.*.[24] As the result of restrictions in heat transfer, the clear increasing gradient in average pore size from the outer regions of the sample, its boundaries being directly exposed to slush of nitrogen, towards its inner content is observed.[25-26] The arrows on the SEM images of Figure VI-2 show the effect of the phenomenon of heat transfer. From the bottom of the arrows, where the sample was in contact with the silicon wafer, and therefore the initial contact with the nitrogen slush, very small pores are formed and the pore size increases along the arrows.

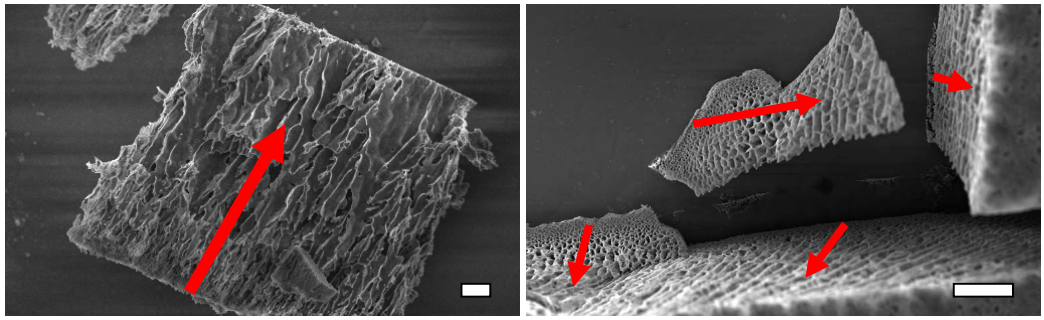

Figure VI-2. SEM images of composite foams obtained after freeze-drying a waterborne mixture of colloids ("hard" silica nanoparticles (Ludox TM-40) and larger "soft" PVL latex: mass ratio of silica/polymer = 4.33 and overall solid contents of the samples = 24.7 wt%). The red arrows show the phenomenon of heat transfer; the direction going from smaller to larger pores. Scale bars 10 μm.

VI.3.3. Reinforcement with "small-hard" nanoparticles

Reinforced structure and high porosities

A series of polymeric foams were prepared using mass ratios of Ludox TM-40 colloidal silica nanoparticles and poly(vinyl laurate) particles of 0, 0.22, 0.38, 0.46 and 0.69, respectively at corresponding overall solids contents of the waterborne mixtures of colloids of 9.3, 12.1, 13.0, 13.6, and 19.7 wt%. SEM analysis at room temperature of the fabricated materials is shown in Figure VI-3.A-E.

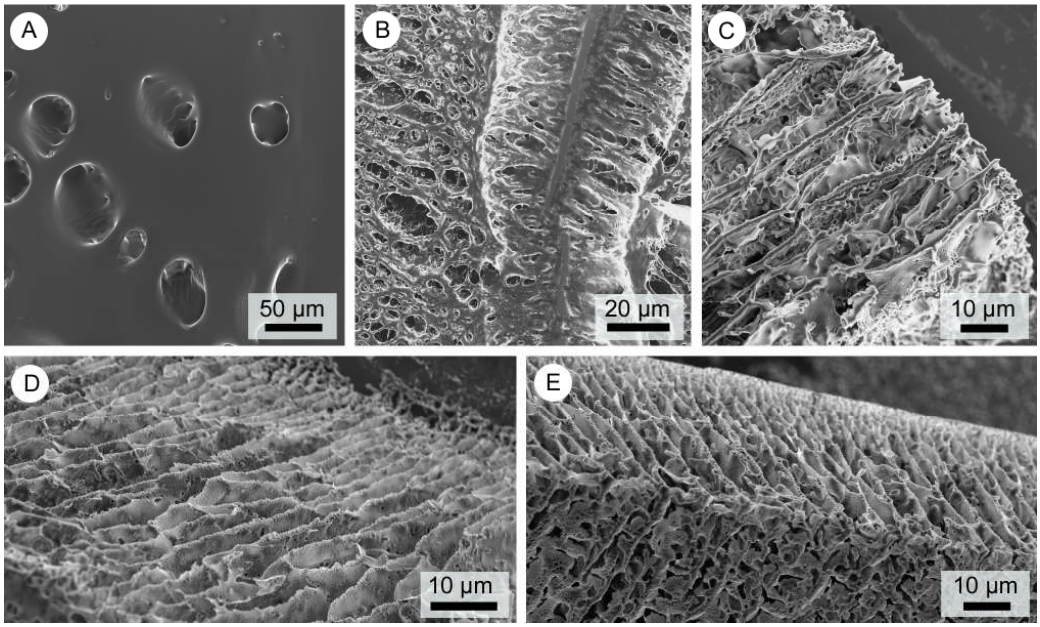

Figure VI-3. SEM images of polymeric foams obtained after freeze-drying a waterborne mixture of "hard" silica nanoparticles (Ludox TM-40) and larger "soft" poly(vinyl laurate) latexes at increasing amounts of silica nanoparticles. Mass ratios of silica/polymer are A = 0, B = 0.22, C = 0.38, D = 0.46, E = 2.22. Overall solid contents of the samples are: A = 9.3 wt%, B = 12.1 wt%, C = 13.0 wt%, D = 13.6 wt%, E = 19.7 wt%.

As shown in Figure VI-3.A, absence of "hard" silica nanoparticles resulted in the collapsing of the polymer foam at ambient temperatures. PVL has a glass transition temperature far below ambient temperature, around -60 ºC,[27] which explains the lack of mechanical strength and deformation of the foam. Upon addition of silica nanoparticles of increasing amounts a porous structure representing the reciprocal template of the ice crystals emerges (Figure VI-3.B-E). These templated composite polymer foams become well-defined when ratios of "hard" nanoparticles to large "soft" polymer latex particles in excess of 0.38 are used. From the quantities of PVL, solid nanoparticles, and water used, the overall calculated porosities ranged from 85% upwards. A series of samples are reported in Table VI-1 in the experimental part, VI.2.5.

Enrichment in silica nanoparticles

Looking at a high magnified image (Figure VI-4) it becomes evident that the cell walls of the composite polymer foam are covered with nanoparticles.

Figure VI-4. Cryo-SEM image of nanocomposite polymer foam obtained after freezing a mixture of a PVL latex and Ludox silica nanoparticles at -210 °C with silica/polymer ratio and total solids content (wt%) of 0.38 and 13.0, respectively. The image was taken after full sublimation of the ice. Scale bar 200 nm.

These armoured structures are a consequence of the difference in size between the large "soft" polymer latex particles and the "hard" silica nanoparticles. The inability of larger particles (~270 nm diameter polymer particles) to approach the solid-liquid interface of the interstitial regions with the channel walls of the growing ice crystals compared to smaller particles (~25 nm diameter silica nanoparticles) generates an enrichment of the nanoparticles near the walls. Similar effects have been observed in composite polymer latex films formed from a blend of silica nanoparticles and a poly(methyl methacrylate-*co*-butyl acrylate) latex.[28]

We envisage that the armoured structure not only provides an enhanced mechanical stability of the composite polymer foam, but also introduces a

unique and tailored surface functionality. This can be of great value when these foams are used in areas that require adhesion or adsorption, such as chromatographic applications. Due to the surface excess of the nanoparticles a near saturated functionalisation is achieved at mass ratios of Ludox TM-40 colloidal silica nanoparticles and poly(vinyl laurate) particles of 0.46 and higher. Increasing the silica content to very high ratios generated composite polymer foams of a more brittle nature.

VI.3.4. Entrapment of "large" polymer particles

Cryo-SEM imaging, Figure VI-5, shows that large "soft" latex particles can become individually entrapped in the ice, whereas throughout sublimation of the samples during cryo-SEM imaging no individual silica nanoparticles could be found.

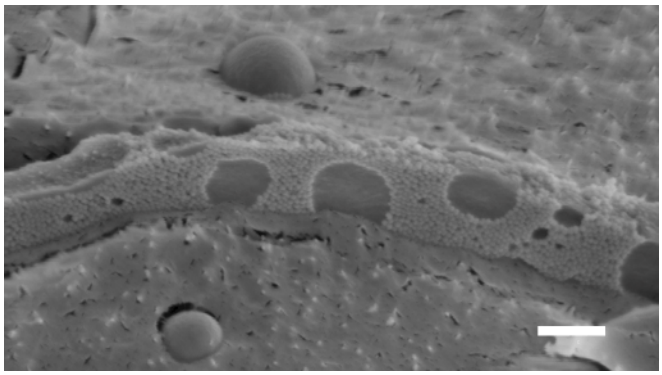

Figure VI-5. Cryo-SEM image of nanocomposite polymer foam obtained after freezing a mixture of a PVL latex and Ludox silica nanoparticles at -210 °C with silica/polymer ratio and total solids content (wt%) of 0.54 and 12.7, respectively. The image was taken after partial sublimation of the ice. Scale bar 300 nm.

Depending on the velocity of the growing water-ice interface, impurities such as particles and/or solute, either become entrapped by the advancing interface or are pushed and swept along with the advancing front thus remaining concentrated in the interstices between the solid ice crystals.[29] In the case of a

particle moving very close to a flat solidification front, the critical velocity v_c marking the border between particle encapsulation and rejection can be expressed by the following equation:[16, 29]

$$v_c = \frac{\Delta\sigma_0 d}{3\eta r}\left(\frac{a_0}{d}\right)^n \qquad \textbf{Equation VI-1}$$

Where η is the viscosity of water, $\Delta\sigma_0$ the difference in interfacial free energy between the entrapped particle in ice and the sum of the surface free energies of ice-water and particle-water, *d* the distance between the particle and the interface, solidification front, a_0 the intermolecular distance of water, *r* the radius of the particle, and *n* an exponent which is larger than 1.[28] This critical velocity is inversely proportional to the radius of the particle but its determination suffers from great experimental uncertainties in values of $\Delta\sigma_0$ and *d.* However, it is clear that the probability of entrapment of large particles is higher, which indeed is observed from our experiments (Figure VI-5).

VI.3.5. Preparation of inorganic foams with super-high porosity

Thermal treatment is a common fabrication route for porous inorganic materials. For instance, Schmid *et al.* reported the formation of hollow silica shells after calcination of polystyrene-silica nanocomposite particles.[30] Inorganic foams were obtained by freeze-drying diluted Ludox colloidal sols or by calcining the composite polymer foams at 600 ºC (Figure VI-6). Pores of similar shape and size were obtained in both cases, but the structure of the cell walls was clearly different. By freeze-drying a 10 wt% Ludox sol, smooth walls were obtained whereas in the case of our polymer/Ludox foams, after thermally

decomposing the polymer out, holes were observed. Extra surface area was created as templated from the polymer particles, see Figure VI-6 for comparison. Although further investigations are required for absolute proof, it is also known that additional thermal treatments re-enforce the structure by crosslinking the silica nanoparticles *via* conversion of silanol groups to siloxane bridges, at temperatures over 300 ºC.[31]

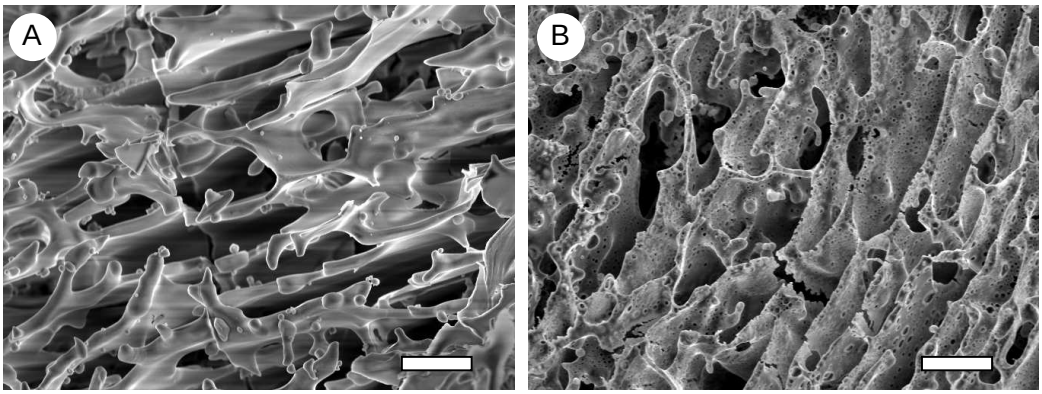

Figure VI-6. SEM images of silica porous structures prepared from (A) freeze-drying a 10 wt% Ludox silica sol, and from (B) successively freeze-drying and calcining a PVL-Ludox sol of about 10 wt% in silica and 7 wt% of PVL (B). Scale bars 10 μm.

This opens new perspectives for the preparation of foams whereby functionality can be tuned by the choice of nanoparticles used. It can thus be suggested that foams produced this way could be extremely promising materials for potential applications as cell growth scaffolds (if bio-compatibles particles like hydroxyapetite nanoparticles are used), sensors, and stationary phase for separation or filtration techniques.

VI.3.6. Versatility of the process using different types of "hard" nanoparticles

Several "soft"-polymer foams were successfully reinforced with different types of "hard"-nanoparticles, *i.e.* Laponite RD clay discs particles (a synthetic trioctahedric hectorite clay, $[Si_8(Mg_{5.45}Li_{0.4})O_{20}(OH)_4]Na_{0.7}$, with approximate diameter of 25-35 nm and a thickness of about 1 nm), aluminium oxide (Al_2O_3) nanoparticles of *ca.* 50 nm diameter, and an in-house prepared polystyrene latex (DLS data showed d_z = 37.2 nm and D_I = 0.15).

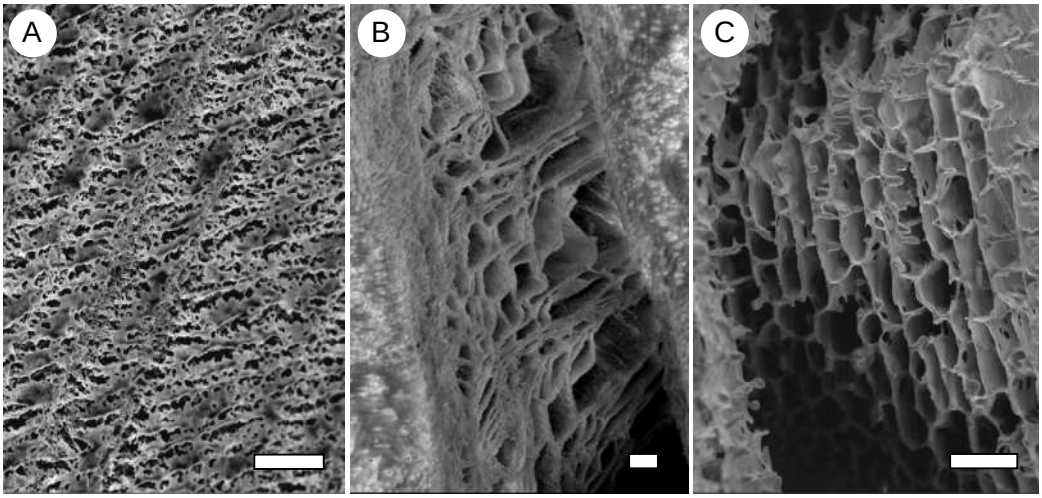

Figure VI-7. SEM images of composite-PVL foams reinforced with (A) Laponite clay (scale bar 10 µm), (B) aluminum oxide (scale bar 20 µm) and (C) polystyrene nanoparticles (scale bar 10 µm).

In case of Laponite clay a mass ratio of clay discs to poly(vinyl laurate) of 0.16 sufficed as a direct result of the higher surface-to-volume ratio these nanoparticles offered compared with the spherical Ludox TM-40 silica sol. The relatively larger Al_2O_3 and poly(styrene) particles required ratios of 0.90 and 0.50 respectively.

VI.3.7. Conducting foams as gas sensors

We increased the complexity of our colloidal dispersion by addition of a third colloidal component, carbon black (C-black) particles with approximate

diameter of 120 nm. These C-black particles were dispersed with the aid of sodium dodecyl sulfate as surfactant. The overall weight percentage of C-black particles in our experiments was 14 wt% with respect to the foam matrix. The foam obtained was conductive, meaning that the percolation threshold value to fabricate conducting multi-component supracolloidal foams was exceeded. In our opinion these conducting cellular materials could be excellent candidates as gas sensor devices.

Existing chemical sensors manufactured from composites of C-black particles and insulating polymer have been demonstrated as room temperature (thus low power) chemical sensors for detecting a range of volatile organic compounds.[32] Such devices are proposed to operate *via* a swelling/expanding effect where adsorbed vapours cause the polymer to swell. This reduces the number of conduction paths through the material, resulting in an increase in resistance. We believe that soft polymer matrixes potentially will provide rapid response times and enhancements in sensitivity as a result of increased rates of gas adsorption/ polymer matrix expansion. Moreover, the armoured structure of the cells in the porous material may provide substrate-specific functionality.

An initial simple test involved a piece of our conducting foam attached to copper wires and multi-meter allowing the facile measurement of resistance across said foam, see Figure VI-8. A distinct reversible response upon exposure to toluene vapour was recorded by placing the polymeric material several millimetres above a drop of toluene. The resistance in this distance increased from 29.2 to 31.5 kΩ and was observed to be reversible and repeatable when the foam was removed from the toluene vapours.

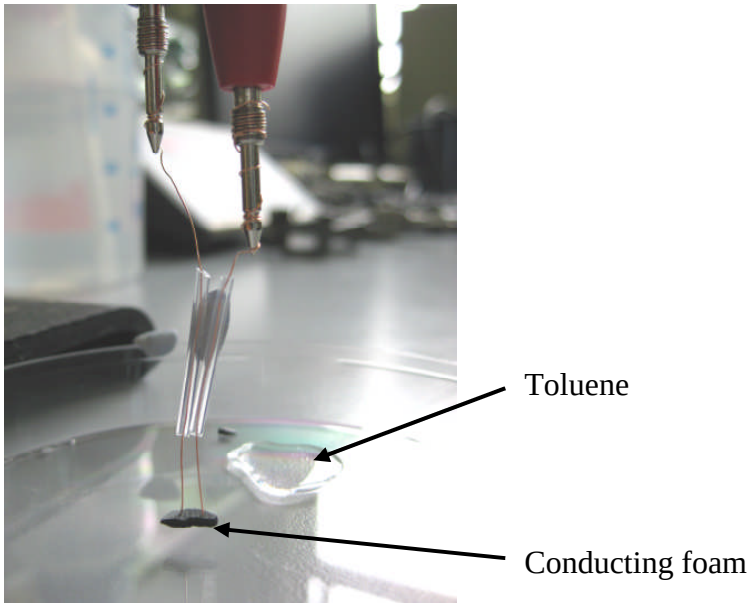

Figure VI-8. Picture of the conducting foam wired to two electrodes for studying the influence of toluene vapours on the resistance of the conducting material.

Consequently, our fabricated conducting nanocomposite polymer foams were integrated onto a printed circuit board heater with two gold terminals (1 mm x 1 mm) using silver paint. This was done in order to simplify the connection to the experimental test equipment as seen in Figure VI-9 (A). Figure VI-9 (B) shows the real-time response of a sensor to these increased ethanol vapour concentrations in air. Figure VI-9 (C) exhibits the average fractional steady state response as a function of increasing vapour concentration. The fractional response is calculated by dividing the change in resistance by the initial resistance baseline. The figure clearly indicates linear response and a higher sensitivity of the films to toluene than ethanol (toluene sensitivity 2.22×10^{-6} ppm^{-1}, ethanol sensitivity 7.8×10^{-7} ppm^{-1}).

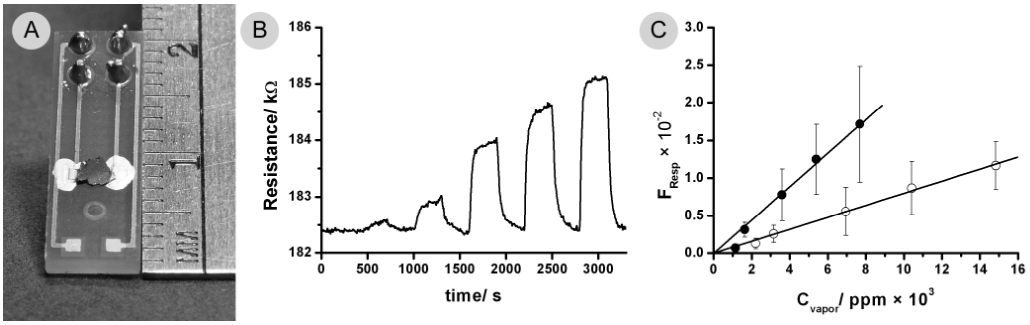

Figure VI-9. (A) Conducting nanocomposite polymer foam integrated onto a printed circuit board heater (scale bar of ruler in cm). (B) Typical electrical resistance response signals vs. time upon exposure to vapour of ethanol in increasing concentration. (C) Average fractional steady state response values to increasing vapour concentration of toluene (●) and ethanol (○).

VI.4. Conclusions

To conclude, we have demonstrated that nanoparticle-reinforced "soft" polymer foams can be prepared by freeze-drying colloidal mixtures of nanoparticles and low glass transition polymer latexes. We demonstrated that the cellular structures depended on the freezing rates. Surface enrichment of the cells with nanoparticles acted as a scaffold and reinforced the polymer matrix, where the nanoparticle excess was the result of a hydrodynamic volume effect. Incorporation of colloidal carbon black as a third and conducting component provided an elegant procedure to fabricate porous conducting "soft" polymer foams which demonstrated potential use as gas sensor materials.

VI.5. References:

1. Colard, C. A. L.; Cave, R. A.; Grossiord, N.; Covington, J. A.; Bon, S. A. F., *Adv. Mater.* **2009,** *21* (28), 2894-2898.

2. Gibson, L. J.; Ashby, M. F., *Cellular Solids - Structure & Properties*. Pergamon Press, Oxford: 1988.

3. Suh, K. W.; Skochdopole, R. E., Foamed Plastics. In *Kirk-Othmer Encycl. Chem. Technol., 3rd Ed.*, Kroschwitz, J. I.; Howe-Grant, M., Eds. Wiley, New-York: 1980; Vol. 11, p 731-743.

4. Xia, Y.; Gates, B.; Yin, Y.; Lu, Y., *Adv. Mater.* **2000,** *12* (10), 693-713.

5. Hilder Emily, F.; Svec, F.; Frechet Jean, M. J., *Electrophoresis* **2002,** *23* (22-23), 3934-53.

6. Zhao, C.; Danish, E.; Cameron, N. R.; Kataky, R., *J. Mater. Chem.* **2007,** *17* (23), 2446-2453.

7. Williams, J. M.; Gray, A. J.; Wilkerson, M. H., *Langmuir* **1990,** *6* (2), 437-44.

8. Colver, P. J.; Bon, S. A. F., *Chem. Mater.* **2007,** *19*, 1537-1539.

9. Schmidt, D. F.; du Fresne von Hohenesche, C.; Weiss, A.; Schaedler, V., *Chem. Mater.* **2008,** *20* (9), 2851-2853.

10. Herzig, E. M.; White, K. A.; Schofield, A. B.; Poon, W. C. K.; Clegg, P. S., *Nat. Mater.* **2007,** *6* (12), 966-971.

11. Talalay, J. A. U.S. Patent 2,432,353, 1947.

12. Talalay, L.; Talalay, A. U.S. Patent 3,238,172, 1966.

13. Lozinsky, V. I.; Galaev, I. Y.; Plieva, F. M.; Savina, I. N.; Jungvid, H.; Mattiasson, B., *Trends Biotechnol.* **2003,** *21* (10), 445-451.

14. Savina, I. N.; Cnudde, V.; D'Hollander, S.; Van Hoorebeke, L.; Mattiasson, B.; Galaev, I. Y.; Du Prez, F., *Soft Matter* **2007,** *3* (9), 1176-1184.

15. Lorinsky, V. I.; Bakeeva, I. V.; Presnyak, E. P.; Damshkaln, L. G.; Zubov, V. P., *J. Appl. Polym. Sci.* **2007,** *105*, 2689-2702.

16. Zhang, H.; Hussain, I.; Brust, M.; Butler, M. F.; Rannard, S. P.; Cooper, A. I., *Nat. Mater.* **2005,** *4* (10), 787-93.

17. Zhang, H.; Cooper, A. I., *Adv. Mater.* **2007,** *19* (11), 1529-1533.

18. Hobbs, P. V., *Ice Physics*. Clarendon Press: Oxford, 1974.

19. Tan, S. L.; Covington, J. A.; Gardner, J. W., *IEE P-Sci. Meas. Tech.* **2006,** *153* (3), 94-100.

20. Kochs, M.; Körber, C.; Heschel, I.; Nunner, B., *Int. J. Heat Mass Transfer.* **1993,** *36*, 1727-1738.

21. Ostrikov, M. S.; Dibrov, G. D.; Danilova, E. P., *Dokl. Akad. Nauk SSSR* **1958,** *118*, 751-4.

22. Chevalier, D.; Sentissi, M.; Havet, M.; Le Bail, A., *J. Food Sci.* **2000,** *65*, 329-333.

23. Woinet, B.; Andrieu, J.; Havet, M.; Le Bail, A., *J. Food Eng.* **1998,** *35*, 395-407.

24. Deville, S.; Saiz, E.; Nalla Ravi, K.; Tomsia Antoni, P., *Science* **2006,** *311* (5760), 515-8.

25. Woinet, B.; Andrieu, J.; Laurent, M.; Min, S. G., *J. Food Eng.* **1998,** *35*, 381-393.

26. Shanti, N. O.; Araki, K.; Halloran, J. W., *J. Am. Ceram. Soc.* **2006,** *89*, 2444-2447.

27. Delgado, J.; Tran, T.-V. T. PCT Int. Appl. WO 9601280, 1996.

28. Luo, H.; Cardinal, C. M.; Scriven, L. E.; Francis, L. F., *Langmuir* **2008,** *24* (10), 5552-5561.

29. Korber, C.; Rau, G.; Cosman, M. D.; Cravalho, E. G., *J. Cryst. Growth* **1985,** *72* (3), 649-62.

30. Schmid, A.; Fujii, S.; Armes, S. P., *Langmuir* **2006,** *22* (11), 4923-4927.

31. Mikhail, R. S.; Khalil, A. M.; Nashed, S., *J. Appl. Chem. Biotechnol.* **1977,** *27* (1), 17-24.

32. Lonergan, M. C.; Severin, E. J.; Doleman, B. J.; Beaber, S. A.; Grubbs, R. H.; Lewis, N. S., *Chem. Mater.* **1996,** *8* (9), 2298-2312.

Chapter VII.

Conclusion and outlook for industrial applications

This chapter highlights the main conclusions of this work. It summarises the achievements of each chapter towards the industrial objectives. Further routes for the development of solids-stabilised polymer additives are briefly discussed.

Poly(vinyl acetate)-based latexes stabilised with poly(vinyl alcohol) are commonly prepared at large scale by industries in emulsion polymerisation. Powders are obtained by spray-drying of dispersions. Often inorganic particles are incorporated as anti-caking agents. The produced powders are widely used in industrial applications such as cement-based formulations for tile adhesives.

The purpose of this work was to prepare poly(vinyl acetate)-based latexes by replacing the polymeric protective colloid with solids-stabilisers. We used silica particles due to their chemical attributes leading to direct integration in cementitious applications. Due to the wide range of commercial grades, silica particles with different surface properties, sizes and shapes were very attractive for use in this kind of system.

Nanoparticles can assemble at liquid-liquid interfaces and have proven their ability to stabilise emulsion droplets, thereby acting as surfactant molecules. To avoid the addition of any co-monomer/co-stabiliser, our research initially focussed on the investigation of the adherence of clay/silica nanoparticles at monomer-water interfaces.

In Chapter II, we showed that synthetic clay particles stabilised poly(vinyl laurate) latexes synthesised in miniemulsion polymerisation. However their physicochemical properties not only restricted their concentration to low solids contents, but also imposed a high pH system requirement leading to the hydrolysis of the monomer of interest for industrial purpose, vinyl acetate.

We then investigated the use of Ludox colloidal silica as solids-stabiliser in Chapter III. Armoured latexes were obtained upon polymerisation of the solids-stabilised monomer droplets in miniemulsion or suspension polymerisation. For this purpose, the surface properties of silica particles were tuned by modifying

the pH of the dispersion. Larger particles of fumed silica exhibited similar surface properties *i.e.* zeta potential. In case of Ludox colloidal silica, we found that the size of the building blocks (in the range of 7-25 nm in diameter) controlled the size of the miniemulsion monomer droplets (diameter from ~310 nm to ~200 nm). This approach was also used in suspension polymerisation to prepare Ludox-stabilised poly(vinyl acetate) particles. Here, small latex particles armoured with silica nanoparticles (< 200 nm in diameter) were also formed *via* secondary nucleation.

This strategy in suspension polymerisation could be extended by using larger solid stabiliser and of different shapes, such as fumed silica. The formation of secondary particles may be avoided in this case.

In Chapter IV, we have shown the synthesis of solids-stabilised latexes of poly(vinyl acetate) in emulsion polymerisation. Colloidal assembly *via* heterocoagulation is a common route for the formation of raspberry-like structures. Adherence of the nanoparticles onto the polymer beads generally requires the addition of co-stabiliser or co-monomer. However, this was not necessary in our system of silica nanoparticles and poly(vinyl acetate)-based latexes potentially due to hydrogen bond interactions. The ease of scaling up these emulsion polymerisation reactions also presents a significant advantage towards industrial application. We described the key mechanistic features of the formation of these Ludox-armoured latex particles throughout the emulsion polymerisation process and showed that disc centrifuge particle sizing could be used as a quantitative tool to monitor the concentration of free silica nanoparticles (stabiliser) in the water phase. We observed a relatively short

nucleation period, followed by the interval for particle growth after which coalescence of the polymer particles occurred as the reaction ran out of free colloidal silica and full coverage of the latex particles ceased to be achieved.

Semi-batch processes controlling the instantaneous concentrations in monomer and also free silica nanoparticles could probably be a straightforward way to prepare latexes of larger polymer particles with narrow dispersity.

A series of poly(vinyl acetate)-based latexes stabilised with Ludox silica nanoparticles were further investigated for industrial applications in Chapter V. Various solid contents, stabiliser concentrations, polymeric compositions, and sizes of colloidal stabiliser were used to prepare latexes of 1 litre emulsion polymerisation reaction batches.

The concentration of calcium cations and pH increase considerably in cementitious application as the hydration reaction/hardening of the material occurs. We therefore studied the colloidal stability of the prepared latexes and the armoured monolayer of silica upon addition of calcium hydroxide. Initially, better colloidal stability of the latex against sedimentation was obtained. With increasing calcium hydroxide concentration, the armoured structure was lost as the charges borne by the silica nanoparticles made them desorb from the polymeric surface. Once the latex is added to cement-based formulations, the loss of their silica shell could potentially be an advantage for the polymer particles to act as an adhesive. However, at pH above 10, coagulation of the latex occurred due to the high ionic strength of the medium.

Powders present numerous advantages in comparison to dispersions. They have a longer shelf life and lower packaging and transport costs. Redispersible

powders are industrially produced by spray-drying colloidal dispersions. Film formation is commonly limited upon addition of water soluble polymer and anti-caking agents. Spray-drying of silica-armoured polymer particles was performed without any additional constituents. Depending on the thickness of the armouring shell (size of the silica nanoparticles), limited coalescence of the latex particles within the powder particles occurred. When film forming was avoided, re-dispersible powders could be obtained. However, a lack of cohesion within the powder particles presented a drawback. Single hybrid polymer particles of approximately one micron in diameter or smaller were observed. Ideally, powder particles should not be smaller than 30 microns, otherwise they are more difficult to handle and present a major respiratory hazard.

Although the initial purpose of this work was to remove poly(vinyl alcohol) from the formulation, little addition of water soluble polymer before spray-drying the dispersion could improve the cohesion within the produced powder particles but still allow their dispersion.

The prepared powders were then tested in cement-based formulations for tile adhesives. Poor results including hard workability of the paste and weak adhesive properties were obtained. In our opinion, the prepared armoured particles are too robust and do not film formed in the material. The nanoparticles of silica not only represent a physical barrier around the polymer beads, but also modify its glass transition temperature. It is well-known that nanoparticles can highly influence rheological properties when blended with polymer materials. The advantage of this effect was used to reinforce the structure of low glass transition temperature foams prepared by freeze-drying dispersions, see Chapter

VI. “Larger-soft” poly(vinyl laurate) latex particles film-formed in the regions between the ice crystals and considerably smaller “hard” nanoparticles, *i.e.* Ludox TM-40 colloidal silica, armoured and maintained the porous structure after sublimation of the micron-sized ice crystals. The material was also developed as gas sensor upon addition of colloidal carbon black for the preparation of conducting nanocomposite foams.

From this work, two synthetic routes can be retained and further developed for the synthesis of solids-stabilised polymer particles: (i) assembly of colloids at liquid-liquid interfaces of monomer droplets in miniemulsion/suspension polymerisation, and (ii) specific adherence of silica nanoparticles onto growing poly(vinyl acetate) particles in emulsion polymerisation.

Design of solids-stabilised polymer particles should be further developed by studying their rheological properties.

Appendix A. Characterisation of colloids

Throughout this work, monomer conversion was commonly measured by gravimetry when possible (otherwise by 1H NMR spectroscopy, see Chapter II). Particle size distribution and zeta potential were measured by light scattering techniques[1-3] and imaging was performed by scanning or transmission electron microscopy.[4-5] The principle of those techniques and protocols for sample preparation are described herein.

A.1. Gravimetry

Gravimetry was performed by sampling the reaction over time and when the reaction was stopped. Samples were weighed as soon as they were taken from the reaction vessel (M_{wet}), dried carefully and then weighed again (M_{dry}). During drying, we assume all the water and the remaining monomer to evaporate. The following equation was used to calculate the monomer conversion X_m:

$$X_m = \left(\frac{M_{dry}}{M_{wet}} - \frac{M_{0,Solid}}{M_{0,Total}} \right) * \left(\frac{M_{0,Total}}{M_{0,Monomer}} \right) \qquad \textbf{Equation A-1}$$

Where $M_{0,Solid}$ is the mass of solid stabiliser, typically silica nanoparticles, $M_{0,Total}$ is the total mass of the system and $M_{0,Monomer}$ is the initial amount of monomer. The ratios $\frac{M_{0,Total}}{M_{0,Monomer}}$ and $\frac{M_{0,Solid}}{M_{0,Total}}$ account for the volatile and non-volatile compounds other than the monomer and polymer, respectively.

A.2. Electrophoretic light scattering

Electrophoretic light scattering measurements were performed on a Malvern Instruments Zetasizer 3000HSa or on a Malvern Zetasizer Nano.

Electrophoretic light scattering measurements analyse the rate of diffusion, or electrophoretic mobility, of charged particles relative to the liquid they are suspended in under the influence of an applied electric field. In addition to their Brownian motion, the particles move in the field towards the oppositely charged electrode. A liquid layer surrounding each particle is moving with them and the potential is measured at its boundary, the slipping plane, this is the zeta potential, see Figure A-1. When an electric field is applied, the particles reach a constant velocity, the electrophoretic mobility, which depends on the strength of the field. The zeta potential, *z*, is related to this electrophoretic mobility, U_E, by the Henry equation:

$$U_E = \frac{2\varepsilon z f(Ka)}{3\eta} \qquad \textbf{Equation A-2}$$

Where, ε and η are the dielectric constant and the viscosity of the media, respectively and $f(Ka)$ is the Henry's function where K^{-1} is the Debye length (reciprocal length) often taken as a measure of the thickness of the electrical double layer, and a refers to the radius of the particle. As described by the model of the diffuse electrical double layer (see section I.2.1), the ionic strength also modify the thickness of the slipping plane.

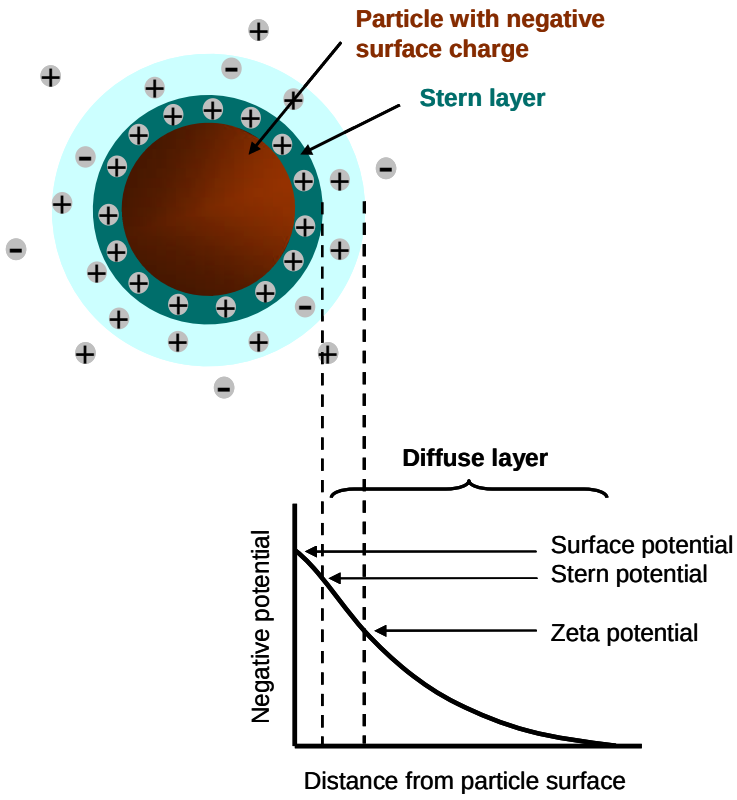

Figure A-1. Schematic representation of the slipping plane and the corresponding zeta potential.

The Smoluchowski approximation was then used assuming the thickness of the electrical double layer to be negligible compared to the particle size; *Ka* is infinite and in this case $f(K\,a)$ is simply equal to 1.5. This approximation holds for the determination of the zeta potential made in aqueous media for moderate electrolyte concentration (> 10^{-3} M).

The electrophoretic mobility is measured using the *Laser Doppler Velocimetry* technique. Two laser beams cross at a specific point in the sample cell to form interference fringes of known spacing. When an electric field is applied, the particles move through those fringes and the intensity of the scattered light fluctuates with a frequency that is related to the particle velocity, that is to say the electrophoretic mobility.

As there is no direct measure of the distance of the slipping plane from the surface, it is impossible to relate the zeta potential to the surface potential. However, the magnitude of the zeta potential gives an indication of the potential stability of the colloidal system. As a general guide, systems with zeta potentials higher than +30 mV or lower than -30 mV are considered to be colloidally stable. The pH has a direct influence on the surface chemistry of the particles; therefore a zeta potential value without a quoted pH is quite meaningless.

Sample preparation and method

A drop of latex was diluted in an aqueous solution of desired ionic strength and the pH was generally modified after dilution to the appropriate value of investigation. The sample was then injected in the supplied cell for electrophoretic measurements and temperature control was set at 25 ºC.

A.3. Dynamic light scattering

Average particle sizes and particle size distributions were measured by dynamic light scattering (DLS) on a Malvern Instruments Zetasizer 3000HS or on a Malvern Zetasizer Nano ZS.

In dynamic light scattering, also called photon correlation spectroscopy, the hydrodynamic diameter is obtained by measuring the particle diffusion in the fluid, and corresponds to a sphere having the same translational diffusion coefficient than the particle. The ionic strength and the pH of the media, having an influence on the slipping plane (see previous section A.2), also affect the measurement.

The size of the particles is calculated from the diffusion coefficient, D (m^2 s^{-1}), by using the Stokes-Einstein equation:

$$d_z = \frac{kT}{3\pi\eta D} \qquad \textbf{Equation A-3}$$

Where, d_z is the hydrodynamic diameter (m), k is the Boltzmann's constant (J K^{-1} or kg m^2 s^{-2} K^{-1}), T is the absolute temperature (K) and η the viscosity (Pa s^{-1} or kg m^{-1} s^{-1}).

The light of the incident beam (in our case, a laser He-Ne of wavelength λ = 633 nm) is scattered by the particles dispersed in a media. The detector records the scattered light at an angle of 90 degrees (Zetasizer 3000HS) or 173 degrees (Zetasizer Nano ZS) and the intensity fluctuations are measured over time. The Rayleigh approximation tells us that the intensity is proportional to the diameter to the power 6 and holds typically for nanoparticles with diameters up to a tenth of the light source wavelength (around 60 nm for a He-Ne laser). Larger particles scatter the light in an isotropic manner which is correctly described by the Mie theory in a complex function with minima and maxima in the plot of intensity over all particle sizes, laser wavelengths and angles of detection.

Due to the Brownian motions of the particles, the smaller the particles are, the faster the fluctuations are, see Figure A-2. However, the interaction of light with matter varies with the particle size.

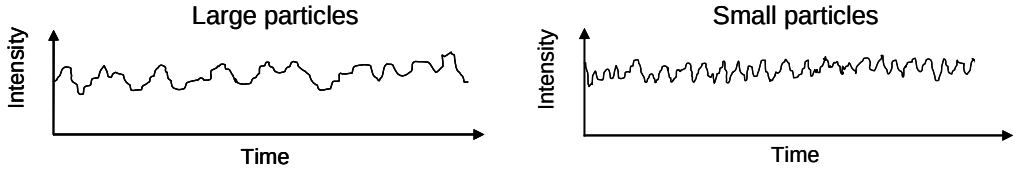

Figure A-2. Schematic representation of typical fluctuations of the intensity for large particles compared to small particles.

A correlator which compares the signals at varying time intervals (τ) calculates the exponential decaying correlation function, $G(\tau) = A\,[1 + B\,g_1(\tau)^2]$. The larger the particles, the slower their correlation will change due to their slower Brownian motion, see Figure A-3.

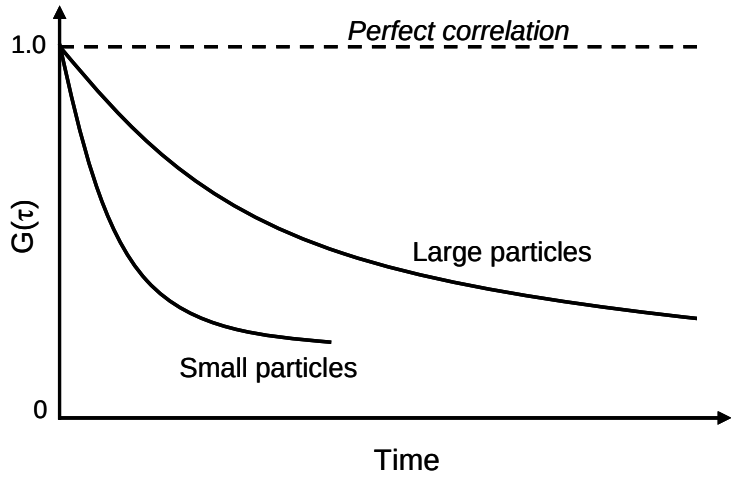

Figure A-3. Graph of the correlation function as a function of time for small or large particles in dynamic light scattering measurements.

The logarithm of the correlation function, $\ln G(\tau)$, is only linear for a large amount of identical particles in Brownian motion and the slope of the fitted line is related to the average particle size. Different methods of analysis have been developed to evaluate the correlation function however none of them can give a perfect accurate particle size distribution as many answers could correspond to similar correlation functions. Contin analysis, most commonly used, involves the calculation of several possible distributions and some statistic model on the most probable solution. Cumulant analysis is described as an example for the determination of the average particle size distribution and its width, the dispersity. Representative results are obtained from expanding a polynomial curve (3rd order) as a fit of the correlation function for a particle size distribution near to monodisperse:

$$LnG(\tau) = a + b\tau + c\tau^2 + d\tau^3 \qquad \textbf{Equation A-4}$$

In this case, the average particle size is obtained from the initial slope of the curve, *i.e.* the value of the second diffusion coefficient *b*, and the dispersity (width of the particle distribution) is calculated from the gap to the linear behaviour given by $2c/b^2$.

Sample preparation and method

A drop of latex was generally diluted in deionised water or, if necessary for stability purposes in an aqueous solution of similar pH and ionic strength to the latex. Polystyrene cuvettes with four clear faces were used and filled with suitable amount of sample for ideal temperature control and 2 minutes were allowed for the sample temperature to stabilise at 25 ºC.

A.4. Imaging by electron microscopy

Electron microscopy is similar in its principle to optical microscopy but in this case the light source is replaced by an electron gun. A high vacuum is required allowing propagation of the electron beam. Electrons are accelerated with an electrical potential and focussed on the sample by a series of electromagnetic lenses, condenser and objective lenses. In optical microscopy, even if all the lenses of the microscope were perfect introducing no distortion into the image, the resolution would be then limited by diffraction due to the wave nature of the photon source. The electron wavelength depends on the acceleration voltage but its magnitude can be over 10 000 times smaller then the photon wavelength considering it is about 0.01 nm at 20 kV compared to the

photon wavelength which is only down to about 200 nm if it is possible to use ultraviolet light.

A.4.1. Scanning electron microscopy

Scanning electron microscopy (SEM) imaging was performed on ZEISS supra 55VP field emission gun scanning electron microscope (FEG-SEM) equipped with an electron backscattered diffraction camera.

Electrical potentials in the range of 1 kV to 30 kV are used and electromagnetic coils allow the user to perfect the alignment and therefore the resolution. This microscope is used in reflection mode and topography images are built up sequentially during the scan of the sample area by detecting the intensity of backscattered and escaping secondary electrons.

Sample preparation and method

Samples for SEM analysis were prepared on silicon wafers (donated by Wacker Chemie AG, Germany) stuck on SEM stubs (purchased from Agar Scientific) by simply evaporating a drop of diluted latex, drying it by convective assembly or freeze-drying samples as for the preparation of foams (Chapter VI). If necessary, samples were made conducting by coating them with a thin metal layer of gold, gold/palladium or platinum. Settings were optimised and best imaging was generally obtained after sputtering 40 seconds at 1.5 kV and 25 mA using the auto mode of a Quorum technologies Polaron SC7640 Auto/Manual high resolution sputter coater. The applied electrical potential was typically set at 5 kV or up to 10 – 20 kV for uncoated samples. The image mode

‘pixel noise reduction’ was commonly used while adjusting the focus and the astigmatism and the pictures were taken using the ‘line average’ mode. Alternatively, in the case of thicker samples, the ‘continuous average’ mode was sometimes used to avoid charging effects but lower resolution was found.

A.4.2. Transmission electron microscopy

Transmission electron microscopy (TEM) analyses were performed on a 1200EXII TEM with a 1K Gatan camera, a Jeol 2000fx TEM, on a Jeol 2011 TEM (200KV LaB6) with 2K Gatan Ultrascan camera or on a Jeol 2010F TEM (200KV FEG) with 4K Gatan Ultrascan camera. Cryo-TEM analyses could also be performed on the two latest.

Higher electrical potentials, from 80 kV to 1 MV are applied and therefore higher resolution is obtained by TEM than SEM. However in this case the microscope is used in transmission mode and only very thin samples (submicron scale) can be analysed. A contrast image is obtained from the partial scattering of the electrons passing through the sample. The higher the electron density of the material, the stronger the electron scattering is and those regions appear darker on the transmitted image.

Sample preparation and method

Samples for (cryo-)TEM analysis were prepared on cupper grids (Formvar-Film grids 200 Mesh Cu or, in cryo conditions, Lacey-Carbon-Film grids 300 Mesh Cu, purchased from Agar scientific or TAAB Laboratories equipment Ltd) by simply evaporating a drop of diluted latex or freezing a thin film of diluted

latex in liquid ethane. The applied electrical potential was typically set at 160 kV and no staining was required due to the high electron density of silica nanoparticles allowing clear contrast between inorganic and polymeric particles.

A.5. References

1. Trotman, A., *PCS training manual*. Malvern Instruments: 1999.

2. Fitch, R. M., *Polymer Colloids: A Comprehensive Introduction*. Academic Press Limited: 1997; p 364.

3. Xu, R., *Particle Characterization: Light Scattering Methods*. Kluwer Academic: 2002.

4. Goodhew, P. J.; Humphreys, J.; Beanland, R., *Electron Microscopy and Analysis*. 3rd ed.; Taylor & Francis: 2001.

5. York, S.; Dobedoe, R.; Wilson, N. *Introductory course on microscopy*; University of Warwick, UK: 2007.

Appendix B. Complement to Chapter III on Laponite clay – poly(vinyl esters) latexes

B.1. Determination of monomer conversion X_m by ^{1}H NMR spectroscopy

Samples of Laponite clay stabilised poly(vinyl laurate) latexes were dried in air. The remaining films were analysed by ^{1}H NMR; a typical spectrum is presented in Figure B-1. Due to its high boiling point the evaporation of vinyl laurate was negligible and the monomer conversion could be calculated from the intensity of the monomer and polymer peaks.

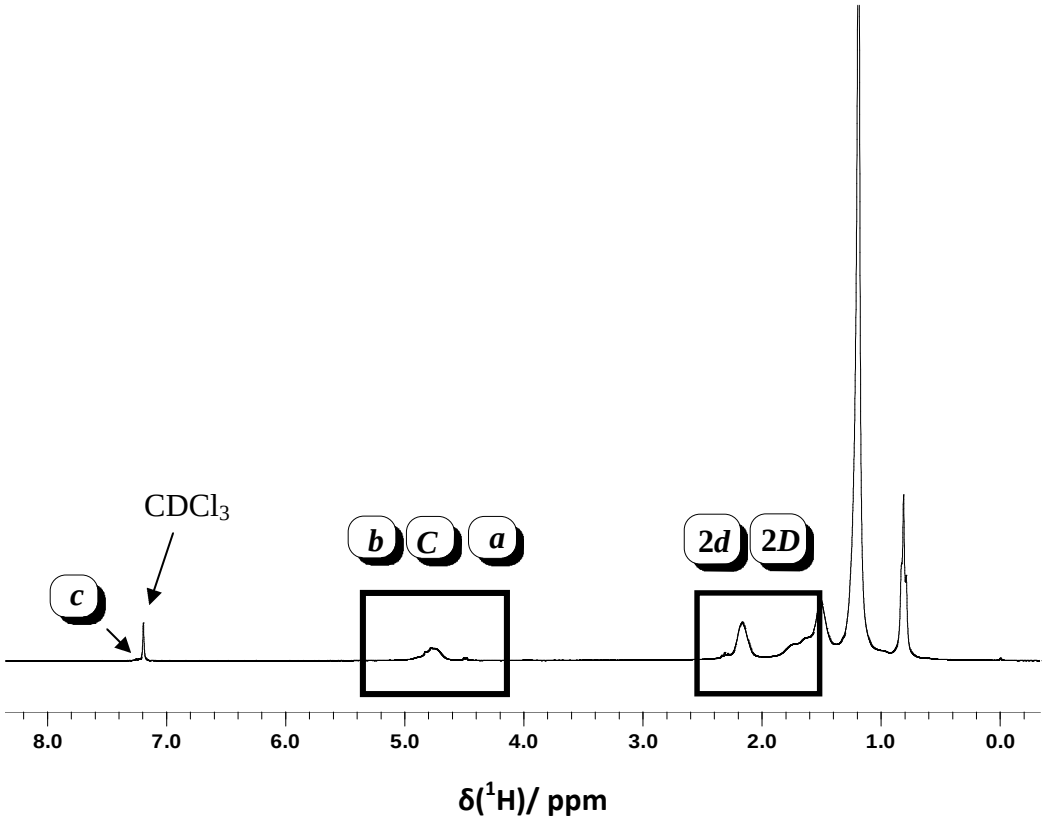

Figure B-1. ^{1}H NMR spectrum of a poly(vinyl laurate) film dissolved in $CDCl_3$ (300 or 400 MHz). Zooms of the squared areas are showed in Figure B-3.

Each hydrogen atom of corresponding ^{1}H NMR signal of shifts higher than 2.0 ppm was annotated with a letter. The annotated molecular structures are displayed in Figure B-2. The zoom of the ^{1}H NMR peaks of interest are showed in Figure B-3. Shifts, multiplicities, integrals and attribution from the data analysis is summarised in Table B-1.

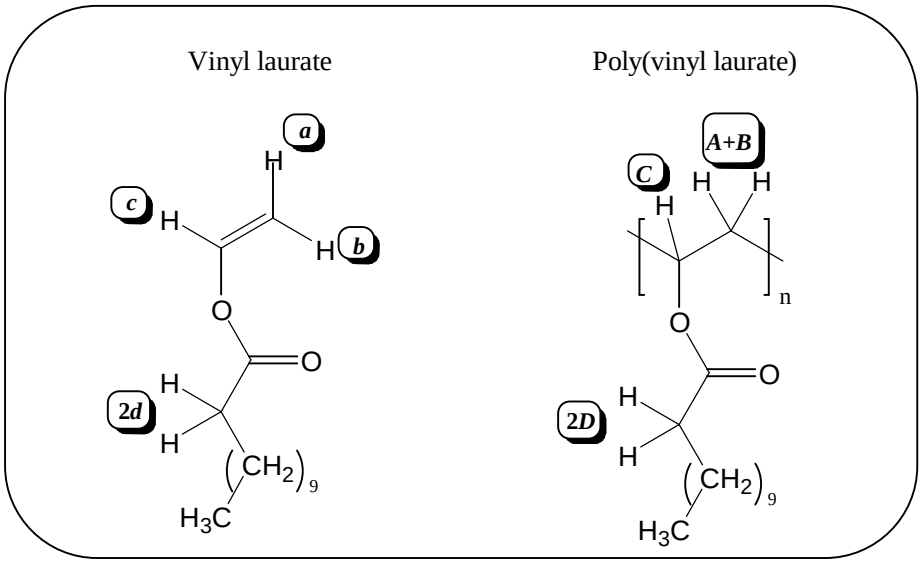

Figure B-2. Molecular structures of vinyl laurate monomer and its polymer annotated for ^{1}H NMR analysis.

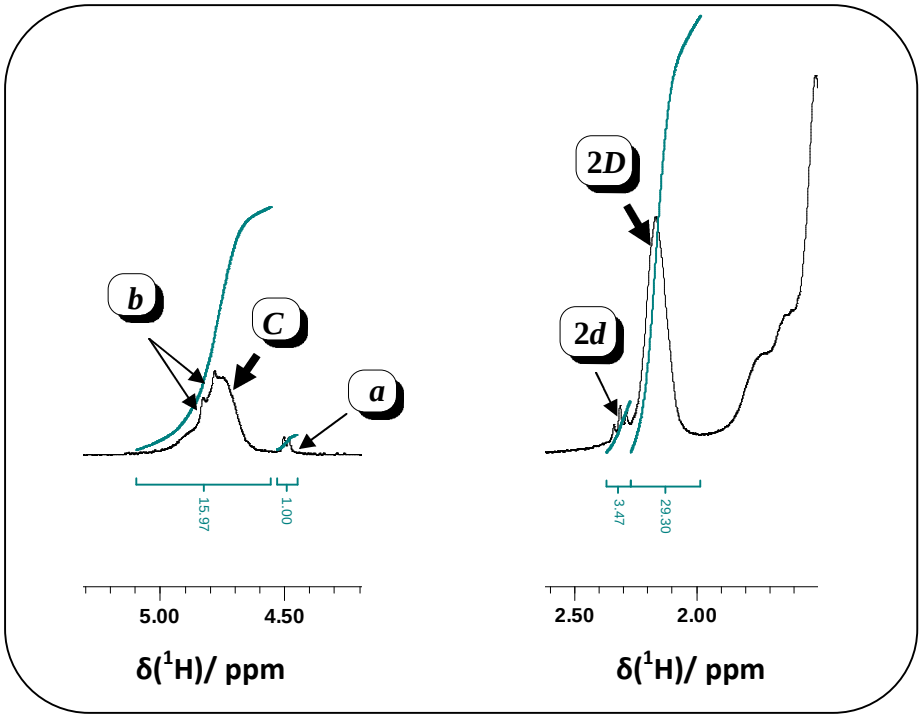

Figure B-3. ^{1}H NMR spectrum of a poly(vinyl laurate) film dissolved in $CDCl_3$ (300 or 400 MHz). Zooms of the squared areas of Figure B-1.

Table B-1. Summary of the shifts, multiplicities, integrals and attribution of the peaks obtained in the range of 2.00 ppm to 6.00 ppm for the poly(vinyl laurate) film spectrum given in Figure B-1.

δ(^{1}H)/ ppm	***Multiplicity***	***Integral***	***Attribution***
2.00 – 2.27	Broad singlet	29.30	(2*D*)
2.27 – 2.37	Triplet	3.47	(2*d*)
4.45 – 4.53	Doublet (of doublet)	1.00	(*a*)
4.57 – 5.60	Broad singlet and doublet (of doublet)	15.97	(*C*) and (*b*)

Monomer conversions were calculated using the intensity of the peaks of the 2-hydrogen atoms (2*d*) (monomer) and the 2-hydrogen atoms (2*D*) (polymer) or the peaks for the hydrogen atoms (*a*) and (*b*) (monomer) and (*C*) (polymer) as follow:

$$X_m(\%) = \frac{D}{d+D} \times 100 \qquad \textbf{Equation B-1}$$

Or,
$$X_m(\%) = \frac{[(b+C)-a]}{b+C} \times 100 \qquad \textbf{Equation B-2}$$

In this work, values of monomer conversion from Equation B-2 are reported due to the higher resolution of the integrated peaks.

B.2. Formulation of all the poly(vinyl laurate)-Laponite clay latexes

Table B-2. Miniemulsion polymerisations of vinyl laurate stabilised with clay and using V-65 initiator. From left to right, symbols are the mass of water, the mass of clay particles, the mass of vinyl laurate monomer, the mass of hexadecane, the mass of initiator, the mass of sodium nitrate, the conversion, the initial calculated concentration in clay particles, and the excess concentration in clay particles.

Experiment	*Initiator*	m_{water}/ *g*	m_0/ *g*	m_M/ *g*	m_{hex}/ *g*	m_I/ *g*	m_{NaNO3}/ *g*	X_m/ *%*	$C_0 \times 10^2$/ $g \times g^{-1}$	$C_{excess} \times 10^2$/ $g \times g^{-1}$
CC-1-123	V-65	52.429	0.522	5.216	0.212	0.031	-	91	0.49	1.00
CC-1-124	V-65	48.149	0.479	4.790	0.195	0.029	0.272	89	0.49	1.00
CC-1-047	V-65	102.983	0.503	10.008	0.406	0.056	-	93	0.15	0.49
CC-1-048	V-65	100.530	0.751	10.009	0.401	0.051	-	93	0.29	0.75
CC-1-043	V-65	100.188	1.003	10.003	0.403	0.051	-	92	0.54	1.00
CC-1-049	V-65	100.280	1.251	10.000	0.405	0.052	-	92	0.69	1.25
CC-1-050	V-65	100.212	1.502	10.011	0.409	0.052	-	93	0.93	1.50
CC-1-107	V-65	50.693	0.356	5.015	0.201	0.025	0.216	88	0.27	0.70
CC-1-108	V-65	50.248	0.501	5.000	0.209	0.029	0.252	87	0.51	1.00
CC-1-109	V-65	50.497	0.702	5.004	0.204	0.027	0.291	85	0.89	1.39
CC-1-110	V-65	50.508	0.851	5.003	0.207	0.026	0.255	83	1.11	1.69

Table B-3. Miniemulsion polymerisations of vinyl laurate stabilised with clay and using AIBN initiator. From left to right, symbols are the mass of water, the mass of clay particles, the mass of vinyl laurate monomer, the mass of hexadecane, the mass of initiator, the mass of sodium nitrate, the conversion, the initial calculated concentration in clay particles, and the excess concentration in clay particles.

Experiment	*Initiator*	m_{water}/ *g*	m_0/ *g*	m_M/ *g*	m_{hex}/ *g*	m_I/ *g*	m_{NaNO3}/ *g*	X_m/ *%*	$C_0 \times 10^2$/ $g \times g^{-1}$	$C_{excess} \times 10^2$/ $g \times g^{-1}$
CC-1-193A	AIBN	100.011	0.503	9.998	0.399	0.052	-	94	0.50	0.20
CC-1-194A	AIBN	100.000	0.753	10.023	0.403	0.054	-	94	0.75	0.18
CC-1-196A	AIBN	100.045	1.125	10.035	0.411	0.052	-	94	1.12	0.13
CC-1-197A	AIBN	100.101	1.500	10.008	0.395	0.056	-	96	1.50	0.27
CC-1-198	AIBN	51.005	- (*)	5.025	0.202	0.044	-	89	n.a.	n.a.

(*) Sodium hydroxide (0.482 g, pH 11.0) was added to work in similar alkaline conditions than with Laponite clay nanoparticles.

B.3. Hydrolysis of vinyl acetate monomer emulsified in Laponite-clay dispersion: pH measurements

The hydrolysis reaction of vinyl acetate leading to acetic acid (pK_a = 4.75) and acetaldehyde products, both soluble in water, is represented in the scheme of Figure B-4.

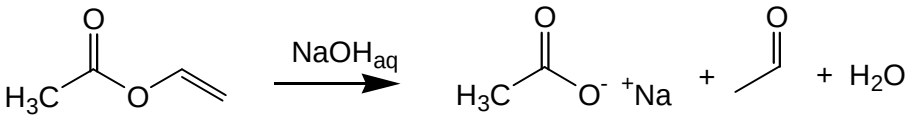

Figure B-4. Reaction of hydrolysis of vinyl acetate in alkaline conditions.

A dispersion of 1.00 g of Laponite clay in 100.00 g water was exfoliated/flocculated with the addition of 0.57 g (0.1 M) of sodium chloride and by ultrasonicating the mixture at 370 W for 4 sub-cycles of one minute (cycle 1). The organic phase containing 10.00 g of vinyl acetate and 0.40 g of hexadecane then added and 6 sonication sub-cycles of one minute were performed to homogenise the sample. The pH monitored during the miniemulsification process, therefore indirectly following the hydrolysis reaction, is represented as a function of time in Figure B-5.

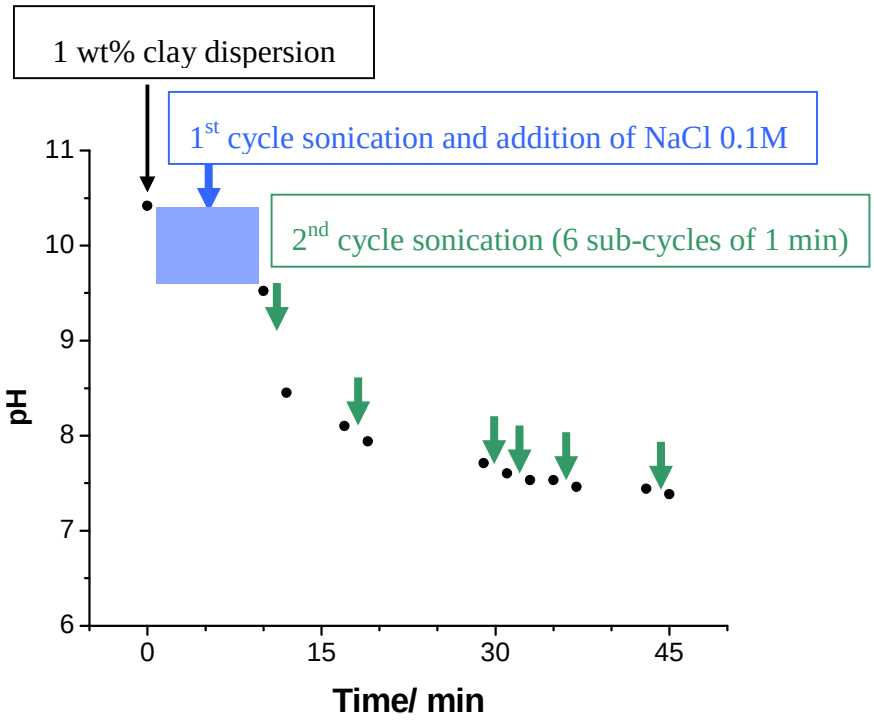

Figure B-5. pH as a function of time of a 1.0 wt% dispersed clay mixture when 10 wt% vinyl acetate are added during ultrasonication.

B.4. Effect of the amount of Laponite clay on the latex particle size

B.4.1. Viscosity of Laponite clay dispersions

Viscosity measurements of clay dispersions were performed at room temperature using a LV2 spindle set at 100 rpm. Ten measurements were taken at 5 seconds intervals, twenty seconds after having started the spindle. The average viscosities of clay dispersions with solids contents ranging from 0.50 up to 1.25 wt% before and after addition of salt are plotted in Figure B-6. A directly proportional dependence was found between the amount of Laponite clay and the viscosity for flocculated (*via* salt) dispersions. Note that at the highest concentration in clay (1.25 wt%), the viscosity of the flocculated dispersion decreased from 48.9 to 45.9 cP over the ten measurements. This is due to work

softening, time-dependent phenomenon, often encountered in clay dispersed systems showing a non-Newtonian behaviour.[1]

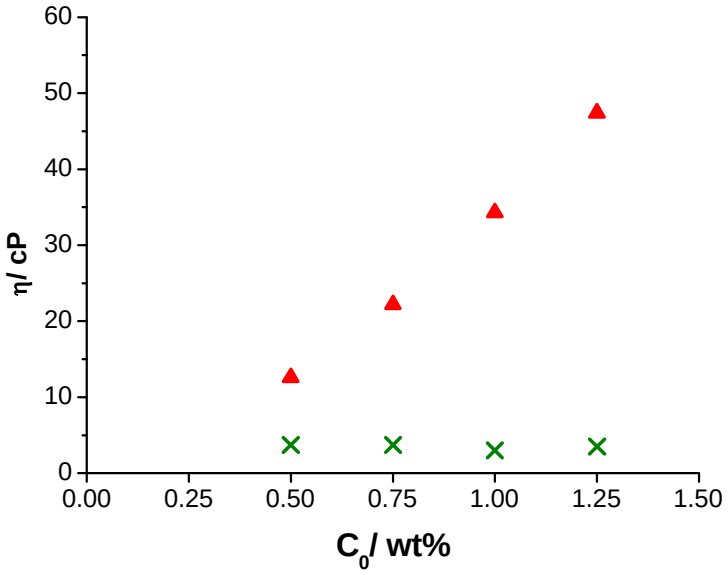

Figure B-6. Viscosities η (cP) of clay dispersions of 0.50, 0.75, 1.00 and 1.25 wt% in deionised water (×) and when flocculated *via* salt (▲) (using an LV2 spindle and the viscometer spindle speed was set at 100 RPM in all experiments).

B.4.2. Semi-empirical model correlating average latex particle size with the amounts of clay and monomer proposed by Bon and Colver[2]

The model describes the partitioning of the Laponite clay platelets between its dispersed state in the continuous phase (water) and its adsorption onto the surface of the miniemulsion droplets of monomer or polymer particles. The overall mass balance in clay nanoparticles is therefore defined as:

$$C_0 = C_{surf} + C_{excess} \qquad \textbf{Equation B-3}$$

Where C_0 is the overall concentration of clay nanoparticles in water in g g^{-1} calculated with m_0/m_{water}. C_{surf} is the concentration of clay nanoparticles

adhered to the oil-water interface (*i.e.*, to the monomer droplets or polymer particles, with respect to the amount of water phase, m_{surf}/m_{water}), and C_{excess} is the excess concentration of clay nanoparticles that remain in the continuous phase, m_{excess}/m_{water}. The clay nanoparticles were dispersed in the aqueous phase and it was assumed that no nanoparticles entered the oil/monomer phase due to its too high energy barrier.

In order to calculate the surface coverage of the droplets, C_{surf}, few assumptions were made: (i) the liquid-liquid interface is "fully" covered, (ii) the monomer droplets/polymer particles and the solid Laponite disks are uniform in size, (iii) the dimensions of the Laponite clay discs are negligible with respect to the size of the monomer droplets/polymer particles, thereby ignoring curvature and thus geometrical constraints so that the disks lie flat on the surface, and (iv) Laponite clay discs are packed in a 2D square lateral geometry.

The interfacial area of one monomer droplet/polymer particle equals:

$$a_{oil} = \pi d_{oil}^{2} \qquad \textbf{Equation B-4}$$

Where d_{oil} is the diameter of the monomer droplets/polymer particles.

The effective area covered by one Laponite clay disk equals:

$$a_{part} = d_{part}^{2} \qquad \textbf{Equation B-5}$$

Where d_{part} is the diameter of a Laponite clay disc.

The total number of monomer droplets/polymer particles is expressed as:

$$N_{oil} = \frac{\frac{m_{oil}}{\rho_{oil}}}{\frac{\pi}{6} d_{oil}^{3}} \qquad \textbf{Equation B-6}$$

Where m_{oil} is the combined amount of polymer and hexadecane, and ρ_{oil} the average density of polymer and hexadecane calculated as follows:

$$\rho_{oil} = \frac{m_{hd}}{m_{hd} + m_{polym}} \rho_{hd} + \frac{m_{polym}}{m_{hd} + m_{polym}} \rho_{polym} \qquad \textbf{Equation B-7}$$

Where $m_{hd}, m_{polym}, \rho_{hd}, \rho_{polym}$ are the amounts of hexadecane, polymer (known from the amount of monomer multiplied by the conversion) and the densities of hexadecane and the polymer, respectively. The total number of Laponite clay disks adhered to the liquid-liquid interface is also calculated with:

$$N_{part} = \frac{4\left(\frac{m_{surf}}{\rho_{part}}\right)}{\pi\, d_{part}{}^{2}\, h} \qquad \textbf{Equation B-8}$$

Where ρ_{part} is the density of Laponite RD and *h* is the height of the discs.

As full coverage is assumed:

$$N_{oil}\, a_{oil} = N_{part}\, a_{part} \qquad \textbf{Equation B-9}$$

By substituting Equations B-4 to B-8 into B-9, the following expression calculating m_{surf} is found:

$$m_{surf} = \frac{3\pi}{2}\left(\frac{\rho_{part}}{\rho_{oil}}\right)\left(\frac{h}{d_{oil}}\right) d_{oil} \qquad \textbf{Equation B-10}$$

Knowing that $C_{surf} = m_{surf} / m_{water}$ *and* $C_{excess} = m_{excess} / m_{water}$, C_{excess} *or* m_{excess} can be expressed from the Equations A-3 and A-10 (see Equation II-1 in Chapter II).

B.5. References

1. Van Olphen, H., *An Introduction to Clay Colloid Chemistry*. 2nd ed.; John Wiley & Sons: 1977.

2. Bon, S. A. F.; Colver, P. J., *Langmuir* **2007,** *23* (16), 8316-8322.

Appendix C. Complement to Chapter III on solids-stabilised droplets for the preparation of silica-armoured polymer latexes

C.1. Formulation of Ludox-stabilised latexes

Table C-1. Miniemulsion polymerisations of styrene using different grade of Ludox colloidal silica as solids-stabiliser at pH ~3. Reactions were conducted at 51 ºC using V-65 initiator. From left to right symbols are the masses of Ludox dispersion, aqueous phase (deionised water and HCl_{aq}), monomer, hexadecane and initiator.

Exp.	*Ludox grade*	$m_{Ludox\ sol}$/ *g*	m_{aq}/ *g*	m_M/ *g*	m_{hex}/ *g*	m_I/ *g*
CC-1-114	TM-40	5.06	53.0	5.05	0.203	0.030
CC-1-199	TM-40	5.00	53.2	5.00	0.201	0.031
CC-1-148	SM-30	5.10	48.5	5.01	0.212	0.025
CC-1-147	HS-40	6.75	60.4	5.01	0.025	0.025

Table C-2. Miniemulsion co-polymerisations of styrene and 4-vinyl pyridine using Ludox colloidal silica TM-40 as solids-stabiliser at pH ~10. Reactions were conducted at 65 ºC with AIBN initiator and at 51 ºC with V-65 initiator. From left to right symbols are the masses of Ludox dispersion, water, styrene monomer, 4-vinyl pyridine monomer, hexadecane and initiator.

Exp.	*Initiator*	$m_{Ludox\ sol}$/ *g*	m_{aq}/ *g*	m_M/ *g*	$m_{4\text{-}VP}$/ *g*	m_{hex}/ *g*	m_I/ *g*
CC-1-189	AIBN	19.21	40.0	5.01	1.00	0.251	0.105
CC-1-191	V-65	6.00	60.4	5.00	1.02	0.242	0.031

C.2. Hand-shaking tests for the formation of solids-stabilised emulsions with Ludox TM-40 silica nanoparticles

Stable oil-in-water emulsions of monomers (such as styrene, vinyl acetate, vinyl pivalate, vinyl laurate and methyl methacrylate) using Ludox TM-40 colloidal silica as solids-stabiliser were obtained when the pH of the aqueous phase was lowered to about 3. As shown in Figure C-1, Vials 1 to 9 contained 10, 20, … up to 90% in volume of the aqueous phase (silica sol) and 90, 80, … down to 10% in volume of styrene monomer (coloured in yellow with an oil-soluble dye [2,4-dihydroxy-4'-nitroazobenzol]), respectively. Stable emulsions were obtained after hand-shaking with monomer contents of 40 – 50% in all cases (down to vial 6 on Figure C-1, bottom part).

The same experiment conducted at various pH showed good stabilisation of o/w emulsions at high pH (~10) in the case of vinyl laurate monomer only. This was attributed to the in situ formation of surfactant (see Chapter II) and a clear difference was observed in the creaming behaviour of the emulsion droplets due to the presence of highly charged nanoparticles and speculated surfactant on the droplet surface (see Figure C-2).

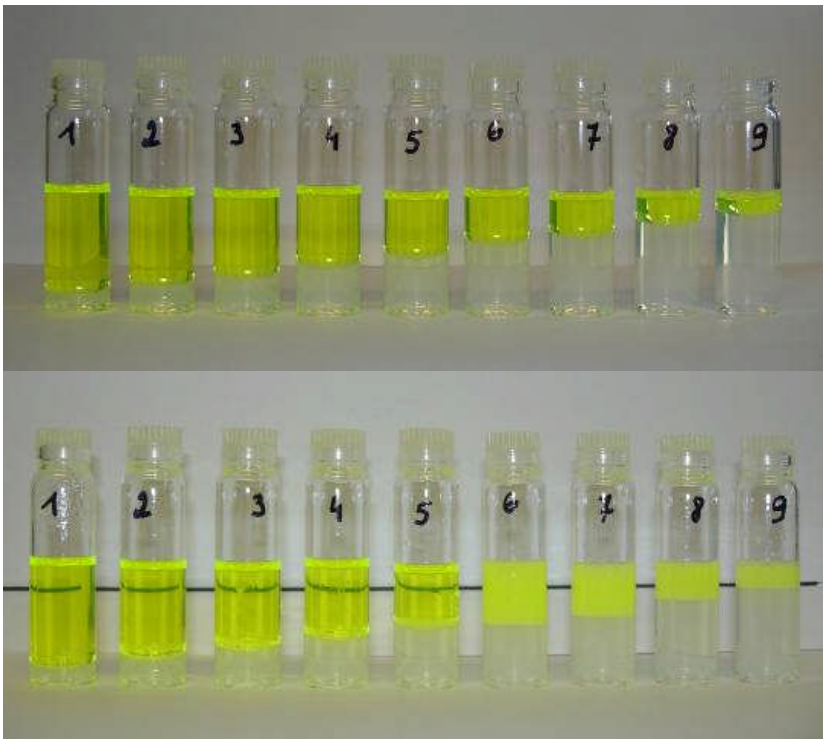

Figure C-1. Styrene monomer and Ludox TM-40 dispersion at pH ~3: Before and after emulsification by hand-shaking, top and bottom respectively. O/w emulsions were obtained up to 40 vol% of monomer.

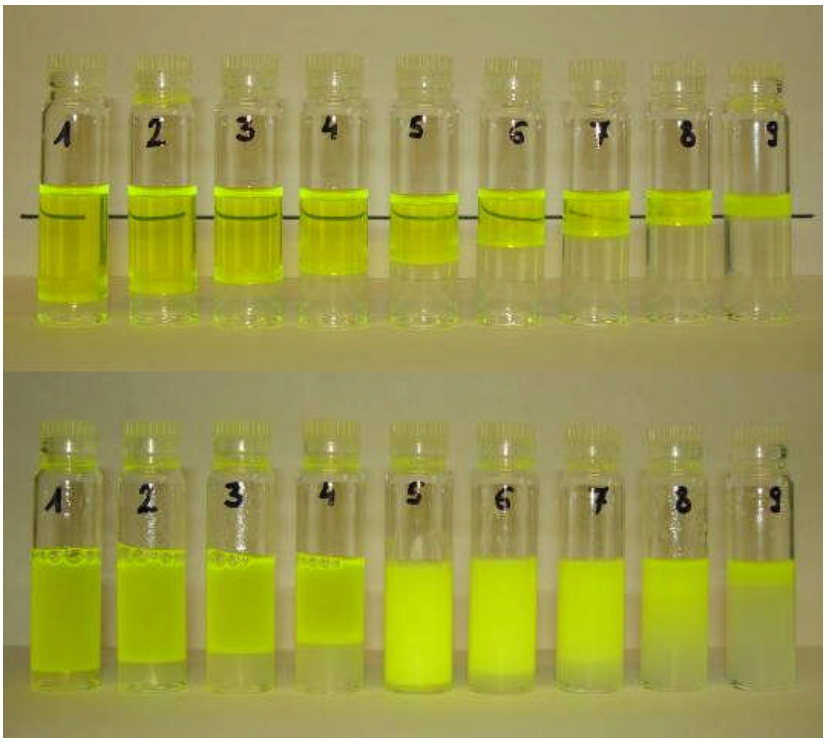

Figure C-2. Vinyl laurate monomer and Ludox TM-40 dispersion at pH ~10: Before and after emulsification by hand-shaking, top and bottom respectively. O/w emulsions were obtained up to 50 vol% of monomer.

C.3. Fumed silica powders as solids-stabiliser for o/w and w/o emulsions of vinyl acetate

Zeta potential measurements (Figure C-3) of hydrophilic fumed silica powders (HDK N20 and HDK D05) showed similar behaviour than Ludox TM-40 silica nanoparticles. By lowering the pH of the aqueous phase down to ~3 *via* addition of HCl (0.1010 M), stable solids-stabilised o/w emulsions of vinyl acetate or styrene were also obtained. As described in section C.2, we prepared a series of hand-shaking samples (see photograph in Figure C-4).

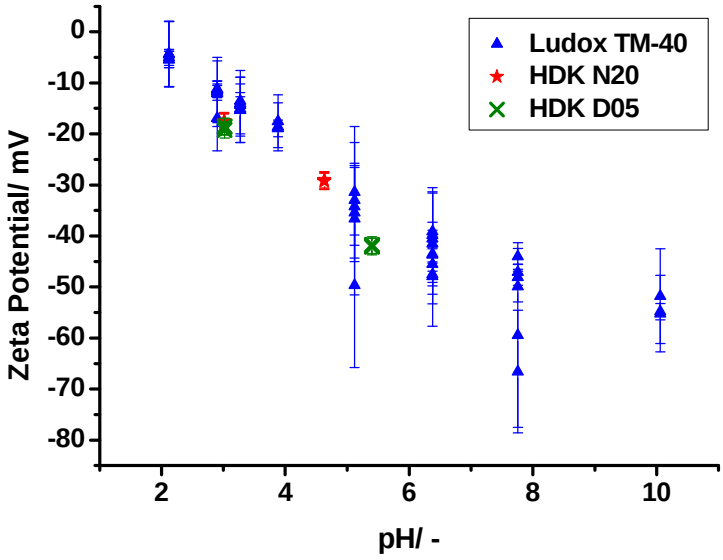

Figure C-3. Graph of the zeta potential of HDK N20, HDK D05 and Ludox TM-40 colloidal silica dispersions as a function of the pH of the aqueous phase.

A range of fumed silica powders hydrophobised by chemical modification (methylation of the residual hydroxyl groups) was investigated for the preparation of solids-stabilised emulsion droplets. Table C-3 summarises the percentage in residual hydroxyl groups of each silica grade as stated by the supplier, their observed capability to disperse (0.5 – 1 wt% powder) in water

and/or vinyl acetate, and in presence of both water and vinyl acetate, the type of solids-stabilised emulsions formed upon hand-shaking. A decrease in the amount of hydroxyl groups onto the fumed silica surface affected their (partial) wetting between the aqueous phase and the monomer (oil) phase in favour to the hydrophobic phase. All emulsions followed the Bancroft rule and fumed silica with 78% residual SiOH (SLM 149/2) was found to be the crossing point. It could be dispersed in both water and vinyl acetate which dictated the type of solids-stabilised emulsion. Silica with full surface methylation showed strong wetting by vinyl acetate and did not stabilise the created vinyl acetate – water interface. However when using non-polar monomers, such as styrene, partial wetting between the two phases occurred and stable water-in-oil emulsions (up to 60 vol% water content) were formed (Figure C-5).

Table C-3. Grades of fumed silica particles with different amounts in residual SiOH groups, their observed dispersion in water and vinyl acetate (✓ good, × very poor/nonexistent), and the type of solids-stabilised emulsion formed for vinyl acetate monomer and water.

Fumed silica grade	***Residual –SiOH***	***Dispersion in water***	***Dispersion in vinyl acetate***	***Type of solids-stabilised emulsion***
HDK D05	100%	✓	×	o/w (pH ~3)
HDK N20	100%	✓	×	o/w (pH ~3)
SLM 149/1	~89%	✓	✓	o/w
SLM 149/2	~78%	✓	✓	o/w or w/o*
HDK HKS-D	~71%	limited	✓	w/o
HDK H20	~33%	×	✓	w/o
HDK H2000	~0%	×	✓	Not stable**

* The phase in which the particles were dispersed constituted the continuous phase of the emulsion.

** When styrene monomer was used, w/o solids-emulsions were obtained.

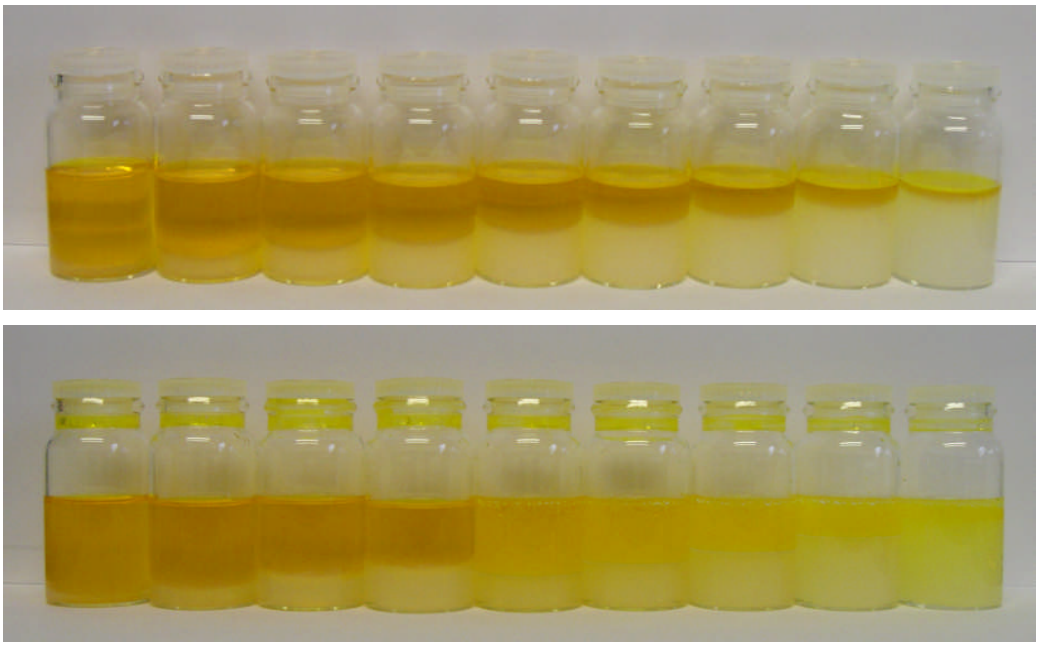

Figure C-4. Vinyl acetate monomer (dyed in yellow) and fumed silica HDK D05 aqueous dispersion at pH ~3: Before and after emulsification by hand-shaking, top and bottom respectively. O/w emulsions were obtained up to 50 vol% of monomer.

Figure C-5. Styrene monomer and fumed silica HDK H2000 aqueous dispersion (initially dyed in red with rhodamine): Before and after emulsification by hand-shaking, top and bottom respectively. W/o emulsions were obtained up to 60 vol% of water.

Appendix D. Complement to Chapter IV on silica-armoured poly(vinyl acetate) latexes made using solids-stabilised emulsion polymerisation

D.1. Formulation and kinetics of Ludox-poly(vinyl esters) latexes

Table D-1. Emulsion polymerisations conducted at 65 ºC using KPS initiator. From left to right symbols are the mass of water, the mass of 40 wt% Ludox(TM-40) dispersion, the mass of monomer, the mass of initiator and the pH of the silica dispersion adjusted with HCl(aq). Vinyl acetate was fed during the emulsion polymerisation processes for experiments cc-3-357 and cc-3-371 (see Chapter IV).

Experiment	*Monomer*	m_{water}/ *g*	$m_{Ludox\ sol}$/ *g*	m_M/ *g*	m_I/ *g*	*pH*/ -
cc-2-342	VAc	100.0	13.0	9.3	0.056	3.0
cc-3-345B	VAc	80.0	39.0	9.3	0.151	3.1
cc-3-345E	VAc	80.0	39.0	14.9	0.151	3.1
cc-3-354	VAc	100.0	13.0	9.3	0.051	4.5
cc-3-355	VAc	100.0	13.0	9.3	0.052	5.5
cc-3-357	VAc	220.0	13.0	n.a.	0.052	4.8
cc-3-367	VAc	885.0	148.3	132.3	0.50	4.5
cc-3-369	VAc	138.0	62.4	50.0	0.25	4.5
cc-3-371	VAc	137.5	62.5	n.a.	0.25	4.5
cc-3-377	VAc	706.3	262.4	240.0	1.00	4.5
cc-3-379	VAc	837.3	130.0	240.0	1.00	4.5
cc-3-381	VAc	170.8	33.3	30.0	0.13	4.5
cc-3-390	VPiv	166.1	33.0	30.0	0.13	4.5

The instantaneous monomer conversion of exp. cc-3-357 and cc-3-371 plotted as function of added vinyl acetate (Figure D-1) revealed the difference in the polymerisation kinetics between the two. Under “starved” conditions in monomer (0.35 mL min^{-1} fed, exp. cc-3-357) the instantaneous conversion

quickly reached and stayed close to 100%. On the other hand, in exp. cc-3-371 we fed monomer (2.25 mL min^{-1}) to ensure an excess in monomer throughout the polymerisation process, "non-starved" regime. This rate was determined from the fastest rate of polymerisation of VAc (50.0 g) in a batch emulsion polymerisation at 65 ºC (exp. cc-3-369); amounts in silica nanoparticles (62 g of Ludox sol) and KPS initiator (0.25 g) in 138 g of water were kept the same. The graph of monomer conversion over time is shown in Figure D-2.

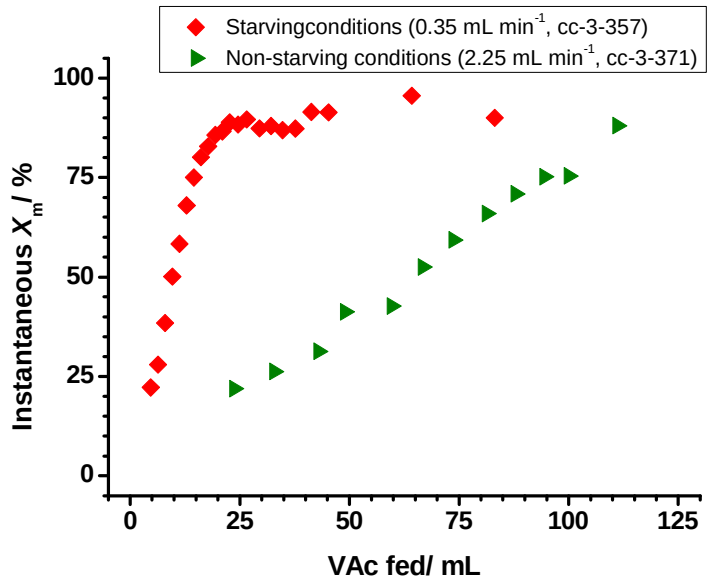

Figure D-1. Instantaneous monomer conversion as a function of the amount of vinyl acetate added for two semi-batch emulsion polymerisation reactions of solids-stabilised polymer particles.

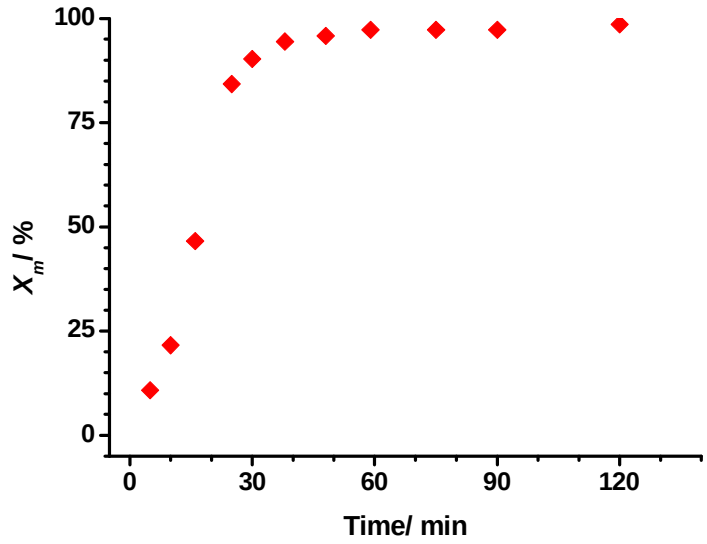

Figure D-2. Conversion of vinyl acetate over time for experiment cc-3-369.

D.2. Armoured structure of the Ludox-poly(vinyl acetate) latexes by transmission electron microscopy

An electron micrograph (Figure D-3) of the Ludox(TM-40) armoured PVAc latex (cc-3-381) at final conversion exhibits partial coalescence of the particle leading to some doublet and triplet coalesced clusters. A lack of colloidal silica stabiliser can be observed in the ‘fused’ areas.

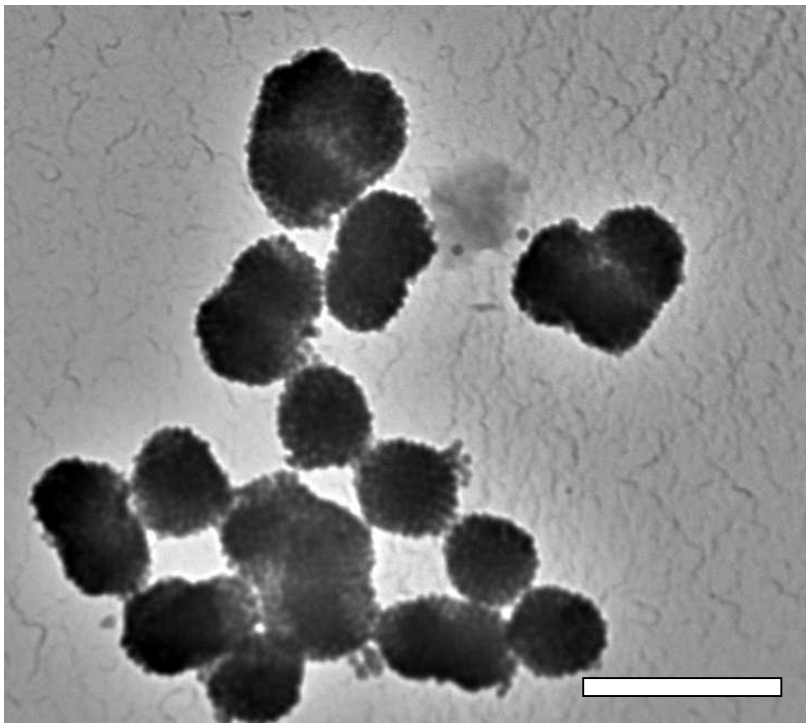

Figure D-3. TEM image of Ludox TM-40 stabilised PVAc latex with a silica-to-monomer ratio of 0.44. Scale bar 500 nm.

D.3. Disc centrifugation particle sizing measurements

D.3.1. Principle of disc centrifugation particle sizing[1]

Disc centrifugation particle sizing (CPS) is a sedimentation method which can be used to measure particle size distributions of colloids by a rotating vertical cylindrical disc containing a gradient fluid at various speeds. When exposed to the centrifugal acceleration, the particles sediment in bands and their velocity can be predicted by the Stokes' law as a function of their diameter. The scattered light from the laser beam (wavelength λ = 480 nm) is detected at the edge of the disc, where the detector is located. The device is described in Figure D-4.

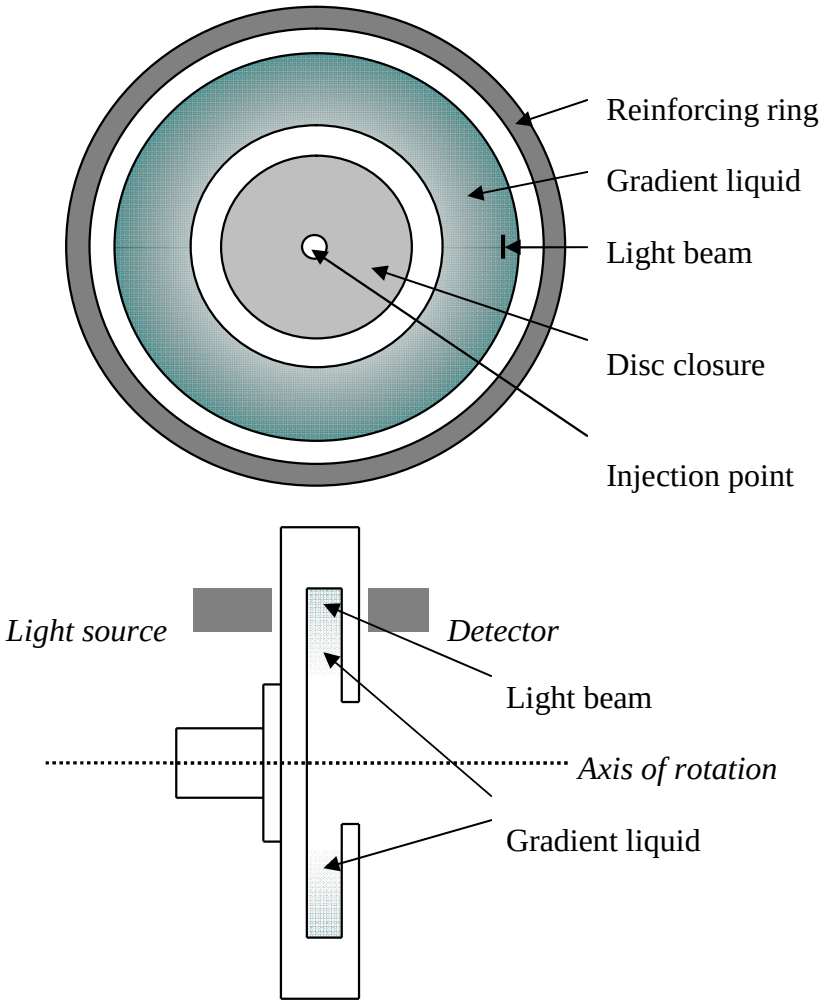

Figure D-4. Hollow disc centrifuge design: front view (top), side view (bottom).

When under the influence of acceleration, particles can be separated upon their size, commonly referred to as 'differential centrifugation' or 'rate zone separation', and upon their density which is known as 'isopycnic separation'.

Pure water cannot be used as a settling fluid as it would provoke streaming of the injected sample which is to say behave like a fluid of higher density rather than like individual particles suspended in water. Density gradient centrifugation was already reported in the 60's by Mateyko and Kopac,[2] and Juhos.[3] They used

Ludox colloidal silica for this purpose. Typically, to analyse a waterborne dispersion down to about 10 nm, a sucrose gradient is built as the settling fluid.

The operational conditions were optimised to analyse Ludox colloidal silica. The more concentrated and monodiperse the sample, the higher the density difference and therefore a steeper gradient should be used to avoid streaming. To allow settling of the particles up to the detector, the highest density of the gradient (highest content in sucrose) located at the edge of the disc has to be lower than the particle density and therefore allows sedimentation upon imposing the centrifugal force by rotation of the disc.

D.3.2. Data analysis to determine the concentration in nanoparticles using disc centrifugation

The CPS was used to correlate intensity of the detection signal to the concentration of nanoparticles. Our gradient was built from two solutions; sucrose of 8.0 wt% (0.23 mol kg^{-1}) and 24.0 wt% (0.70 mol kg^{-1}).

We initially injected a series of calibration standards of Ludox TM-40 silica nanoparticles dispersed in water. Representative data is shown in Figure D-5 for various concentrations of silica nanoparticles, 0.11 wt%, 0.22 wt%, 0.28 wt%, 0.33 wt% and 0.39 wt%.

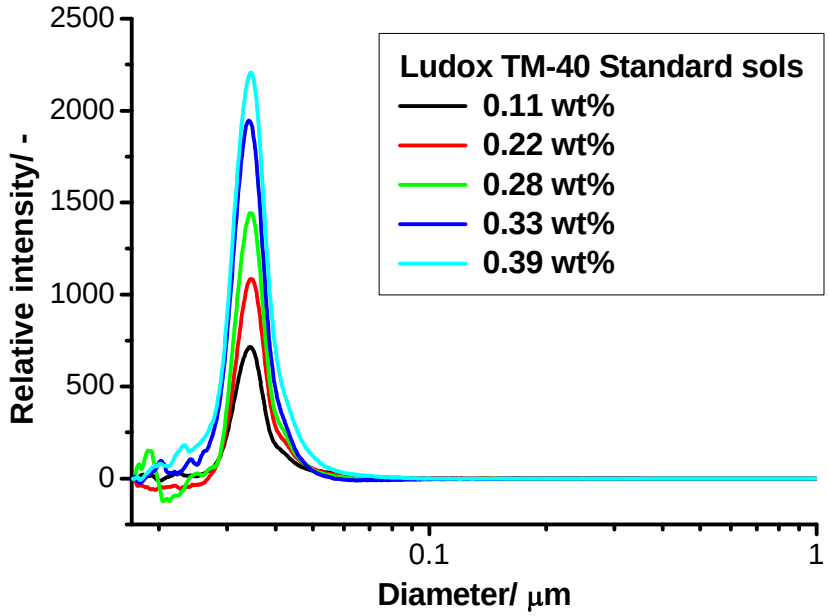

Figure D-5. Traces obtained by CPS analyses of approximately 0.1 g for each Ludox TM-40 standard sol of known concentration in colloidal silica nanoparticles prepared from a 40 wt% Ludox TM-40 sol.

Note from the disc centrifugation data, the signal of the silica nanoparticles appeared around 35 nm in diameter which differed from our TEM mean value of 24 nm. We believed that this shift was potentially due to several factors such as a possible difference between the calculated density and the actual density of the nanoparticles of silica, a sedimentation process depending on the hydrodynamic volume rather than actual size, and the silica particles were not of perfect spherical shape. However the mean position of the peak was not of main importance as we were interested in the intensity of the detector signal, and the shape of the signal, which did not change between samples and throughout the emulsion polymerisation process.

In order to measure the intensity of the signal from the detector, we compared three different methods to analyse the traces. We used the CPS software to measure (1) the full area under the peak, (2) the area of half of the

peak, and finally, (3) the height corrected by the baseline (subtracting the intensity at a diameter of 0.26 nm to the highest intensity of the peak), see Figure D-6. This diameter was chosen arbitrarily to attempt to minimise errors induced by the noise observed at the end of the runs and the automatic baseline generated by the software manifestly based on the absorption recorded at the end of the measurements. Settings parameters are specified in the experimental part of Chapter IV.

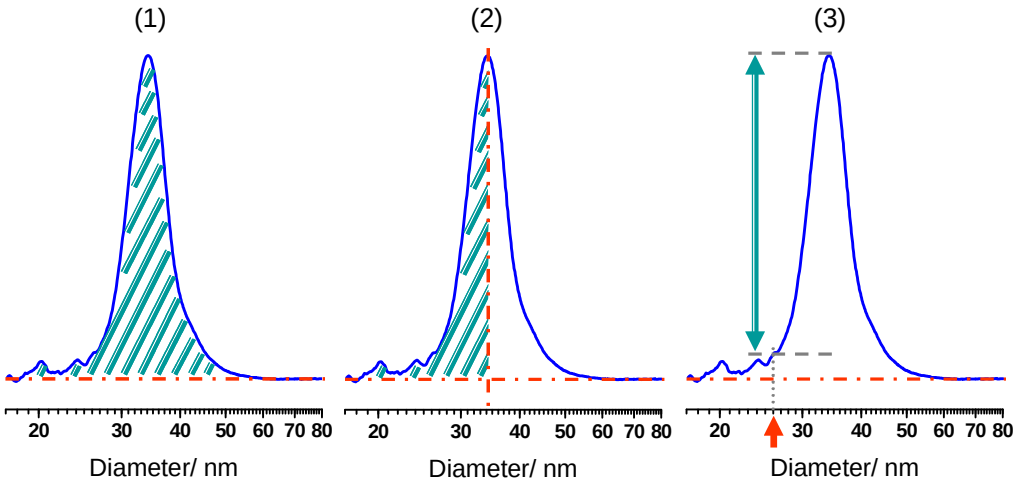

Figure D-6. Cartoon of the three types of analysis performed for each trace (1) by full-area, (2) by half-area and (3) by height after 'baseline correction'. The y-axis is the relative light intensity measured by the detector. The horizontal red dashed-line represents the 'zero' made by the software at a diameter of 17 nm.

Each colloidal silica standard was injected 3 times and all traces obtained were analysed by methods (1), (2) and (3), and corrected by the mass of sample injected. The average of the three measurements is plotted with the standard deviation against the concentration in colloidal silica in Figure D-7.

(1) Full-area

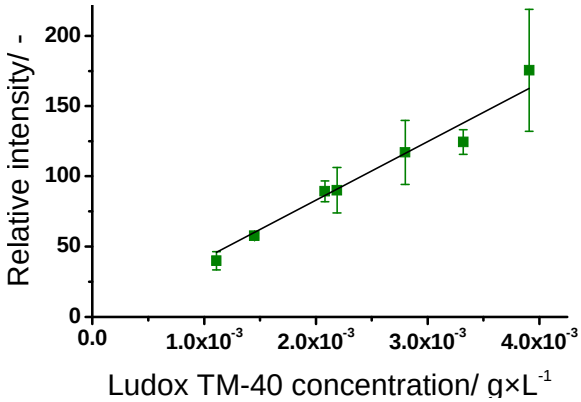

(2) Half-area

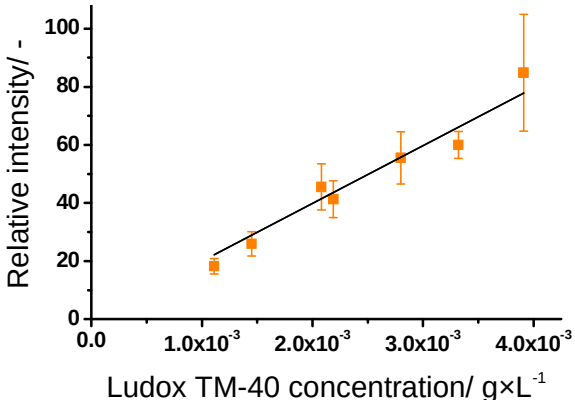

(3) Height

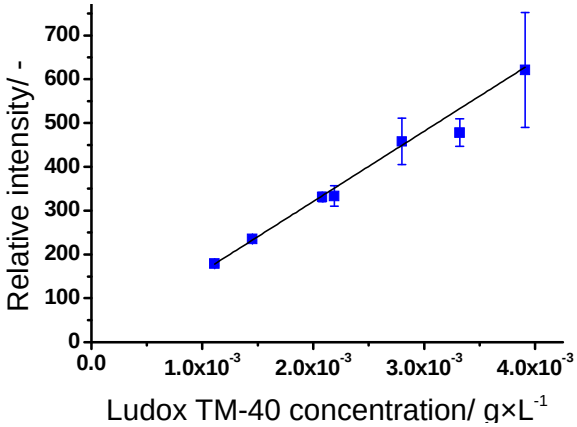

Figure D-7. Graphs of dependence between the concentration in silica nanoparticles and the relative intensity of the peak obtained by CPS measurements for the three different analysis methods described in Figure D-6: (1) Full-area (linear fit: y = 41555 x, R^2 = 0.967), (2) Half-area (linear fit: y = 19919 x, R^2 = 0.955) and (3) Height (linear fit: y = 155598 x, R^2 = 0.983).

By plotting relative signal intensities versus concentration in colloidal silica, a linear trend is observed for the three types of analysis with excellent linear regression (R^2 over 0.95). The peak is uniform in shape and size which gives a good indication for reproducibility and comparison between samples.

In order to determine the most accurate methods of the three methods to analyse, relative standard deviations, σ_{rel}, were compared and plotted in Figure D-8. They were calculated over three measurements made for each concentration in nanoparticles and normalised by dividing by the relative intensity of the signal measured. The irregularities observed on the graph are simply attributed to the fact that each sample was injected only 3 times.

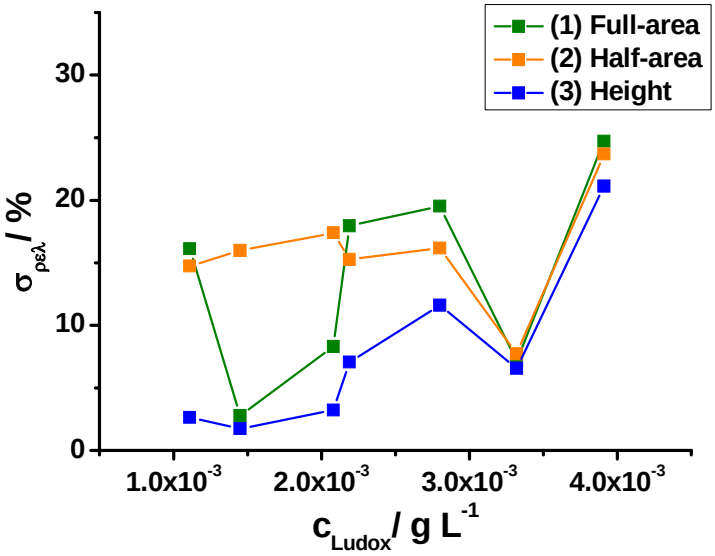

Figure D-8. Graph of the relative standard deviations, σ_{rel}, from the analysis with the three different methods of the Ludox standard sol CPS measurements.

From these analyses we found a very clear linear trend between the concentration in colloidal silica nanoparticles and the signal intensity given by the CPS. All cases, reported a high R^2, from 0.955 with method (2), 0.967 with method (1) and 0.982 with method (3). However the differences between standard deviations are less negligible as can be seen in Figure D-8. The third method, using the height of the peak, exhibits a smaller standard deviation and hence was more accurate for single measurements, especially for smaller concentration in silica nanoparticles. We therefore further pursued the analyses of emulsion polymerisation samples using this method.

D.3.3. Reproducibility and variation between gradient fluids for disc centrifugation measurements

This technique has demonstrated exemplary reproducibility due to the injection of PVC calibration standard prior to each injection of samples. However in our case, as we are not analysing the particle size distribution but intensity of the detected signal, more parameters have to be taken into account.

The intensity of the scattered light depending on the refractive index of the dispersed medium, we expected the sucrose concentration to be determinant for the detection of the nanoparticles. Since a sucrose gradient fluid cannot be used for longer than 5 or 6 hours, several gradients had to be prepared in order to analyse Ludox standards and series of samples with each injection taking approximately half an hour. Herein we checked the influence of which on the measurements. The detector is located at the edge of the rotating disc where the sucrose concentration of the gradient is highest. In Figure D-9, the graph displays the results obtained using 8.0 – 20.0 wt% gradient in comparison with

8.0 – 24.0 wt% gradient to investigate the influence on detection of the nanoparticles. A noticeable shift in the detector response was found.

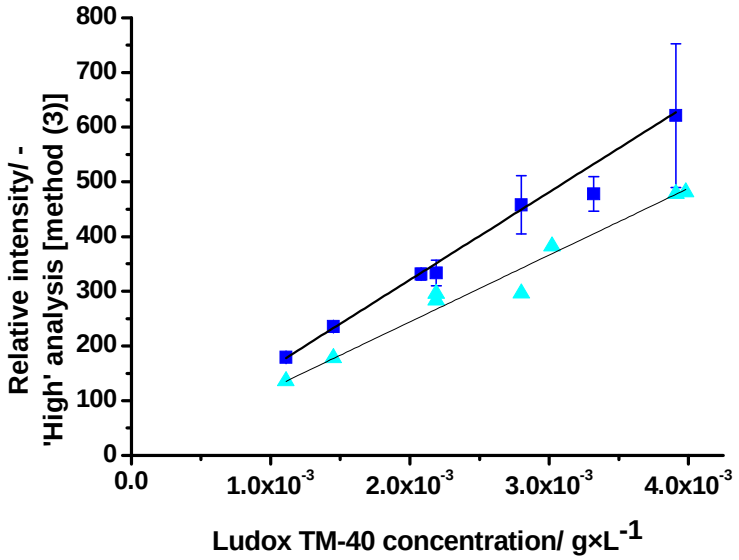

Figure D-9. Relative intensity from the colloidal silica analysed by CPS versus concentration using two different gradient fluids of sucrose: 8.0 to 24.0 wt% (■) and 8.0 to 20.0 wt% (▲).

D.3.4. Stability of the gradient fluid

We also tested the repeatability of the measurement as a function of time using the same sucrose gradient fluid. Two different samples were alternatively injected four times each over a period of four hours. After analysing the data as described above, the variation between the different traces was found to be random. Any change in the refractive index of medium, induced by a warm-up during the centrifugation process for instance, was minimal and could not be observed.

D.4. References

1. Analytik Ltd analytical solutions, C. I. E., *CPS Disc Centrifuge DC24000, System Documentation* **2009**.

2. Mateyko, G. M.; Kopac, M. J., *Ann. N. Y. Acad. Sci.* **1963,** *105*, 185-285.

3. Juhos, E. T., *J. Bacteriol.* **1966,** *91* (3), 1376-7.

Appendix E. Complement to Chapter V on the stability of silica-armoured poly(vinyl esters) latexes, production of powders and their application in tile adhesive formulations

E.1. Formulation of Ludox-poly(vinyl esters) latexes

Emulsion polymerisation reactions of vinyl acetate (co-vinyl neodecanoate) were conducted in a 1 L double-jacket reactor with the overhead stirrer speed set at 312 rpm for about 3-4 hours at 65 ºC using KPS initiator (potassium persulfate). (See experimental part in Chapter IV for details.)

Suspension polymerisation reactions of vinyl acetate were conduced in a ~300 mL double-jacket reactor equipped with a homogeniser (Heidolph Silent Crusher) and the overhead stirrer speed set at 200 rpm. While the mixture was homogenised at 18,000 rpm for 30 minutes the temperature was kept at 15 ºC. Polymerisations were conducted for about 3-4 hours at 65 ºC using AIBN initiator (2,2′-azobis(2-methylpropionitrile)). (See experimental part in Chapter III for details.)

Table E-1. Composition of emulsion polymerisation reactions. From left to right symbols are the mass of water, the mass of Ludox sol, the mass of vinyl acetate (VAc), the mass of vinyl neodecanoate (VEOVA-10) and the mass of initiator.

Experiment	*Ludox grade*	m_{water}/ *g*	$m_{Ludox\ sol}$/ *g*	m_{VAc}/ *g*	$m_{VEOVA\text{-}10}$/ *g*	m_I/ *g*
cc-3-367	TM-40	885.0	148.3	132.3	-	0.50
cc-3-377	TM-40	706.3	262.4	240.0	-	1.00
cc-3-379	TM-40	837.3	130.0	240.0	-	1.00
cc-3-383	TM-40	706.3	262.0	215.0	24.0	1.00
cc-3-384	TM-40	706.1	262.1	192.0	48.0	1.00
cc-3-410	SM-30	891.2	91.4	241.1	-	1.02

E.2. Standard dry formulation for tile adhesives

Table E-2. All constituents for the preparation of cement-based adhesives upon addition of water are listed with their relative solid content. RD-Powders were standards of PVOH-PVAc powders or the prepared silica-PVAc powders.

Components	*wt% content*
OPC CEMI / Milke 52,5 (Ordinary Portland Cement)	32.00
Sand F34	54.32
Durcal 65 (limestone)	6.00
Culminal 9142 (Methyl hydroxyethyl cellulose)	0.40
Metastar 501 (calcinated clay)	2.00
$Al_2(SO4)_3$*18 H_2O	0.58
Calciumformiat (accelerator)	0.70
RD-Powder (redispersible powder)	0.40

E.3. Determination of slip and workability of the prepared tile adhesive pastes

Table E-3. Summary of the first series of additives tested in tile adhesive formulation. Samples 4 TL 'Powder A' and 4 TL 'Powder B' contained two standard PVOH-PVAc powders (Wacker Chemie AG®) as additive and, samples 4 TL cc-3-377 and 4 TL cc-3-379 contained the corresponding silica-PVAc powder.

Sample	Water/ ml kg^{-1}	Viscosity/ $\times 10^3$ mPa s	slip (with 415 g tile after 5 min)	Workability at once	workability after 1h
4 TL 'Powder A'	250	644	0 mm	smooth running, little sticky, low toughening, very little air bubbles in the mortar, little air bubbles at application	skin formation, little thickening, some air bubbles, easy to agitate
4 TL 'Powder B'	250	672	0 mm	smooth running, low sticky, low toughening, very little air bubbles in the mortar, little air bubbles at application	little skin formation, little thickening, some air bubbles, very easy to agitate
4 TL cc-3-377	270	1528	0 mm	very strong thickening over time, very rough-running, very toughening, after sagging no wetting of the 415g-tile	no longer to handle - to tough
4 TL cc-3-379	270	912	0 mm	strong thickening over time, rough-running, very toughening; after sagging only little wetting of the 415g-tile	hard workability, very tough

Table E-4. Summary of the first series of additives tested in tile adhesive formulation. Sample 4 TL 'Powder A' contained a standard PVOH-PVAc powder (Wacker Chemie AG®) as additive and, samples 4 TL cc-3-383, 4 TL cc-3-384 and 4 TL cc-3-410 contained the corresponding silica-PVAc powder.

Sample	Water/ ml kg^{-1}	Viscosity/ $\times 10^3$ mPa s	Slip (with 415 g tile after 5 min) / wetting	Workability at once	workability after 1h
4 Tl 'Powder A'	250	620	1 mm / good	smooth, many air bubbles, good trowel stickiness, easy to apply, nice mortar ridges	little skin formation, no ripening of the mortar, very little air bubbles, good to agitate, little thickening
4 Tl cc-3-383	310	650	0 mm / crosslinked	smooth, some air bubbles, good trowel stickiness, good to apply, nice mortar ridges	little skin formation, no ripening of the mortar, very little air bubbles, good to agitate, little thickening
4 Tl cc-3-384	320	550	*	Creamy, good to apply, many air bubbles, nice mortar ridges	Scarcely skin formation, no ripening of the mortar, very little air bubbles, very good to agitate, little thickening
4 Tl cc-3-410	315	650	0 mm / crosslinked	Creamy, good to apply, many air bubbles, nice mortar ridges, good trowel stickiness	No skin formation, no ripening of the mortar, very little air bubbles, good to agitate, little thickening

* After 3 minutes compete sagging, very thin mortar ridges, no adhesion to the big tile

E.4. Pull off measurements

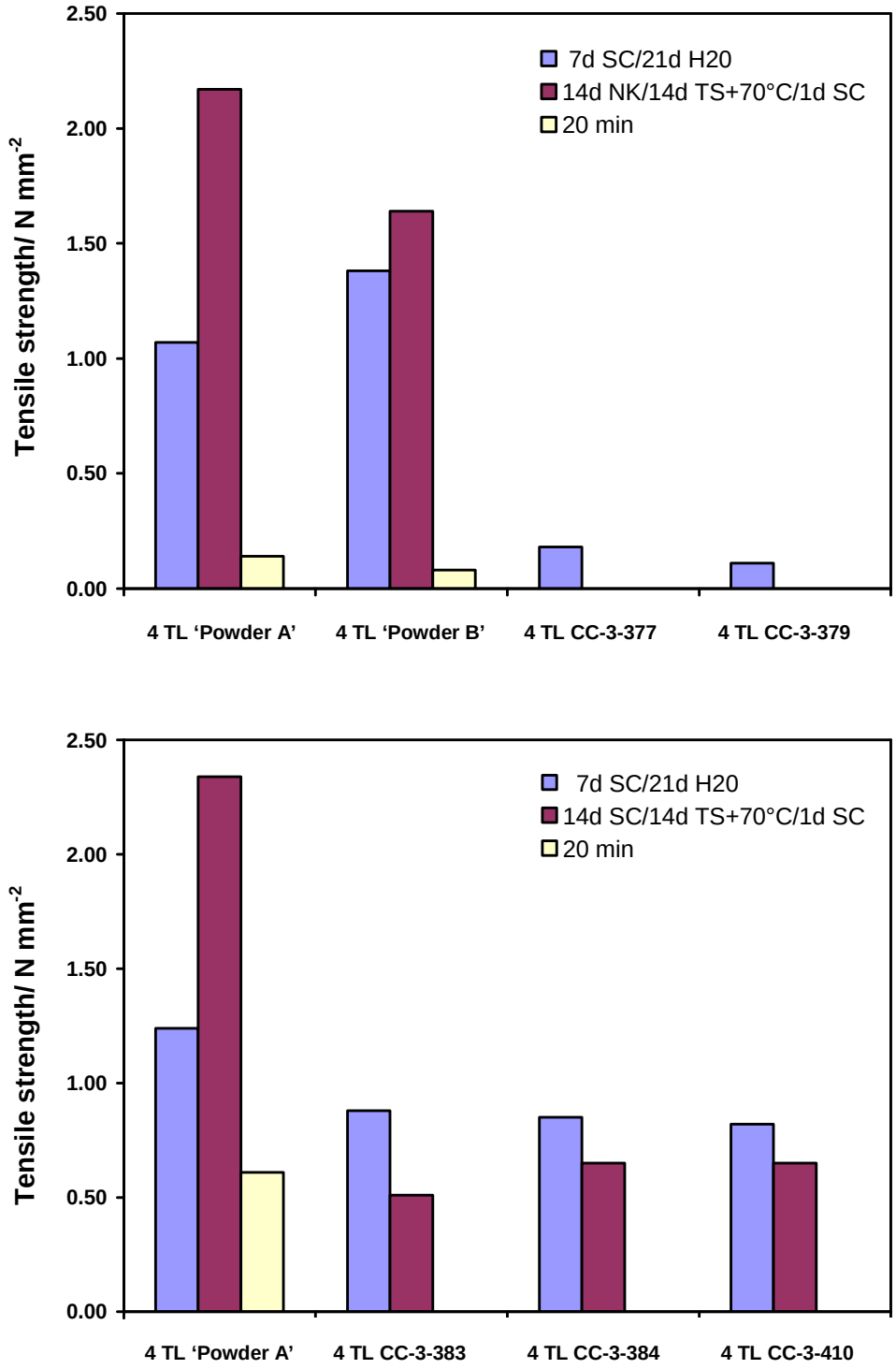

Figure E-1. Graphs of the pull off tests performed at 250 N s^{-1} after wet and temperature storage (PML-543) and 20 minutes open time (PML-505).